Technische Universität München

ZIEL – Zentralinstitut für Ernährungs- und Lebensmittelforschung

Nachwuchsgruppe Intestinales Mikrobiom

Impact of the interplay between bile acids, lipids, intestinal *Coriobacteriaceae* and diet on host metabolism

Sarah Just

Vollständiger Abdruck der von der Fakultät Wissenschaftszentrum Weihenstephan für Ernährung, Landnutzung und Umwelt der Technischen Universität München zur Erlangung des akademischen Grades eines

Doktors der Naturwissenschaften (Dr. rer. nat.)

genehmigten Dissertation.

Vorsitzender:	Prof. Dr. rer. nat. Siegfried Scherer
Prüfer der Dissertation:	1. Prof. Dr. rer. nat. Dirk Haller
	2. Prof. Dr. rer. nat. Martin Klingenspor

Die Dissertation wurde am 14.02.2017 bei der Technischen Universität München eingereicht und durch die Fakultät Wissenschaftszentrum Weihenstephan für Ernährung, Landnutzung und Umwelt am 12.06.2017 angenommen.

Abstract

The gut microbiome is a highly diverse ecosystem which influences host metabolism via for instance via conversion of bile acids and production of short chain fatty acids. Changes in gut microbiota profiles are associated with metabolic diseases such as obesity, type-2 diabetes, and non-alcoholic fatty liver disease. However, beyond alteration of the ecosystem structure, only a handful of specific bacterial species were shown to influence host metabolism and knowledge about molecular mechanisms by which gut bacteria regulate host metabolism are scant. The family *Coriobacteriaceae* (phylum Actinobacteria) comprises dominant members of the human gut microbiome and can metabolize cholesterol-derived substrates such as bile acids. Furthermore, their occurrence has been associated with alterations of lipid and cholesterol metabolism. However, consequences for the host are unknown. Hence, the aim of the present study was to characterize the impact of *Coriobacteriaceae* on lipid, cholesterol, and bile acid metabolism *in vivo*. For this purpose, a gnotobiotic mouse model colonized with a consortium of four *Coriobacteriaceae* strains was established (*CORIO* mice). Germ-free (GF) and specific pathogen-free (SPF) mice were used as controls. Mice were fed diets varying in their fat source and amount with or without supplementation of primary bile acids (BA).

The most striking finding was that *CORIO* mice fed BA diet were characterized by a two-fold increase in white adipose tissue (WAT) mass. This increase in WAT mass was not associated with adipocyte hypertrophy but was accompanied by metabolic disturbances including increased plasma levels of leptin and insulin and marked changes in epididymal WAT proteome. Furthermore, changes in hepatic lipid metabolism including a higher concentration of fatty acids and shifts towards monounsaturated fatty acids were observed in these mice. Interestingly, systemic hypercholesterolemia was detected in all *CORIO* mice, regardless of the diet. In a second trial, the importance of dietary fat source (plant vs. animal) was demonstrated in SPF and GF mice. SPF mice fed BA in combination with a lard-based high-fat diet (L-HFD-BA) were characterized by higher WAT mass and disturbed glucose tolerance when compared to animals fed BA and a palm oil-based HFD-BA (P-HFD-BA). In contrast, GF mice did not show these effects. Changes in gut microbiota profiles, such as a reduction in *Lachnospiraceae* was characteristic of SPF mice on L-HFD-BA. Impact of these different diets on *Coriobacteriaceae*-derived alterations of host metabolism will have to be investigated in the future. In summary, the present thesis demonstrates that the combination of gut-derived *Coriobacteriaceae* and bile acid supplementation modulates host metabolism substantially. Moreover, dietary fat source plays an important role in the regulation of host metabolism and impact gut microbiota profiles.

Zusammenfassung

Die Darmmikrobiota ist ein komplexes Ökosystem, welches den Wirtsmetabolismus unter anderem durch die Umwandlung von Gallensäuren oder die Produktion von kurzkettigen Fettsäuren beeinflusst. Veränderungen in der Darmmikrobiota sind mit verschiedensten metabolischen Erkrankungen wie Übergewicht, Typ-2-Diabetes und nicht-alkohol-bedingter Fettleber assoziiert. Bisher konnten jedoch nur wenige Bakterienarten identifiziert werden, die den Wirtsmetabolismus modulieren. Des Weiteren sind die molekularen Mechanismen, wie Darmbakterien auf den Wirt und damit auf die Entstehung von metabolischen Erkrankungen Einfluss nehmen nur wenig bekannt.

Die Familie der *Coriobacteriaceae* (Phylum Actinobacteria) beinhaltet dominant vorkommende Mitglieder der humanen Darmmikrobiota und kann unter anderem Cholesterinderivate wie Gallensäuren umwandeln. Die Konsequenzen für den Wirt sind bisher jedoch unklar. Daher war das Ziel der vorliegenden Arbeit, den Einfluss von *Coriobacteriaceae* auf den Lipid-, Cholesterin- und Gallensäurestoffwechsel des Wirtes zu untersuchen. Dafür wurden keimfreie Mäuse mit einem Konsortium bestehend aus vier *Coriobacteriaceae*-Stämmen (*CORIO* Mäuse) kolonisiert. Keimfreie und spezifisch pathogen frei–gehaltene (SPF) Mäuse dienten als Kontrollen. Alle Mäuse wurden mit verschiedenen Diäten, die sich in ihrer Fettquelle und –menge sowie dem Zusatz primärer Gallensäuren (BA) unterschieden, gefüttert.

Bemerkenswerterweise besaßen BA-gefütterte *CORIO* Mäuse doppelt so viel weißes Fettgewebe wie die Kontrollmäuse. Dieser Anstieg an weißer Fettmasse war nicht mit einer Zunahme der Fettzellgröße assoziiert, führte jedoch zu Stoffwechselstörungen wie erhöhte Plasmakonzentrationen von Insulin und Leptin und markanten Änderungen im Proteom des epididymalen Fettgewebes. Zusätzlich konnten in diesen Mäusen Veränderungen im hepatischen Lipidstoffwechsel wie zum Beispiel ein Anstieg an Fettsäuren und Verschiebungen in Richtung einfachungesättigter Fettsäuren beobachtet werden. Interessanterweise wurde in allen *CORIO* Mäusen, unabhängig von der Diät, eine Hypercholesterinämie festgestellt. In einem weiteren Versuch wurde die Relevanz der Nahrungsfettquelle (pflanzlich versus tierisch) in SPF und keimfreien Mäusen gezeigt. Hierbei zeigten SPF Mäuse, die mit einer Schweineschmalz- und Gallensäuren-angereicherten Diät (L-HFD-BA) gefüttert wurden, ein höheres Gewicht des weißen Fettgewebes sowie einer gestörten Glukosetoleranz. Diese Effekte wurden bei keimfreien Mäusen jedoch nicht beobachtet. Veränderungen in der Darmmikrobiota wie eine Reduktion der *Lachnospiraceae* war charakteristisch für L-HFD-BA gefütterte Mäuse. Der Einfluss dieser verschiedenen fettreichen Diäten auf Funktionen der *Coriobacteriaceae* und ihre daraus resultierenden Wirkungen auf den Wirtsmetabolismus bleibt zu untersuchen.

Zusammenfassend zeigt die vorliegende Arbeit, dass die Kombination von *Coriobacteriaceae* und Gallensäuregabe den Wirtsmetabolismus erheblich beeinflusst. Darüber hinaus spielt die Quelle des Nahrungsfettes eine wichtige Rolle in der Regulation des Wirtsstoffwechsels und beeinflusst das Profil der Darmmikrobiota.

Table of content

1   Introduction

The present thesis is primarily focused on the interplay between host metabolism and a specific taxonomic family of gut bacteria, the *Coriobacteriaceae*. Hence, the following sections in the introduction provide background information on the gut microbiota (the communities of microorganisms in the intestine), its functional role, and mechanisms involved in the regulation of host metabolic functions such as bile acid and lipid metabolism.

1.1   The gut bacterial ecosystem and metabolic diseases

The gut of each human individual harbors up to $3.8x10^{13}$ bacteria belonging to approximately 500 – 1.000 species with the highest density in the colon, referred to as gut microbiota [1–3]. The widely stated ratio of bacterial to human cell of 10:1 was recently updated to closer to 1:1 by Sender *et al.* [2]. The gut microbiota is dominated by the phyla Firmicutes, Bacteroidetes, Actinobacteria, Verrucomicrobia and Proteobacteria. The diversity, composition, and metabolic functions of the gut microbiota vary highly between individuals and are influenced by diet, life-style, use of antibiotics as well as genetics [4–10]. The interplay between gut microbiota and the host as well as between gut microbes themselves plays an important role in digestion, immunity, and metabolism [11, 12]. Furthermore, the gut microbiota can modulate the absorption of dietary nutrients and influence the endocannabinoid system, which can further induce lipogenesis in adipocytes [13, 14]. This indicates that the interplay between diet and the gut microbiota is crucial for the host's health.

Several research groups assessed the effect of diet on the gut microbiota and the development of metabolic diseases, including obesity and type-2 diabetes (T2D). In human, obesity has been associated with changes in fecal microbiota profiles, including reduction and alterations in bacterial diversity [15–19]. Moreover, a negative correlation between the Bacteroidetes/ Firmicutes ratio and obesity was observed in mice and humans in some studies [16, 20–23], but not in others [24–26]. Fecal microbiota profiles in T2D patients were shown to differ from that in healthy persons, although results from different studies are conflicting [27–32]. These contradictory results could be due to differences in study design, number of subjects, consideration of confounders like anti-diabetic therapies and methodologies used for microbiome analysis [33, 34]. Infusion of microbiota from lean donors to patients with metabolic syndrome improved insulin sensitivity and increased the abundance of butyrate-producing gut bacteria as measured by Human Intestinal Tract Chip (a custom-made Agilent microarray) [35], suggesting that manipulation of the gut bacterial ecosystem might be one opportunity to increase insulin sensitivity and thereby human health. Moreover, compositional shifts in the gut microbiota were also observed in human patients and animals with

non-alcoholic fatty liver disease (NAFLD) or non-alcoholic steatohepatitis (NASH) as well as symptomatic atherosclerosis compared to healthy controls [36–41].

Interestingly, feeding of high-fat diet (HFD) to mice and rats revealed that some animals are resistant whereas others are prone to the development obesity, which is usually accompanied by differences in microbial composition, gut permeability, plasma lipopolysaccharide concentration, and inflammation [42, 43]. Furthermore, various mouse strains differ in their response to HFD and in their gut microbiota, such as the obesity-resistant SWR/J and obesity-prone AKR/J mice [44, 45], suggesting an strong impact of the gut microbiota on the development of obesity.

All the aforementioned publications show that changes in the gut microbiota diversity and composition are associated with metabolic diseases like obesity, T2D, NAFLD and NASH. However, causality and consequences of these differences are not fully clarified and knowledge of molecular mechanisms by which gut bacteria affect host health is scant. In the next paragraphs, known mechanisms how intestinal bacteria can modulate host health are presented.

As toll-like receptors (TLRs) play an important role in host defense against pathogens, these data show that the interaction between gut microbes and the host are important for the development of metabolic diseases. In line with this, rats prone to diet-induced obesity (DIO) showed increased TLR4 activation, increased intestinal permeability and plasma lipopolysaccharide (LPS) concentrations [43]. TLR5-deficient mice have increased fat mass and exhibit features of the metabolic syndrome like hyperlipidemia and insulin resistance [46]. Furthermore, chronic fructose feeding to TLR4 knock out mice resulted in strongly reduced hepatic steatosis and plasma alanine aminotransferase levels, a marker for liver damage [47]. The effects of obesity on gut barrier function and endotoxin concentrations are controversially discussed. Several authors also stated increased gut permeability and/ or LPS levels induced by HFD in mice [42, 48, 49], whereas others reported no evidence for an impaired gut barrier function of DIO in mice [50]. A recent publication showed that the housing conditions, which modulate gut bacterial composition, were crucial for gut barrier function when comparing conventional- and specific pathogen free (SPF)-housed mice [51]. Also the production of short chain fatty acids (SCFA) by the gut microbiota could be of importance in the development of metabolic diseases [25, 52]. However, results are conflicting and will therefore not be dealt with any further in this thesis.

One host factor which might be influenced by the gut microbiota and modulate host adipose tissue is the fasting-induced adipose factor (Fiaf; also referred to as angiopoietin-like protein 4, Angptl4). Fiaf is a secreted inhibitor of lipoprotein lipase (LPL)-meditated lipolysis of plasma triglyceride-rich lipoproteins which increases plasma triglyceride levels and uptake into tissues [53]. The comparison

of GF and conventional mice fed a western-style, high-fat/ high-sugar diet, revealed the inhibition of intestinal Fiaf by the gut microbiota which might induce body weight gain and hints towards an important role of the microbiota in fat-storage in adipocytes [13, 54]. However, measurement of circulating Fiaf levels did not differ between GF and conventional housed mice [22]. Summed up, data regarding Fiaf are controversial and its role in microbiota-mediated fat storage remains to be investigated.

Branched-chain amino acids (BCAAs) were associated with insulin resistance. Pedersen *et al*. (2016) revealed that serum BCAAs levels, synthesized by intestinal bacteria like *Prevotella copri* and *Bacteroides vulgatus*, were increased in insulin-resistant patients [55]. Furthermore, this study showed that *Prevotella copri* CB7 was able to induce insulin resistance and impair glucose tolerance in mice. In line with this, in obese and T2D patients, levels of BCAAs were negatively correlated with insulin resistance [56, 57]. However, more studies are needed to investigate how BCAAs modulate insulin resistance in detail.

Choline metabolism by intestinal microbiota was shown to modulate the development of NAFLD. Feeding of HFD to a susceptible mouse strain (129S6) revealed that choline is excessively metabolized by the intestinal microbiota which then induced the development of NAFLD [58]. This is in line with the observations that the occurrence of this disease is also observed in mice fed a choline-deficient diet [59, 60]. Moreover, NASH patients had a higher abundance of alcohol-producing bacteria like *Escherichia coli* which resulted in higher serum ethanol levels [38]. In line with this, obese *ob/ob* mice fed a standard laboratory diet, exhibited a higher endogenous ethanol production compared to wild type mice [61]. This might be a hint how obesity and the accompanied changes in gut microbiota composition could induce the development of NAFLD and it progression to NASH.

Changes in bile acid composition as well as an increased bile acid pool were also observed in obesity and T2D [62–65]. Surprisingly, serum glycine- and taurine-conjugated forms of chenodeoxy and deoxycholic acid (CDCA and DCA, respectively), glycocholic acid (GCA) and total bile acid concentrations were increased after Roux-en-Y gastric bypass compared to overweight and obese patients [66]. Additionally, changes in fecal bile acid composition in NAFLD and NASH patients were accompanied with changes in the gut microbiota [67].

More and more clinical studies evaluate the effects of modulating the bile acid metabolism via the two key regulators farnesoid X receptor (FXR; also referred to as FXR-α and Nr1H4) and the G protein-coupled bile acid receptor TGR5 (also referred to as GPBAR1) using semisynthetic agonists and antagonists as well as bile acid sequestrants [68, 69]. Only some will be introduced in the next

section. Treatment with FXR agonists like GW4064, WAY-362450 and obeticholic acid (OCA, INT-747) protected against cholestatic liver damage, cholesterol gallstones, lowers serum triglyceride and cholesterol levels and improves insulin sensitivity and inflammatory status in different animal models [70–79]. In a human trial, OCA increased insulin sensitivity, and reduced markers of hepatic inflammation and fibrosis in T2D and NAFLD patients [80]. Guggulsterone, which is the bioactive substance of the plant extract guggul and an antagonist of FXR, decreased hepatic cholesterol and exhibited hypolipidemic effects [69, 81, 82]. However, with respect to human trials the effect of Guggulsterone are not consistent [83]. One semi-synthetic TGR5 agonist, INT-777, induced intestinal GLP1 secretion and reduced the formation of vascular lesions in mice [84, 85]. Moreover, bile acid sequestrants like cholestyramine and colestimide are used for the treatment of hypercholesterolemia and dyslipidemia. These sequestrants form complexes with bile acids in the intestine leading to increased fecal bile acid and fat excretion. Thereby, they reduce FXR activation, increase bile acid *de novo* synthesis and thus decrease cholesterol levels [69, 86].

In summary, the gut microbiota composition and function are important for the development of metabolic diseases. However, it is necessary to identify specific bacterial taxa involved in these diseases. So far, only a few bacterial strains exhibiting pro-obesity effects (e.g. *Clostridium ramosum* DSM1402 and *Enterobacter cloacae* B29) or anti-obesity effects like *Akkermansia muciniphila* MucT (ATTC BAA-835) have been identified [87–90]. **As bile acid metabolism is affected by the gut microbiota and influences the host energy homeostasis, bacteria which interfere with bile acid metabolism are interesting targets in the context of metabolic disease development. The next section will focus on one specific family of gut bacteria which is able to transform bile acids: The *Coriobacteriaceae*.**

1.2 *Coriobacteriaceae*

The family *Coriobacteriaceae* belongs to the phylum Actinobacteria and currently includes 15 genera: *Adlercreutzia, Asaccharobacter, Atopobium, Collinsella, Coriobacterium* (type genus), *Cryptobacterium, Denitrobacterium, Eggerthella, Enterorhabdus, Gordonibacter, Olsenella, Paraeggerthella, Parvibacter, Senegalimassilia* and *Slackia* (**Figure 1**) [91–104].

Most *Coriobacteriaceae* grow as small rods or coccobacilli, are gram-positive, non-motile, non-spore-forming, non-hemolytic, mesophilic, usually neutrophilic and acidotolerant. Most are strictly anaerobic but some are reported to be aerotolerant (*Eggerthella lenta, Enterorhabdus* spp.), microaerophilic (*Olsenella* spp.) or facultative anaerobes (*Atopobium vaginae*) [92, 93, 95, 105, 106]. When compared with Firmicutes and Bacteroides, Actinobacteria represent a minor fraction of the

sequence-based gut bacterial diversity (<2 to 5 % of total 16S ribosomal ribonucleic acid (rRNA) gene sequences). Nonetheless, some species such as *Collinsella aerofaciens* and *Atopobium spp.* are prevalent and dominant residents of the human intestine [1]. Moreover, *Atopobium* and *Eggerthella* spp. were shown to be correlated with several clinical pathologies including abscesses and bacteremia [107].
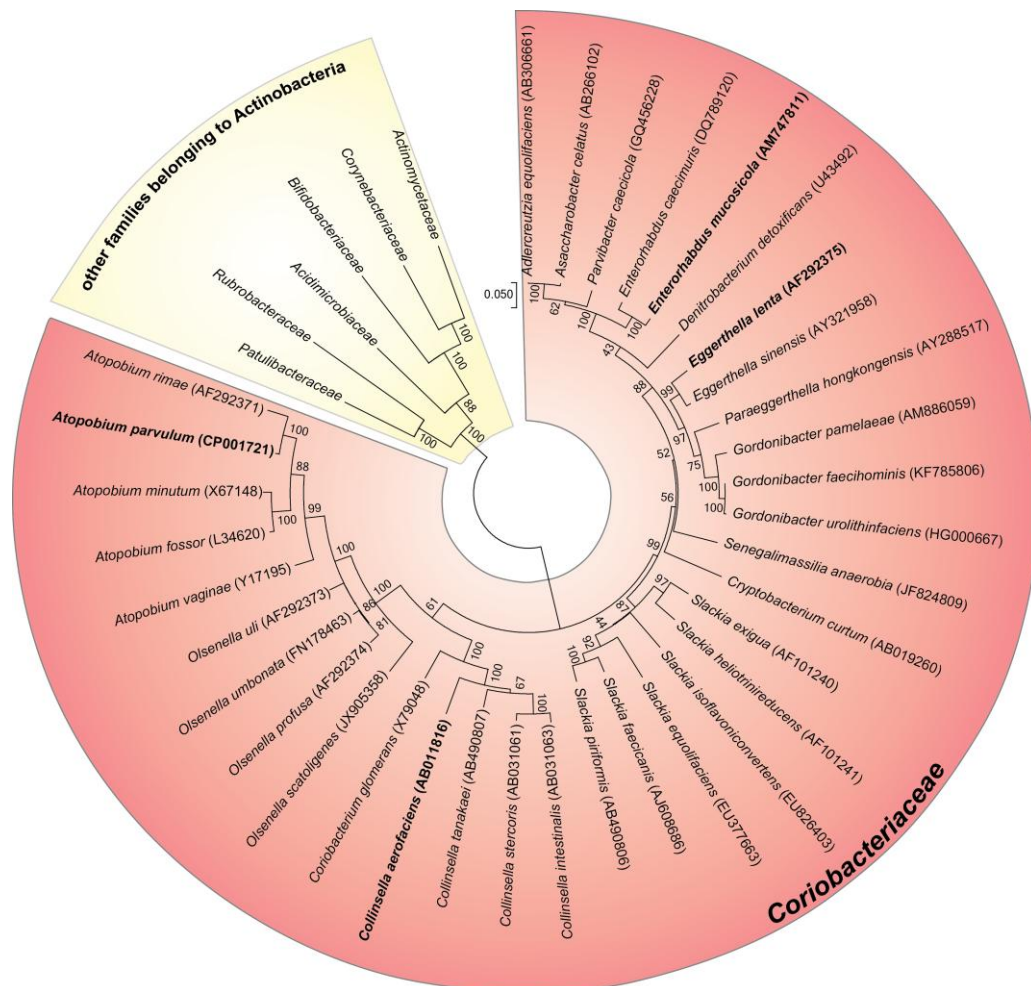
Figure 1: Phylogenetic tree of the family *Coriobacteriaceae* based on 16S rRNA gene sequences.
The tree was created using the Maximum Likelihood method based on the General Time Reversible model. Sequences were obtained from the All-Species Living Tree (https://www.arb-silva.de/projects/living-tree). The tree is drawn to scale, with branch lengths measured in the number of substitutions per site. The analysis involved 40 nucleotide sequences. All positions with less than 70% site coverage were eliminated. That is, fewer than 30% alignment gaps, missing data, and ambiguous bases were allowed at any position. The percentage of trees in which the associated taxa clustered together is shown next to the branches. There were a total of 1426 positions in the final dataset. Evolutionary analyses were conducted in MEGA7 [108–113]. Species, selected for *in vivo* experiments, are shown in bold letters.
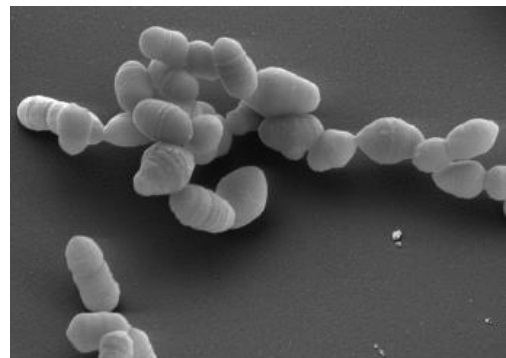
Some species like *Egg. lenta*, *C. aerofaciens* and *E. mucosicola* express bile acid- and steroid-metabolizing enzymes, which will be further explained in section 1.3 [114, 115]. Furthermore, the occurrence of *Coriobacteriaceae* was connected to host lipid and cholesterol metabolism [116, 117], and higher fecal cholesterol concentrations have been associated with decreased relative

abundances of *Coriobacteriaceae* [118]. In another study, their occurrence in the mouse gut correlated with decreased hepatic glycogen and glucose levels, enhanced triglyceride synthesis and the activity of Cyp3a11, a hepatic detoxification enzyme [117]. Additionally, Thorasin *et al.* (2015) could show that some *Collinsella* and *Eggerthella* species possess active lipases *in vitro*. However, until now it is not known whether this lipolytic activity also takes place *in vivo* and whether it modulates host metabolism [119].

All these studies indicate a possible function of *Coriobacteriaceae* on host lipid, cholesterol and bile acid metabolism. The four cultured species of this family that were selected for *in vivo* studies are presented in greater detail in the following section.

Atopobium parvulum (*A. parvulum*)

A. parvulum, formerly *Streptococcus parvulus*, was first described in 1937 by Weinberg *et al*. Its whole genome was sequenced in 2009 and it is reported to have one 16S rRNA operon [97, 120]. It is frequently isolated from human oral cavity and known to play a role in oral infections. Additionally, its abundance in human feces increases with aging [121–123]. *A. parvulum* ferments

Figure 2: Scanning electron micrograph of *A. parvulum* [97]

glucose mainly to lactose, acetic and formic acid [107, 121, 124]. Interestingly, the genus *Atopobium* was shown to be overrepresented in cirrhotic patients [125, 126].

Furthermore, *A. parvulum* may impact host metabolism via apelin [127]. Apelin is produced and secreted by the adipose tissue. Its expression is upregulated by insulin and it modulates glucose homeostasis. The plasma concentration of Apelin was found to be increased in obese patients and mice compared to lean controls [127, 128]. In contrast to *A. parvulum*, the occurrence of *Eggerthella et rel.* was negatively correlated to apelin expression [127]. Moreover, *Atopobium* spp. were higher abundant in mice having NASH than in NAFLD and healthy controls and their abundance was positively correlated with hepatic triglyceride levels, total plasma lipids and bile acids [126].

### *Collinsella aerofaciens* (*C. aerofaciens*)

C. aerofaciens, formerly *Eubacterium aerofaciens*, was originally isolated from human feces [106, 129] and belongs to the human core microbiome [1, 130–133]. It has also been found in feces of newborns [123]. The fermentation of different sugar sources by *C. aerofaciens* leads to the production of molecular hydrogen, ethanol, formate and lactate [100, 107].

Interestingly, the occurrence of the genus *Collinsella* was shown to correlate with increased intestinal cholesterol absorption and levels of plasma non-high density lipoprotein (HDL) in hamsters [118, 134]. Furthermore, their abundance was higher in patients with symptomatic atherosclerosis, which is characterized by lipid and cholesterol accumulation and the recruitment of macrophages to the arterial wall [41], and patients with T2D compared to healthy subjects [135]. However, the authors of the latter study did not specify whether they adjusted for confounders like the use of antidiabetic drugs. Moreover, the abundance of *C. aerofaciens* was positively correlated with uptake of dietary protein, potassium, zinc, iron and vitamin B2 in Mongolian adults [136].

Eggerthella lenta (*Egg. lenta*)

Egg. lenta, formerly *Eubacterium lentum*, was also originally isolated from human feces [106] and is part of the human core microbiome [91, 131]. The whole genome was sequenced in 2009 and contains three 16S rRNA operons [120, 137]. The type strain is bile-resistant, produces ammonia from arginine, can reduce nitrate and does not produce acids from glucose, [91, 107, 137].
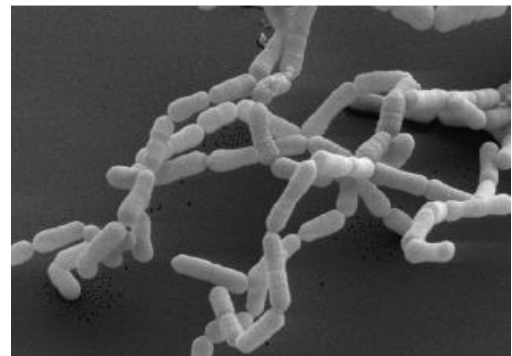
Figure 3: Scanning electron micrograph of *Egg. lenta* [137]

The metabolism of dietary catechins, which have antioxidative and anti-inflammatory capacities, by *Egg. lenta* affects their bioavailability [138, 139]. Additionally, this species can dehydroxylate dietary lignans to the biologically active enterolignans, enterodiol and enterolactone [140]. Qin *et al*. (2012) showed that *Eggerthella* spp. were higher abundant in T2D patients compared to healthy controls. However, they did not include confounders like antidiabetic medication in their analysis [27]. Forslund *et al*. (2015) controlled for metformin treatment and did not observe a correlation between the occurrence of *Eggerthella* spp. and T2D [28]. Further, *Egg. lenta* is involved in mixed and invasive infections as well as bacteremia in immunocompromised hosts [137, 141–143].

Enterorhabdus mucosicola (*E. mucosicola*)

E. mucosicola was first isolated in 2009 from ileal mucosa of an inflamed TNF$^{\Delta ARE/wt}$ mouse – which is a murine model of ileal inflammation - and can convert the isoflavones daidzein and genistein to the metabolic active compounds equol and 5-hydroxy-equol. Additionally, it is bile-sensitive [92, 144]. The relative abundance of *Enterorhabdus* spp. was found to be reduced in diabetic, leptin-resistant *db/db* mice [127]. Furthermore, prediabetic patients had a higher relative abundance of *Enterorhabdus* spp. compared to healthy controls, although the general abundance was quite low [145].

As described above, some members of the family *Coriobacteriaceae* exhibit enzymes involved in bile acid transformation. Therefore, bile acid metabolism in general as well as enzymes, involved in bile acid transformation, expressed by *Coriobacteriaceae* are described in the next section.

1.3 Bile acid metabolism

The liver plays an important role in the digestion of dietary compounds due to the production of bile. Bile is composed of water, conjugated bile acids, mucin, cholesterol, phospholipids, and anorganic salts and has a pH value of 7.1. In the gall bladder, mixed micelles are formed by these components [146, 147]. In humans, the majority of bile acids is conjugated to glycine whereas there are mainly taurine-conjugates in mice [148]. Upon stimulation by cholecystokinin (CCK), bile is secreted into the duodenum [86, 149]. The bile forms micelles with dietary lipids and lipid soluble vitamins. This process is necessary for cleavage and absorption of dietary fat [86, 149–152].

Bile acids are water-soluble and amphipathic steroids. Primary bile acids, cholic acid (CA) and CDCA, which are converted to α- and β-muricholic acid (MCA) in rodents, are synthesized in liver hepatocytes from cholesterol via two different pathways: classical and acidic [86, 150, 151, 153]. In the classical pathway cholesterol is directly converted to 7-hydroxycholesterol, whereas in the acidic pathway it is transformed via two intermediates. In both pathways, the rate limiting enzyme is cholesterol 7α-hydroxylase (Cyp7a1) [86, 149, 150]. Bacterial modifications, including deconjugation, dehydroxylation, and dehydrogenation of primary bile acids, lead to the formation of 15 − 20 so called secondary bile acids [150]. As unconjugated bile acids are strongly cytotoxic, they are conjugated to taurine or glycine in the liver [86].

Some intestinal bacteria, including *Coriobacteriaceae* and members of the genera *Bacteroides*, *Clostridium*, *Lactobacillus*, and *Bifidobacterium* are able to transform bile acids by various enzymes. Before transformation can take place, the bile acids have to be deconjugated which is mediated by microbial bile salt hydrolase (BSH) (**Figure 4**) [115, 154–156]. Hydroxysteroid dehydrogenases (HSDHs) can then epimerize various hydroxyl groups of bile acids via an oxo intermediate. This epimerization can be carried out by a single bacterial species (intraspecies) or in cooperation of different species (interspecies) [157]. In bacteria, several bile acid inducible (bai) genes involved in bile acid dehydroxylation were found [154]. **Table 1** shows presence of BSH and HSDH genes in *Coriobacteriaceae*.
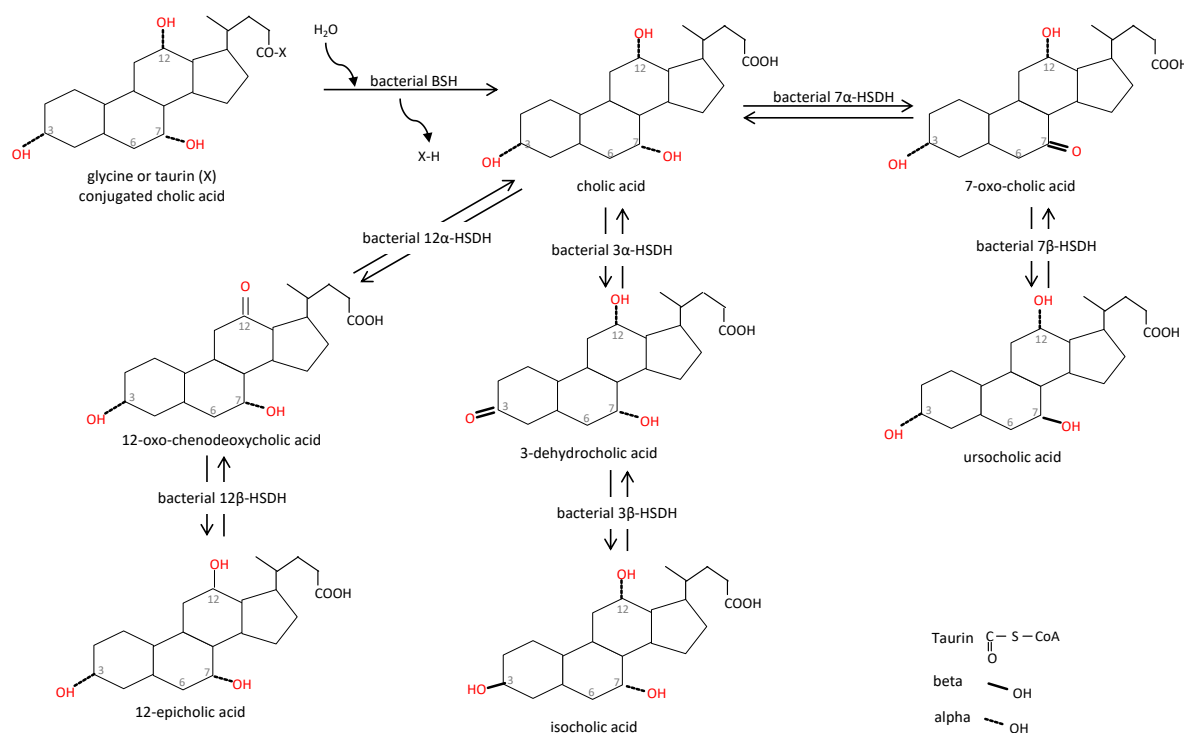
Figure 4: BSH and HSDH activity of *Coriobacteriaceae*
[154, 156, 158, 159].

Table 1: Bile acid-converting enzymes in *C. aerofaciens*, *Egg. lenta* and *E. mucosicola*

	C. aerofaciens	*Egg. lenta*	*E. mucosicola*
Bile salt hydrolase EC 3.5.1.24 = choloylglycine hydrolase	x[2,5]	x[5]	x[2,5]
12α-HSDH (EC 1.1.1.176)	x[8]	x[7]	x[8]
3 α-HSDH (EC 1.1.1.50)	x[8]	x[6,7]	x[8]
3 β-HSDH (EC 1.1.1.51)		x[1]	
7 β-HSDH (EC 1.1.1.201)	x[5]		
21-HSDH (EC 1.1.1.150)		x[6,3]	
16 α-HSDH		x[4]	

1 = http://www.brenda-enzymes.org/; 2 = https://www.patricbrc.org/portal/portal/patric/Home; 3, [160]; 4, [161, 162]; 5, [158]; 6, [114]; 7, [157]; 8, [115]

Most of the bile acids in the intestine (95 %) are actively or passively reabsorbed in the ileum, transported back to the liver via the portal vein where they are bound to albumin. Afterwards, they are again available for secretion. This process is called enterohepatic circulation and is important for cholesterol and bile acids homeostasis [86, 148, 149] (**Figure 5**). Due to this re-circulation and food intake-dependent release of bile acids, their serum concentration varies throughout the day. This implies that bile acids might also inform the peripheral tissue that nutrients and energy will become available [86]. Bile acids which escape re-absorption are excreted in feces, which is the only way for mammals to eliminate cholesterol and its derivatives [149].

In the terminal ileum, mainly conjugated but also unconjugated bile acids are taken up by apical sodium bile acid transporter (ASBT, *Slc10a2*). This transporter has a higher affinity for dihydroxy bile acids like CDCA and DCA [148]. The transporters are under a tight control to ensure bile acid

homeostasis which is mainly regulated by FXR (described below) [148]. In mice and human, ASBT expression is inhibited by bile acids via an FXR-mediated and small heterodimer partner (SHP)-dependent pathway [163]. Once in enterocytes, bile acids are bound to the intestinal bile acid-binding protein (IBABP) and are transported to the basolateral side, where they can be secreted into the circulation via several transporters like the heterodimeric organic solute transporter (OST) α and β. In human and mice, OST expression is also regulated by FXR [148].
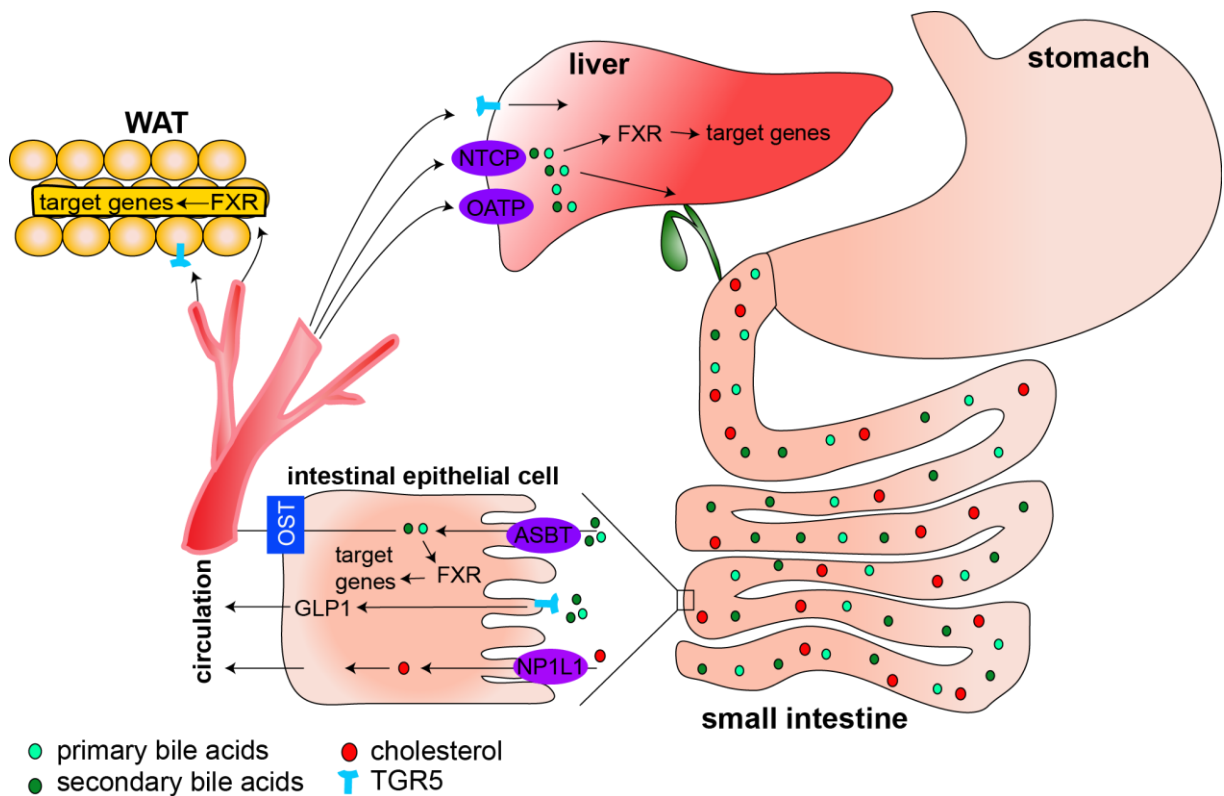
Figure 5: Simplified representation of the uptake, distribution and target receptors of bile acids.
ASBT, apical sodium bile acid transporter; FXR, farnesoid X receptor; GLP-1, glucagon like peptide 1; NP1L1, Niemann Pick 1 like 1 receptor; NTCP, sodium taurocholate Co-Transporting Polypeptide; OATP, organic anion transport peptide; TGR5, G-protein-coupled receptor 1.

Hepatocytes take up conjugated and unconjugated bile acids from portal and sinusoidal blood mainly via the sodium taurocholate Co-Transporting Polypeptide (NTCP) and a subset of the family of organic anion transport peptide (OATP) [148]. The transport of bile acids across the canalicular membrane is critical and rate-liming as it regulates the bile flow. The bile acid concentration in the canalicular lumen is 100-1000 fold higher than in the cytoplasm. This concentration differences imply an ATP-dependent secretion of the bile acids which is mainly mediated by the bile salt export pump (BSEP) [148].

Beside their importance for dietary lipid absorption, bile acids regulate their own as well as cholesterol and lipid homeostasis and act as signaling molecules in many metabolic processes. The best investigated targets of bile acids are FXR and the G-protein-coupled receptor TGR5 [86].

Furthermore, bile acids activate other receptors like muscarinic receptors, pregnane X receptor (PXR), the vitamin D receptor (VDR), Formyl-peptide receptors (FPRs) [164–167].

FXR is known as the nuclear receptor for bile acids and was identified in 1995 by the research groups of Forman and Seol [168, 169]. FXR belongs to the nuclear receptor superfamily class II. Ligands of this receptor subfamily are endogenous lipophilic compounds like cholesterol, lipids, bile acids and metabolites thereof. Several receptors regulating host metabolism like retinoic acid receptor (RARα), PXR, peroxisome proliferator-activated receptor (PPAR), constitutive androstane receptor (CAR), liver X receptor (LXR) and retinoid X receptor (RXR) also belong to this receptor subclass. Their activation leads to the formation of a heterodimeric complex with RXR before binding to response elements in promoter regions of the target genes [148]. Bile acids, conjugated as well as unconjugated, are the natural ligands for FXR with the conjugated and unconjugated forms of CDCA being the most potent ones. Furthermore, glucose and insulin are regulators of FXR. FXR occurs, due to different promoter usage and alternative splicing, in 4 different isoformes (1 to 4), which differ in tissue distribution [86, 170]. FXR-α is mainly expressed in liver, gut, kidney, adrenal cortex and adipose tissue [86, 171]. FXR is the key regulator of bile acid homeostasis but exhibits also a tremendous number of direct and indirect target genes involved in lipid, glucose, and cholesterol homeostasis (**Table 2**).

Table 2: List of major direct and indirect targets of FXR

Target	Mode of action	function
ApoA-I	inhibition	HDL cholesterol reduction [172]
APOB	Inhibition	Assembly and secretion of VLDL [173]
APOC2	Induction	Activation of LPL [173]
APOC3	Inhibition	Inhibition of LPL [173]
ASBT	Inhibition via SHP	Ileal bile acid uptake [163]
BAAT and BACS	Activation	Bile acid conjugation [170]
BSEP	Activation	Bile export in gallbladder [174]
ChREBP	inhibition	Hepatic glycolysis [175]
CYP7A1	Inhibition via SHP	Bile acid *de novo* synthesis [176]
FGF19/15	Activation	Inhibition of Cyp7a1 and stimulation of bile flow [177]
HNF4	inhibition	Bile acid homeostasis [174, 178]
PPARα in humans	activation	Lipid, glucose and energy homeostasis [170, 179, 180]
PPARγ	activation	Adipocyte differentiation, lipid storage and glucose metabolism [181–184]
I-BABP	Increase	Ileal bile acid binding [185]
Insulin signaling	inhibition	White adipose tissue [70]
LPK	Inhibition	Glycolysis [170]
LXR	Inhibition via SHP	Bile acid de novo synthesis [186], cholesterol and lipid homeostasis [187, 188]
NTCP	inhibition	Hepatic uptake of bile acids [189]
OST α and β	Activation	Bile acid transport [148]
SHP	activation	Bile acid homeostasis [174]
SREBP1c	Inhibition via SHP	main regulator of fatty acid and triglyceride biosynthesis [190]

Apo, apolipoprotein; ASBT, apical sodium bile acid transporter; BAAT, bile acid-CoA:amino acid n-acetyltransferase; BACS, bile acid-CoA synthetase; BSEP, bile salt export pump; ChREBP, Carbohydrate-responsive element-binding protein; CYP7A1, cholesterol 7α-hydroxylase; FGF, fibroblast growth factor; HNF, hepatocyte nuclear factor; PPAR, peroxisome proliferator-activated receptor; I-BABP, ileal bile-acid-binding protein; LPL, lipoprotein lipase; LXR, liver X receptor; LPK, L-pyruvate kinase; NTCP, sodium taurocholate Co-Transporting Polypeptide; OST, organic solute transporter; SHP, small heterodimer partner; SREBP, sterol regulatory binding protein.

TGR5 is a member of the rhodopsin-like subfamily of GPCRs (Class A) and is conserved among mammals. The expression of TGR5 is universal but levels vary between tissues: high in gall bladder and low in brown adipose tissue (BAT), liver, intestine, monocytes/ macrophages and some areas of the central nervous system [86, 191–193]. Hepatic TGR5 is only expressed in sinusoidal endothelial cells, which are exposed to high bile acid concentrations from enterohepatic circulation [192]. Many bile acids can activate TGR5, with lithocholic acid (LCA) being most potent. TGR5 modulates glucose and energy homeostasis as well as inflammatory responses (**Table 3**).

Table 3: TGR5 targets

Target	Mode of action	function
Type 2 iodothyronine deiodinase (D2)	Activation	Energy homeostasis [194]
Glucagon-like peptide 1 (GLP1) in intestinal L-cells	Activation	Glucose homeostasis [192, 195, 196]
Pro-inflammatory cytokines in macrophages	Inhibition	Immunomodulatory properties [197]
Peroxisome proliferator-activated receptor gamma coactivator 1-alpha (PGC1α)	Activation	Energy expenditure [86]

All the aforementioned data clearly prove the important role of bile acids are important for lipid and cholesterol homeostasis. Interestingly, the metabolic syndrome is commonly defined by the presence of three of the following diseases: abdominal obesity, hyperlipidemia, hypercholesterolemia, hypertension and hyperglycemia [198]. Therefore, the next section deals with lipid metabolism and the effects of bile acids on it.

1.3.1 Bile acids modulate lipid metabolism

As described above, bile acids are needed for the emulsification of dietary lipids. Emulsified lipids can then be broken down to fatty acids and monoacylgylcerol (MAG) by gastric and pancreatic lipases (**Figure 6**). These cleavage products can be passively or actively absorbed by intestinal epithelia cells via fatty acid translocase (CD36/FAT) [199]. In the endoplasmic reticulum of intestinal epithelial cells, monoacylgylcerol acyltransferase (MGAT) and diacylglycerol acyltransferase (DGAT) re-synthesize triglycerides from the absorbed fatty acids and MAG. Triglycerides are then incorporated in chylomicrons in the Golgi apparatus and secreted due to their size into the lymph whereas short chain fatty acids are transported into systemic circulation [199, 200]. Interestingly, HFD feeding increases MGAT2 activity in small intestine which was associated with higher fat absorption [201]. In line with this, healthy subjects show a low hepatic MGAT activity whereas it is induced in diabetic and obese rodents [202, 203]. In the liver, triglycerides are packed in very-low-density lipoproteins (VLDL) which are secreted into circulation [199]. The secretion of chylomicrons and VLDL is for the supply of heart, skeletal muscle and adipose tissue with fatty acids which are for energy

expenditure and storage. The release of fatty acids from chylomicrons and VLDL is carried out by lipoprotein lipases (LPL) [204].

Bile acids further modulate lipid homeostasis via FXR. One target gene of FXR, sterol regulatory element binding protein 1c (SREBP1c) is a key factor in hepatic fatty acid and triglyceride synthesis. Interestingly, SREBP1c might also be activated by insulin [205, 206]. In *ob/ob* mice, hepatic SREBP1c protein levels and expression of its target genes were significantly higher compared to those of wild type mice which led to increased hepatic fatty acid synthesis and induced steatosis [207].
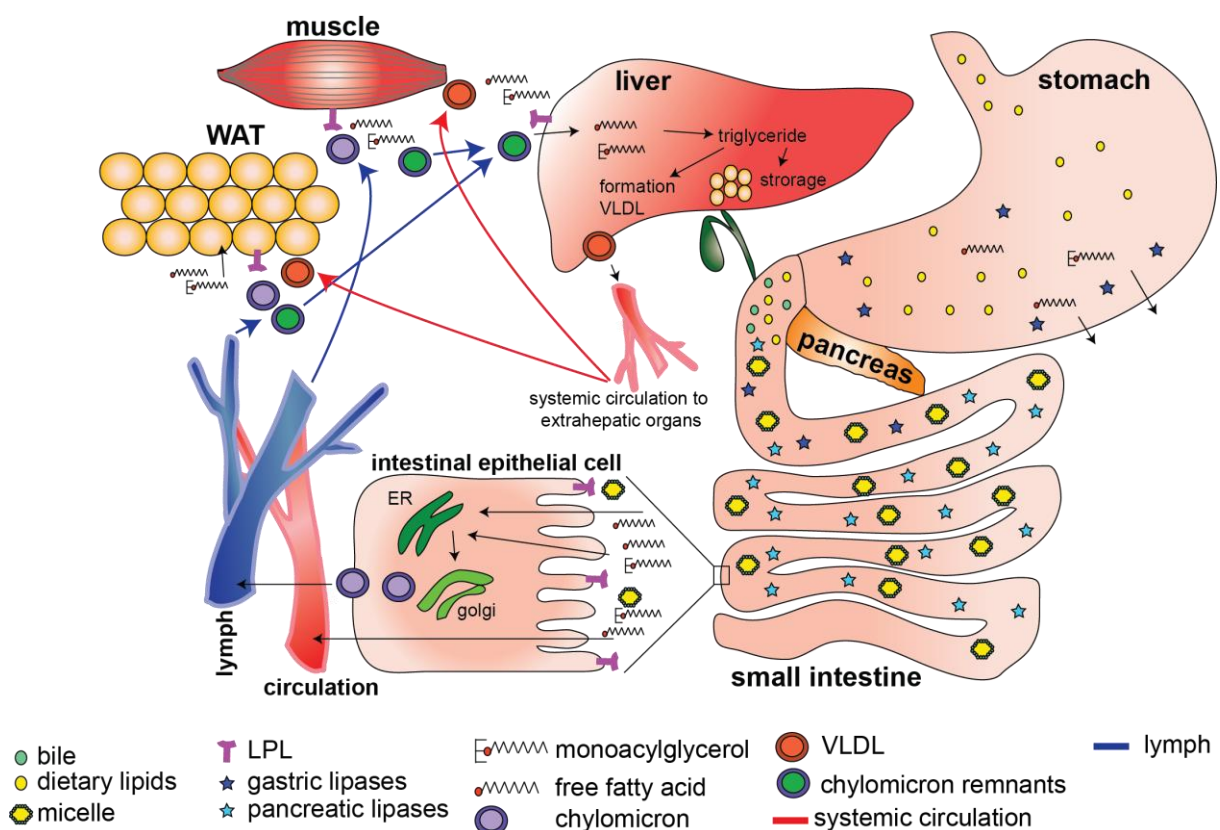
Figure 6: Schematic overview of dietary lipid absorption.
LPL, lipoprotein lipases; ER, endoplasmic reticulum; VLDL, very low density lipoprotein; WAT, white adipose tissue.

FXR additionally regulates LXR via SHP. LXR increases expression of genes involved in cholesterol and lipid metabolism like Cyp7a1, hydroxymethyl glutaryl (HMG)-CoA synthase/reductase, apolipoprotein E, SREBP1c, fatty acid synthase (FAS) and LPL. The activation of LXR target genes results in increased lipogenesis in liver and adipose tissue and the reduction of hepatic gluconeogenesis [208]. Interestingly, LXR is also regulated by insulin [208]. In murine models of atherosclerosis, activation of LXR strongly reduced the formation of atherosclerotic plaques presumably by the reduction of plasma cholesterol concentration [209]. The LXR target gene stearoyl-CoA desaturase 1 (SCD1)

regulates the synthesis of monounsaturated fatty acids (MUFAs) like palmitoleic acid (C16:1n7) and oleic acid (C18:1n9). These two MUFAs are the most abundant ones in human plasma, membranes and adipose tissue [207, 210]. In liver, SCD1 expression was positively correlated with hepatic free fatty acids, cholesterol esters, phospholipids and total lipid concentrations and is important for triglyceride synthesis [211, 212]. Interestingly, in obese and hyperglycemic *ob/ob* mice, SCD activity in adipose tissue and liver was strongly increased compared to wild type mice [213, 214]. Furthermore, SCD gene expression was positively associated with triglyceride storage in adipocytes leading to an increase in cell volume [215]. Studies also showed that SCD expression was induced by dietary saturated fatty acids and inhibited by polyunsaturated fatty acids (PUFAs) [215, 216].

Therefore, changes in lipid and bile acid metabolism in patients with metabolic syndrome indicate that therapeutic modulation of bile acid homeostasis is a promising way to treat metabolic diseases.

2 Hypothesis and aim of the thesis

The human gut microbiota is a highly diverse and complex ecosystem that influences metabolic responses of the host. However, little is known about specific bacteria and associated molecular mechanisms underlying the modulation of host metabolism. Some species of the bacterial family *Coriobacteriaceae* are dominant members of the microbiota and can metabolize bile salts and steroids. In animal models, the occurrence of *Coriobacteriaceae* as assessed by sequencing was found to be positively correlated with hepatic concentrations of triglycerides, activity of Cyp3a11, and plasma cholesterol levels. In humans, their relative abundance has been associated with chronic metabolic diseases such as obesity and type-2 diabetes. Hence, we hypothesized that *Coriobacteriaceae*-derived functions play an important role in host metabolic responses, in particular lipid homeostasis.

Therefore, the primary aim of the present thesis was to assess the role of these bacteria in mouse metabolism, with particular focus on bile acid and lipid metabolism. For this purpose, GF mice were colonized with a consortium of four *Coriobacteriaceae* strains and were fed diets varying in their fat type and amount, with or without supplementation of primary bile acids. Major readouts included organ and tissue weights, metabolic parameters (e.g. leptin, insulin, glucose levels and tolerance test), bacterial colonization, bile acids/lipids composition and the expression of key enzymes involved in their metabolism.

3 Methods

3.1 Occurrence of *Coriobacteriaceae* in human fecal metagenomes

The genomes of *Collinsella* (*C.*) *aerofaciens* DSM 3979[T], *Atopobium* (*A.*) *parvulum* DSM 20469[T], *Eggerthella* (*Egg.*) *lenta* DSM 2243[T] and *Enterorhabdus* (*E.*) *mucosicola* DSM 19490[T] were mapped against an integrated gene catalogue (IGC) generated from human fecal samples [217] (**Figure 7**). This work was performed by Dr. Stanislas Mondot at INRA, France. Briefly, the reference dataset consisted of fecal metagenomes from normal weight, underweight, overweight, obese and morbid obese individuals (**Table 4**) of three different nationalities (185 Chinese, 177 Danish, and 59 Spanish). Coding sequences of the four strains were extracted and blasted [218] against the IGC database. Best blast hit sequences with both a similarity and query length coverage ≥ 90 % were retained and used as a proxy to collect information on the relative abundance of *Coriobacteriaceae* in each metagenome. The relative abundance of each gene was $\log_{10}$ transformed and averaged for each group of metagenomes. Finally, a z-score was applied on the averaged gene abundance. Significance (p-value < 0.05) was analyzed using Turkey HSD test with correction for false discovery rate. Results were illustrated as a heat map using the R programming environment.

Table 4: classification of the metagenome data sets

Category	Abbreviation	Number of metagenomes	Body mass index (BMI)
Under weight	UW	19	<18.5
Normal weight	N	194	18.5 ≥ x ≤ 25
Over weight	OW	102	25 ≥ x ≤ 30
Obese	O	76	30 ≥ x ≤ 35
Morbid obese	MO	30	≥ 35

Mapping of *Coriobacteriaceae* to IGC database
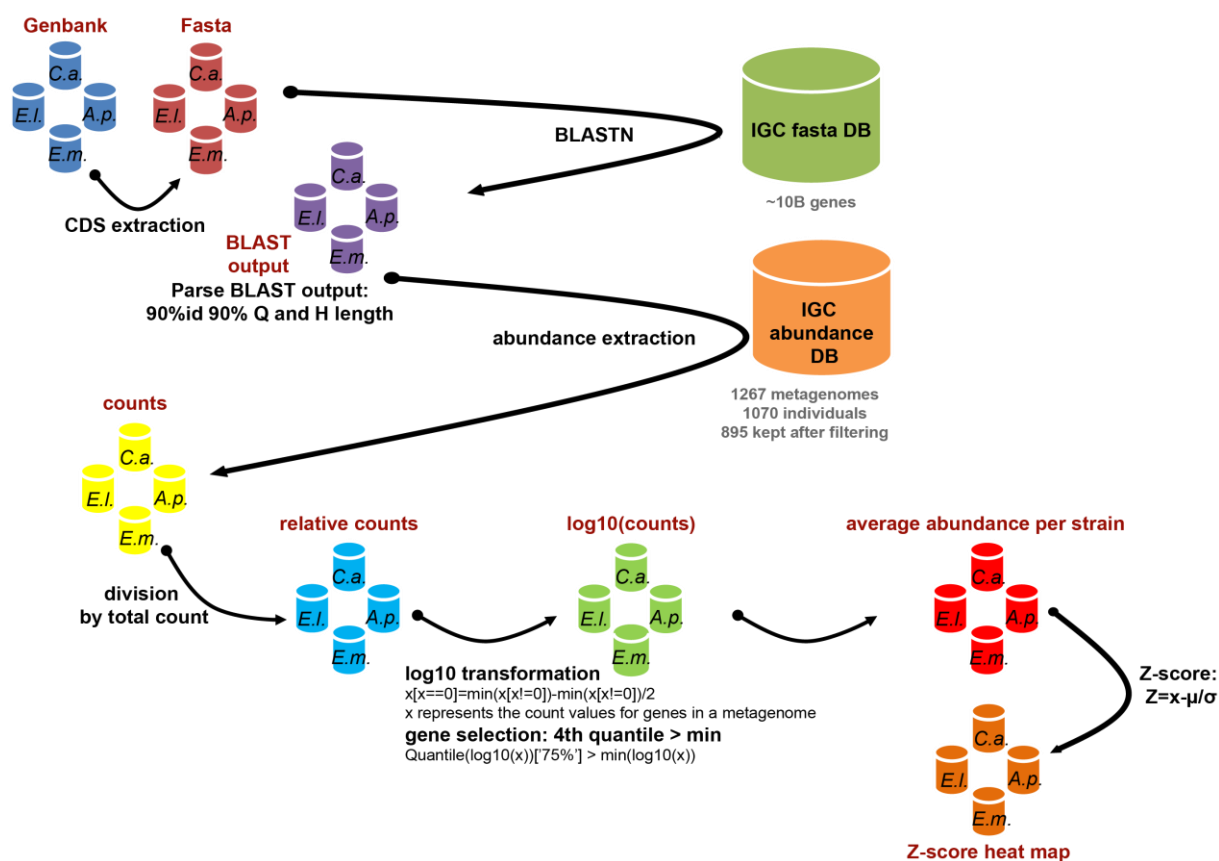
Figure 7: Mapping of *Coriobacteriaceae* genomes to the integrated gene catalogue (IGC) database.
This scheme illustrates the steps of metagenomic queries used to evaluate the occurrence of *Coriobacteriaceae* in human metabolic diseases. This work is a courtesy of Dr. Stanislas Mondot at INRA. BLASTN, basic local alignment search tool for nucleotide sequences; CDS, coding sequences; DB, data base; Fasta, fasta format; Q and H, Query and Hit of blast analysis.

3.2   *St*rains and cultivation

Four strains of the family *Coriobacteriaceae* were used for functional characterization *in vitro* and *in vivo* experiments: *C. aerofaciens* DSM 3979[T] (taxonomic ID: 411903), *A. parvulum* DSM 20469[T] (ID 521095), *Egg. lenta* DSM 2243[T] (ID 479437) and *E. mucosicola* DSM 19490[T] (ID 1121866). All strains were cultivated on Wilkins-Chalgren-Agar or -broth (WCA, Fischer Scientific) supplemented with 0.05 % (w/v) L-Cystein (Carl Roth), 0.02 % dithiothreitol (DTT; Sigma Aldrich) as reducing agents and 0.0025 mg/ ml Phenosafranin (Sigma Aldrich) as redox potential indicator. The medium for *A. parvulum* also contained 0.02 % Tween80 (Fluka) to stimulate growth [107]. Strains were grown at 37 °C under strictly anaerobic conditions either in an anaerobic chamber (Whitley Hypoxystation H85, Meintrup DWS Laborgeräte GmbH) containing a H_2/ N_2 gas mixture (10:90) or in Hungate tubes (VWR International) containing 9 ml WCA medium gassed with N_2. Cryo-stocks were prepared from overnight cultures by mixing bacterial suspensions 1:1 with filter-sterilized glycerol in culture medium (40 % vol/ vol) under sterile but aerobic conditions before freezing at −80 °C in the form of

200 µl aliquots. For colonization of mice, the strains were cultivated overnight (approx. 16 h) in Hungate tubes previously inoculated with 200 µl pre-culture (consisting itself of one cryo-aliquot in 9 ml medium in Hungate incubated for 24 h). Two dilutions of the bacterial cultures were counted using a Thoma Chamber and an average number of cells per ml was calculated for each strain. The strains were then mixed at an equal cell density of 5×10^9/ ml in an empty sterile, Hungate tube gassed with N_2.

3.3 Functional characterization of *Coriobacteriaceae* strains *in vitro*

3.3.1 Bile salt hydrolase (BSH) activity assay

BSH (choloylglycine hydrolase, EC 3.5.1.24) catalyzes the cleavage of conjugated bile acids to release free bile acids and the amino acids taurine or glycine. This process is needed for further transformation of bile acids. First, protein databases, including GenBank at the National Center for Biotechnology Information (NCBI) and BRENDA, were checked for the availability of BSH protein sequences in the four strains.

Next, BSH activity was tested *in vitro* as described elsewhere [219] (**Figure 8**). Briefly, after autoclaving and cooling down to 50 °C in a water bath, WCA agar was supplemented with 0.5 % (w/ v) tauro-conjugated deoxycholic acid (TDCA; Sigma Aldrich) prepared as filter-sterilized stock solution of 12.5 %. After two days of equilibrium of the agar plates in the anaerobic chamber, all strains were grown for 72 hours at 37 °C. *Clostridium* sp. FSA-380-WT-2B was used as positive control. Active BSH cleaves the taurine moiety of TDCA and the resulting free bile acid molecules either precipitate around colonies, thereby forming a halo, or induce whitening of colonies. WCA agar plates without TDCA were used as controls.
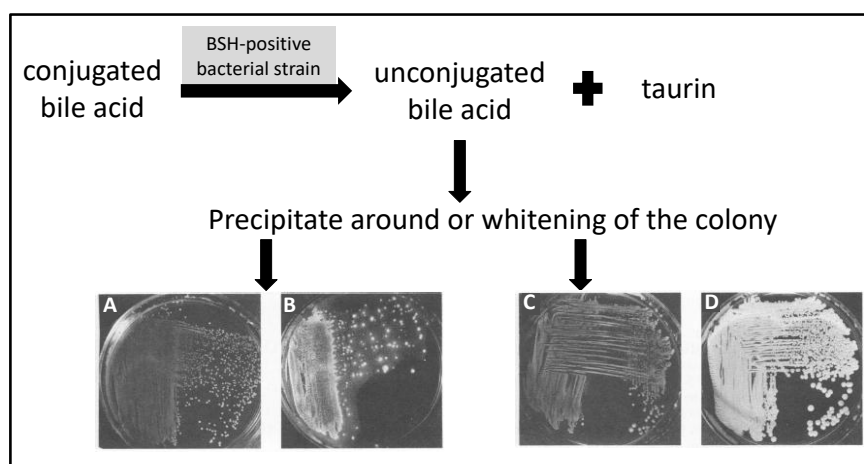

Figure 8: Principle of the *in vitro* BSH activity assay.
The conjugated bile acid TDCA is cleaved into DCA and taurine in the presence of BSH. DCA precipitates and leads to the formation of halos around (B) or to whitening of (D) colonies. (A and C) Agar without TDCA used as growing negative controls. Figure was modified from the literature [219, 220].

3.3.2 Lipase activity assay

Lipase (triacylglycerol acylhydrolases, EC 3.1.1.3) activity of the *Coriobacteriaceae* strains was tested using Rhodamin B-olive oil agar (modified from Kouker and Jaeger (1987) [221]) (**Figure 9**). Briefly, autoclaved WCA agar was cooled down to 50 °C and supplemented with 2.5 % (v/ v) filter-sterilized olive oil (A&P, Tengelmann) and Rhodamin B (0.01 g/ l, Sigma Aldrich). The medium was poured into Petri dishes after vigorous mixing. After two days of equilibrium in the anaerobic chamber, the plates were inoculated with *Coriobacteriaceae* strains and incubated for 48 h. *Escherichia (E.) coli* and *Acinetobacter johnsonii* MG844 (a gift from Dr. Mareike Wenning, Chair for Microbial Ecology, TU Munich) were used as negative and positive control, respectively. Lipase activity leads to the release of free fatty acids that form a complex with Rhodamine B. This complex can be observed visually by exposing the plates with UV light (360 nm), resulting in fluorescence.
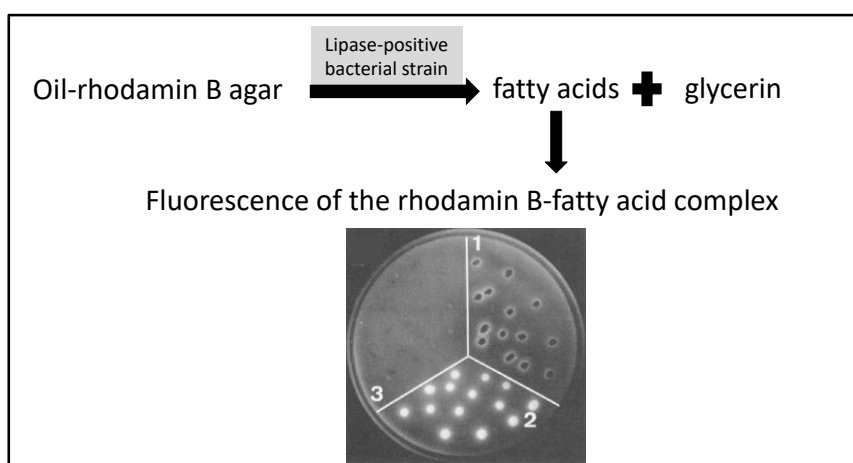
Figure 9: Principle of the lipase activity assay.
Strains were grown anaerobically on olive oil-rhodamin B WCA. Lipase-positive strains cleave triglycerides from oil into fatty acids and glycerin. The free fatty acids form a complex together with rhodamin B, resulting in visible fluorescence upon UV light. The picture shows *Pseudomonas aeruginosa* PAC1R (1), *Staphylococcus aureus* (2) and *E. coli* (3). 1 and 2 formed fluorescent halos around the colonies, indicating lipase activity, whereas 3 did not. Modified from Kouker and Jaeger (1987) [221].

3.4 Strain-specific 16S ribosomal RNA (rRNA)-based real time quantitative polymerase chain reaction (qPCR) assay

After animal experiments, it was necessary to specifically quantify the four *Coriobacteriaceae* strains used for colonization. Therefore, a qPCR assay based on 16S rRNA gene copy numbers was developed. Specificity and limit of detection were determined and standard curves were prepared for each strain (see details below). Additionally, primer sequences to detect all bacteria were taken from Haarmann and Knol (2006) [222].

Briefly, genomic DNA was isolated from pure cultures as follows: 600 µl overnight culture, 400 µl Phenol:Chloroform:IsoAmyl alcohol (25:24:1; Sigma Aldrich), and 500 mg autoclaved zirconia/silica beads (0.1 mm; BioSpec Products) were mixed. Bacterial cells were disrupted by mechanical lysis using a FastPrep®-24 (3 times, 40 sec; 6.5 m/ s) (MP Biomedicals) fitted with a 24 x 2 ml cooling adaptor, followed by heat treatment (95 °C, 5 min) and centrifugation (15000 x g, 5 min, 4 °C). Supernatants were treated with RNase (0.1 µg/ µl; VWR International) for 30 min at 37 °C. DNA was purified using the gDNA clean-up kit following the manufacturer's instructions (Macherey-Nagel). Concentrations and purity were checked using NanoDrop® (Thermo Fisher Scientific) and samples were immediately used or stored at -20 °C. Purity of the strains was controlled by microscopic observation before DNA extraction and by sequencing the 16S rRNA gene using primer 27F (5'-AGAGTTTGATCCTGGCTCAG-3') and 1492R (5'-GGTTACCTTGTTACGACTT-3'), as described previously [223].

The Universal Probe Library (UPL) system from Roche was used for qPCR, where primer-probe combinations guarantee higher specificity than intercalate fluorescence systems. Primer and probes were designed using the Roche UPL assay design center (https://lifescience.roche.com/en_de/brands/universal-probe-library.html). The final primer pairs (Sigma Aldrich) and probes (Roche) used are listed in **Table 5**. A 2-step qPCR program was used for all assays (95 °C 5 min; 45 cycles of 95 °C for 10 sec and 60 °C for 20 sec; cooling at 4 °C). Specificity was validated *in vitro* using different genomic DNA and primer concentrations of each strain and mixtures thereof (**Suppl. Fig. S1**). A template DNA concentration of 2.5 ng/ µl and 200 nM of each primer (stock solution 20 µM) achieved the highest specificity and lowest background signal. Each qPCR approach was validated using equal mixture of all strains (each 2.5 ng/ µl) and increasing concentrations of the target strain. The ct-value only decreased with higher DNA concentrations of the target strain and was unaffected by raising concentrations of the non-target strains.

Table 5: Primers and probes used for 16S rRNA copy number based qPCR

Bacterial strain	Forward primer	Reverse primer	UPL-Probe (# and sequence)	Amplicon length [nt]
A. parvulum	gaagaacaccagtggcgaag	tgtttgctcccctagctttc	#73, gctgagga	74
C. aerofaciens	gtgttgccatcgggtgat	aaggggcatgatgacttgac	#70, ccgccgcc	92
Egg. lenta	ctaatccgagggctcaacc	gcattccaccgctacacc	#34, agaggcag	93
E. mucosicola	cgcctaagcggaacctcta	gcattccaccgctacacc	#91, gaggagag	109
All bacteria (EUB)	tcctacgggaggcagcagt	ggactaccagggtatctaatcctgtt	#66, cagcagcc	453

For each strain, a standard curve was generated. Therefore, 16S rRNA genes were amplified in triplicates by standard PCR using pure genomic DNA of each strain and the universal primers 27F and 1492R. For the EUB standard curve, fecal DNA of three SPF housed C57BL/6N mice was used as template for the standard PCR. PCR products were loaded on a 1.5 % agarose gel, specific bands

were excised, and amplicons were cleaned using the PCR clean-up system (Stratec Biomedical). DNA concentration was measured using the dsDNA high sensitivity kit for Qubit measurement (Invitrogen^{TM}), and the number of amplicons was calculated with the "DNA Copy Number and Dilution Calculator" web tool of Thermo Fisher Scientific. Standard curves were performed from 10^{10} to 10^1 gene copies spiked into fecal DNA of three germfree C57BL6/N mice, results in a total of 6 replicates per strain per dilution. These standard curves (**Table 6**) were used for calculation of 16S rRNA copy numbers in fecal samples and intestinal content, then expressed per 1 µg DNA. Fecal and caecal DNA of GF mice was used as negative control.

Table 6: Equation and Pearson coefficient for calculation of strain-specific 16S rRNA gene copy numbers

Species	Formula	Coefficient of determination (r²)
A. parvulum	y = -1.555ln(x) + 42.442	0.995
C. aerofaciens	y = -1.688ln(x) + 43.564	0.999
Egg. lenta	y = -1.528ln(x) + 42.145	0.985
E. mucosicola	y = -1.796ln(x) + 46.151	0.995
All bacteria (EUB)	y = -1.828ln(x) + 44.134	0.997

To help with the interpretation of results, copy numbers as obtained by the qPCR assays were determined from known cell numbers of each *Coriobacteriaceae* strain. For that purpose, liquid overnight cultures were prepared in triplicates, bacterial counts were calculated using a Thoma Chamber and DNA was isolated from 5×10^9 cells of each triplicate culture using the protocol described in 3.7. The qPCR assays and calculation of 16S rRNA copy numbers were performed as described above. Results are shown in **Table 7**.

Table 7: 16S rRNA copy numbers corresponding to 5×10^9 cells of each strain

	A. parvulum	*C. aerofaciens*	*Egg. lenta*	*E. mucosicola*
specific primer-probe combinations	9.5 ± 0.2	9.7 ± 0.1	9.3 ± 0.2	9.3 ± 0.5
EUB	8.7 ± 0.2	8.8 ± 0.1	8.7 ± 0.1	8.5 ± 0.2

Data are expressed as $\log_{10}$ 16S rRNA copies/ 1µg DNA (mean ± standard deviation; n = 6 replicates per strain)

3.5 Design of animal experiments

Male C57BL/6N mice were housed under SPF or GF conditions with 12 h light/dark cycles at 24 - 26 °C. To exclude litter and cage effects, the mice from different litters were mixed up and housed in at least three separate cages per experimental group. All mice were fed autoclaved standard chow diet (Ssniff Spezialdiäten GmbH) *ad libitum* and were sacrificed by CO_2. Sterility of germfree mice was checked by cultivation of feces on blood agar, lysogeny broth (LB) agar and WCA (Sigma Aldrich) as well as gram staining. A mold-trap was used to indicate the presence of mold. No contaminations were observed during any time of the experiments.

For identification of *Coriobacteriaceae*-specific effects on the host, germfree (GF) mice (n = 8-14) were associated with 1×10^9 cells per strain at week 5 of age (see section 3.2 for details on the preparation of strains) (**Figure 10**).
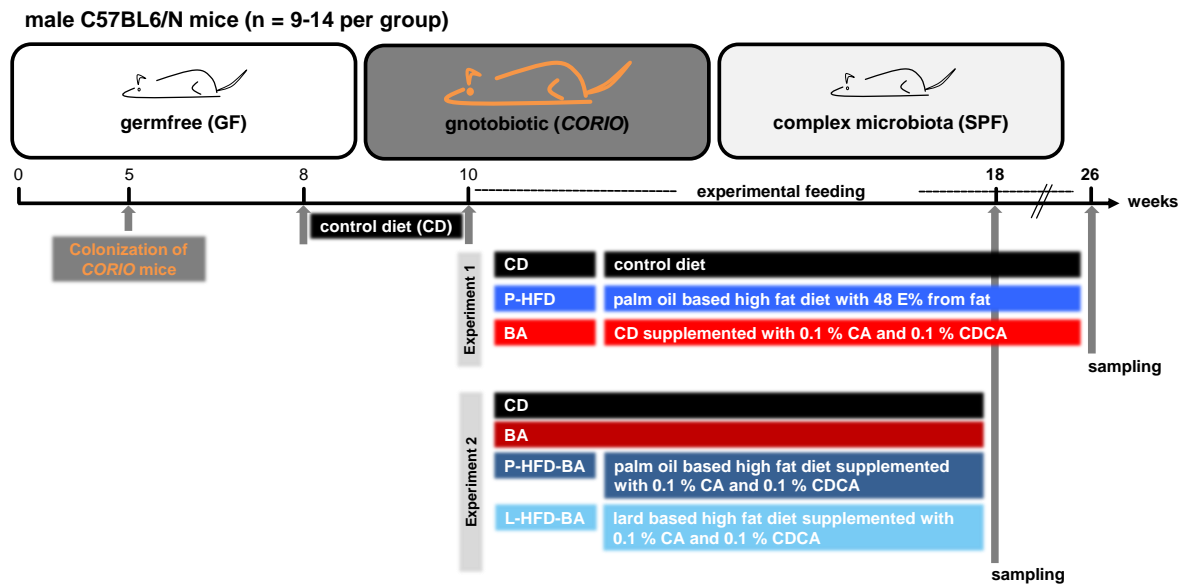
Figure 10: Design of animal experiments.
GF mice were associated with 10^9 cells of each bacterial strain at the age of 5 weeks (*CORIO* mice). At week 8 of age, diet was changed from chow to the experimental control diet (CD) to allow metabolic adaptation. After two weeks, mice were randomly divided into the different feeding groups. In experiment 1, mice were fed either CD, CD supplemented with CA and CDCA (each 0.1%) (BA), or palm oil-based high-fat diet (P-HFD). In experiment 2, mice were fed either CD, BA, palm oil- or lard-based HFD supplemented with 0.1% CA and 0.1% CDCA (P- or L-HFD-BA). The feeding period was 16 weeks in experiment 1 and 8 weeks in experiment 2.

One and two weeks after association, feces was collected from mice to assess the efficacy of colonization by cultivation (calculation of colony forming units) and 16S rRNA gene copy number assays by qPCR (see section 3.4). GF and SPF mice were used as controls. In all animal experiments, diet was changed from chow (Ssniff Spezialdiäten) to experimental control diet (CD) for two weeks prior to starting dietary challenges, to allow metabolic adaptation. Afterwards, mice were randomly divided into the different feeding groups: Experiment 1: CD, CD supplemented with CA and CDCA (each 0.1 %) (BA), or palm oil based high-fat diet (P-HFD); Experiment 2: CD, BA, palm oil- or lard-based HFD supplemented with CA and CDCA (each 0.1 %) (P- or L-HFD-BA). All experimental diets were purchased from Ssniff Spezialdiäten GmbH and their composition is illustrated in **Table 8** . In experiment 1, the feeding period was 16 weeks, while it was 8 weeks in experiment 2.

Table 8: Composition of the different diets used in animal experiments.
All diets were purchased from ssniff Spezialdiäten GmbH.

diet	CD	BA diet	P-HFD	P-HFD-BA	L-HFD-BA
product number	S5745-E902	S5745-E905	S5745-E912	S5745-E915	S5745-E935
energy [MJ/ kg]	15.3	15.3	19.7	19.7	19.7
fat [kJ%]	13.0	13.0	48.0	48.0	48.0
casein [%]	24.0	24.0	24.0	24.0	24.0
corn starch [%]	47.8	47.6	27.8	27.8	27.8
maltodextrin [%]	5.6	5.6	5.6	5.6	5.6
saccharose [%]	5.0	5.0	5.0	5.0	5.0
cellulose[%]	5.0	5.0	5.0	5.0	5.0
L-cystin [%]	0.2	0.2	0.2	0.2	0.2
vitamins [%]	1.2	1.2	1.2	1.2	1.2
minerals/ trace elements [%]	6.0	6.0	6.0	6.0	6.0
cholin-Cl [%]	0.2	0.2	0.2	0.2	0.2
soy oil [%]	5.0	5.0	5.0	5.0	5.0
palm oil [%]			20.0	20.0	
porc lard [%]					20.0
cholic acid [%]		0.1		0.1	0.1
chenodeoxycholic acid [%]		0.1		0.1	0.1
fatty acid composition [%]					
C12:0	0.01	0.01	0.01	0.01	0.05
C14:0	0.02	0.02	0.21	0.21	0.29
C16:0	0.58	0.58	9.18	9.18	5.37
C18:0	0.18	0.18	1.11	1.11	2.88
C20:0	0.02	0.02	0.10	0.10	0.08
C16:1	0.01	0.01	0.05	0.05	0.60
C18:1	1.29	1.29	9.19	9.19	9.64
C18:2	2.65	2.65	4.67	4.67	4.55
C18:3	0.29	0.29	0.35	0.35	0.49

Weekly, body weight of the mice was measured. At the end of the trials, fasting blood glucose was measured using the FreeStyle Lite system (Abbott - Diabetes Care). Therefore, mice were fasted for 6 hours and one little piece of their tail was cut off for collecting blood. In the second experiment, in addition to fasting glucose levels, an oral glucose tolerance test (OGTT) was performed with 5 to 6 mice per group to have a closer look at the glucose metabolism. For this purpose, fasted mice receive 2 g glucose per kg body weight via gavage. Blood glucose levels were measured 15, 30, 60, and 120 min after gavage. Total area under the curves (AUC) were calculated for each animal using the following formula:

$$AUC \left[\frac{mg \; x \; min}{dl} \right] = (0.5x(t_0 + t_{15})x15) + (0.5x(t_{15} + t_{30})x15) + (0.5x(t_{30} + t_{60})x30) + (0.5x(t_{60} + t_{120})x60).$$

All mice were sacrificed with CO_2 at the end of the feeding period. Organs were dissected, their weight was recorder whenever appropriate and they were either directly snap-frozen or fixed in 4 % formalin for 24 to 48 hours depending on the organ.

3.6 Ethical statement

Animal use was approved by the local institution in charge (Regierung von Oberbayern, approval no. 55.2-1-54-2531-156-13). All animals were housed in the mouse facility of the Technische Universität München, ZIEL - Institute for Food & Health.

3.7 DNA isolation from feces and intestinal content

Metagenomic DNA was obtained from fecal pellets or caecal content of the fist experiment after mechanical lysis using a Fastprep and two freezing and thawing cycles followed by purification via precipitation according to a protocol published previously [224]. Genomic DNA from ileal and colonic from the first experiment as well as caecal content from the second experiment was isolated using a modification of this protocol. Briefly, intestinal content was transferred into 2 ml tubes containing 500 mg zirconia/silica beads (0.1 mm; BioSpec Products). After addition of 600 µl stool DNA stabilizer (Stratec Biomedical), 250 µl 4 M Guanidinethiocyanat (Sigma Aldrich), and 500 µl 5 % N-laurolylsarcosine (Sigma Aldrich), samples were mixed and incubated for 60 min at 70 °C with constant shaking. This was followed by mechanical lysis using a FastPrep®-24 (3 times, 40 sec, 6.5 m/ sec) (MP Biomedicals). After addition of 15 mg Poly(vinylpolypyrrolidone) (PVPP, Sigma Aldrich), the suspension was vortexed and centrifuged for 3 min at 15.000 x g and 4 °C. 500 µl of the clear supernatant was transferred in a new 2 ml Eppendorf tube, mixed with 5 µl RNase (VWR International, stock concentration 10 mg/ ml) and incubated for 20 min at 37 °C with constant shaking. Then the genomic DNA was purified following instructions of the NucleoSpin® gDNA clean-up kit (Macherey Nagel). DNA quantity and quality was measured with NanoDrop® (Thermo Fisher Scientific).

3.8 High-throughput 16S rRNA gene amplicon analysis

Diet can modulate intestinal microbiota profiles, which can be analyzed by next generation sequencing (NGS) of 16S rRNA genes. For this purpose, metagenomic DNA using two different isolation protocols (see 3.7) was isolated from caecal content of SPF mice fed CD, HFD or BA diet for 16 weeks (experiment 1), or CD, BA, P- or L-HFD-BA for 8 weeks (experiment 2).

After DNA isolation, the V3/V4 region of 16S rRNA genes was amplified (25 cycles) from 12 ng of metagenomic DNA using primer 341F and 785R [225] following a 2-step procedure to limit amplification bias [226]. Libraries were double-barcoded (8-nt index sequence on each forward and revers primer). Amplicons were purified using the AMPure XP system (Beckmann Coulter), pooled in an equimolar amount, and sequenced in paired-end modus (PE275) using a MiSeq system (Illumina) following the manufacturer's instructions.

Sequences were analyzed as described previously [227]. Raw sequence reads were processed using IMNGS (www.imngs.org) [228], a pipeline developed in-house based on UPARSE [229]. Parameters were: barcode mismatches allowed, 2; expected error allowed, 3; Phred quality threshold, ≥ 3; trimming length, 3 nt; min. sequence length, 300 nt; max. sequence length, 600 nt (see IMNGS website for further information). Operational Taxonomic Units (OTUs) were clustered at 97 % sequence similarity and only those occurring at a relative abundance ≥ 0.25 % total reads in at least one sample were further analyzed. For each OTU, the final taxonomy was assigned using the most detailed taxonomic classification among SILVA [230] and RDP [231]. Downstream diversity and composition analyses were done using the Rhea pipeline, a set of R scripts that allows standardized analysis of OTU tables, including normalization steps, alpha- and beta-diversity analysis, taxonomic composition, statistical comparisons, and calculation of correlations [232]. EzTaxon classification [233] was used for OTUs showing significant differences in relative abundances between feeding groups to identify the closest described species.

3.9 Blood measurements and hepatic triglycerides

Blood samples were analyzed at INRA, Micalis (team AMIPEM), France. The procedures were as described previously [37]. Plasma insulin, leptin, TNFα, IL-6, IL-27, INFβ, INFγ, IL-1α, IL-1β, IL.23, IL-17a, IL-12p70, IL-10 and MCP1 concentrations were measured using a Luminex 100 IS system (Luminex Corporation) with a Milliplex MAP mouse serum adipokine panel kit (Millipore). For hepatic triglycerides, portions of frozen liver were homogenized in chloroform-methanol (2:1) to extract total lipids. The organic extract was dried, reconstituted in isopropanol, and triglyceride concentrations were measured with a triglyceride determination kit (Sigma Aldrich) and expressed as mg/ g liver.

3.10 Bile acid measurements

Bile acids were measured at the Institute of Food Chemistry, University of Hamburg. Bile acid measurement was performed according to Wegner *et al*. (2016) [115]. Briefly, caecal content was lyophilized and homogenized. 5 mg of the powder were resuspended in 250 µl methanol containing an internal standard mixture (IS), vortexed for 10 min and centrifuged for 10 min at 12,000 x g and 4 °C. Then, 5 µl supernatant were mixed with 40 µl methanol and used for liquid chromatography electrospray ionization tandem mass spectrometry (LC-ESI-MS/MS) analysis. Adipose tissue (100 mg) was spiked with 10 µl IS and mixed with 4 ml methanol. This suspension was then homogenized with an Ultra-Turrax (intensity 4) and centrifuged for 10 min at 12,000 x g and 4 °C. Afterwards, 1000 µl supernatant were transferred to a new glass vial, evaporated until dryness. The residue was re-dissolved in 100 µl methanol and used for LC-ESI-MS/MS analysis.

The analysis of bile acids and cholesterol were performed on an Agilent 1260 Infinity Quaternary LC System (Agilent Technologies) coupled to a triple quadrupole API 4000 QTRAP® MS (AB Sciex Germany GmbH) equipped with a turbo ion spray source, operating either in positive or negative ion mode. A Kinetex® C18 reversed phase column equipped with a Kinetex® C18 security guard column (Phenomenex Inc.) was used for separation of the analytes (constant flow rate of 200 µl/ min.).

3.11 Free fatty acids and lipid measurement

<u>Free fatty acids analysis</u>: For the analysis of free fatty acids in WAT, 10-50 mg tissue were mixed with 2 ml methanol and 10 µl IS. Then the samples were homogenized 3 times for 20 sec using Ultra-Turrax (intensity 4) and centrifuged for 10 min at 4 °C and 4,000 rpm. 1 ml of the supernatant was then mixed with 3 ml Methyl tert-butyl ether and 50 µl IS, sonicated for 10 min at room temperature (RT) and homogenized for 10 min at RT using a vortex mixer (2200 U/ min). The last three steps were repeated three times. Then, the organic phase was taken off and sterile filtrated using a PTFE-filter. 1.5 ml filtrate were transferred into a glass vial and dried using nitrogen flow. Afterwards, the residue was resuspended in 300 µl MTBE, transferred in a new glass vial and dried using nitrogen flow. Last, the residue was resuspended in 50 µl C19:0-Methanol solution (1 mg/ ml) and esterified using 25 µl trimethylsulfonium hydroxide solution and analyzed by gas chromatography flame ionization detector (GC-FID). The used GC-FID method is shown in **Table 9**.

Table 9: Parameter and conditions used in the GC-FID method

Gas chromatograph	Hewlett Packhard HP 6890 Series GC System			
mobile phase	nitrogen			
flow rate	2 ml/ min			
column	Agilent CP-SIL 88 (50 x 250 µm x 20 µm)			
Step	°C/min	next [°C]	hold [min]	run time [min]
Initial	-	90	2	2.00
Ramp 1	15	150	0	6.67
Ramp 2	3	180	0	16.67
Ramp 3	30	230	10	28.34
autosampler	Agilent 6890 Series Injector			
Injector temperature	200 °C			
Injection volume	1 µl			
Split	75:1			
Software	ChemStation, Agilent Version Rev.A.10.02 1757			
Integration conditions	peak slope/ sensitivity: 15 mind. peak width: 0.01 mind. peak area: 2 mind. peak height: 2			

<u>Lipid analysis</u>: Measurement of total fatty acids and phospholipids was done at the Institute of Clinical Chemistry and Laboratory Medicine, University of Regensburg, Germany. Total lipid analysis was performed as described by [234]. Briefly, fatty acid methyl esters (FAME) were generated by overnight incubation with acetyl-chloride and methanol at RT. FAMEs were then extracted with

hexane. Afterwards, FAMEs were separated by a highly polar BPX70 column coated with 70 % cyanopropyl polysilphenyl-siloxane using a Shimadzu 2010 GC-MS system. FAMEs were characterized and identified by selected ion monitoring mode of the most intense fragments. Quantification was done using an external calibration with C21:0 as internal standard. The desaturation index as indicator for SCD1 activity was calculated as follows [235]:

$$C16:0 = \frac{concentration\ of\ C16:0}{concentration\ of\ C16:1(n7)\ +\ concentration\ of\ C18:1(n7)}$$

$$C18:0 = \frac{concentration\ of\ C18:0}{concentration\ of\ C18:1(n9)}$$

Phospholipids were isolated and measured as described by [236]. Briefly, lipids were isolated according to Bligh *et al*. (1959) [237]. Lipids were quantified by ESI-MS/MS in positive ion mode using a quadrupole mass spectrometer (Quattro Ultima, Micromass). Non-natural occurring lipid species were used as internal standards. Product ion spectra were generated in a negative ion mode using API 4000 Q-Trap (Applied Biosystems).

3.12 Fluorescence *In Situ* hybridization (FISH)

Fluorescence *In Situ* hybridization (FISH) was carried out on proximal colon in order to confirm the colonization status of *CORIO* mice. Therefore, formalin-fixed paraffin-embedded (FFPE) colon tissue was cut in 5 µm sections using a microtome (Leica Biosystems). Three different probes were used: (I) ATO291 (5'-GGTCGGTCTCTCAACCC-3'; binding to *C. aerofaciens*, *A. parvulum* and *Egg. lenta*; [123]), (II) EUB338 (5'-GCTGCCTCCCGTAGGAGT-3'; binding to all bacteria, [238]) and (III) COR653 (5'-CCCTCCCMTACCGGACCC-3'; binding to *C. aerofaciens*; [123]).

Tissue sections were transferred onto Superfrost Plus microscope slides (Thermo Fisher Scientific) and dried overnight at RT. The following day, the tissue sections were heated up for 15 min at 60 °C and incubated three times for 2 min in xylene, followed by 2 min in 96 % ethanol, 80 % ethanol and 60 % ethanol for deparaffinization. Thereafter, sections were fixed by incubation in 4 % formaldehyde for 5 min.

Then, tissues were incubated for 5 min in 3x phosphate buffered saline (PBS, Invitrogen™) and twice for 1 min in 1x PBS. Dehydration was performed by incubating the tissue sections in 60 % ethanol, 80 % ethanol and 96 % ethanol for 3 min each. After drying the slides for 3 min, tissues were circled with a liquid barrier marker (Roti; Carl Roth) and put in a water filled incubation chamber. Each section was covered with 50 µl lysis buffer (20 mM Tris-HCl, 2 mM EDTA, 1.2 % (v/ v) Triton-X-100, 40 mg/ ml lysozyme, sterile filtrated) and incubated for 45 min at 37 °C in a hybridization oven (Thermo Fisher Scientific) for permeabilization.

Subsequently, tissue sections were washed with water and a second dehydration step was carried out. Therefore, tissue sections were incubated in 60, 80 and finally 96 % ethanol for 3 min each. After a final wash with 1 x PBS, hybridization was carried out. Hence, hybridization buffer (50 °C; 20 mM Tris-HCl, 0.9 % NaCl, 0.01 % 20% SDS solution, sterile filtrated) containing 0.5 ng/ µl of the probes ATO291 and EUB338 or ATO291 and COR653 was pipetted cautiously on the tissue. To prevent draining of the tissue section, the hybridization chamber was filled with pre-warmed hybridization buffer and closed with parafilm. Tissues were incubated overnight at 50 °C. The following day, tissues were washed thrice with preheated washing buffer (48 °C; 20 mM Tris-HCl, 0.064 M NaCl, sterile filtrated). Then, the nuclei were stained with 4',6-Diamidin-2-phenylindo (DAPI). Therefore, DAPI stock solution was added to the washing buffer (DAPI end concentration: 1 µg/ ml), the sections were incubated for 30 min at RT in the dark and then washed again thrice with preheated washing buffer. Following, sections were mounted with aqueous mounting reagent (Aquatex by Merck) and covered with a cover glass.

Sections were analyzed with a confocal laser scanning microscope (Olympus FluoView FV10i) using the channels DAPI, Cy5.5 (blue) for EUB338 and COR653 and Cy3 (red) for ATO291. Double positive cells appeared pink. For all samples of one run, the same laser intensity was used. Sections of SPF and GF mice were used as controls. Of each mouse, three pictures were taken at 60 x magnification.

3.13 Lable-free quantification of eWAT proteome

Proteomic anaylsis of epididymal white adipose tissue (eWAT) was done in cooperation with Prof. Küster, Chair for Proteomics and Bioanalytics, TU Munich. Protein isolation was performed according to a protocol from Prof. Küster. Briefly, 30 mg snap frozen eWAT of 5 to 6 mice of each BA fed group were homogenized in 250 µl tissue lyses buffer (50 mM Tris/HCl pH 7.6, 8 M urea, 10 mM Tris(2-carboxyethyl)phosphine hydrochloride, 40 mM Chloroacetamide, protease (cOmpete Protease Inhibitor Cocktail Tablets, Roche) and phosphatase inhibitor mixture (PhosSTOP, Roche)) using a sterile mortar and pestle on ice. Afterwards, protein concentration was measured using Pierce™ 660nm Protein Assay (Thermo Fisher Scientific) following manufacturer's instructions. For each sample, at total amount of 75 µg protein was diluted with four volumes of 50 mM Tris HCl (pH 7.6). Next, sequencing grade trypsin (Promega) was added in a protease-to-protein ratio of 1:100 (w/ w) using a 1 µg/ µl trypsin stock solution. Following, the samples were predigested for four hours at 37 °C and 700 rpm. Thereafter, trypsin was again added in a 1:100 (w/ w) manner and samples were incubated overnight at 37 °C and 700 rpm. The next day, samples were cooled down to RT and acidified to a pH of 2 with 50 % (v/ v) formic acid (FA). Samples were then centrifuged at 14,000 x g for 5 min at RT and supernatants were used for desalting.

Desalting was performed using C18-Peptide Clean-up Sep-Pak columns 50 mg (Waters). First, columns were activated with 1.5 ml methanol (MeOH) and equilibrated with 1.5 ml 80 % acetonitrile (ACN), 20 % H_2O and 0.1 % formic acid (FA). Following, columns were washed five times with 1.5 ml 2 % ACN, 98 % H_2O and 0.1 % FA. Then they were loaded with the samples. Flow through was recovered and applied a second time onto the column. Afterwards, peptides on the column were washed five times with 2 % ACN, 98 % H_2O and 0.1 % FA. Finally, peptides were eluted twice by adding 150 µl 40 % ACN, 60 % H_2O, 0.1 % FA. Then the eluates were dried completely using an acid-resistant vacuum concentrator CentriVap Concentrator (Labconco). Dried peptides were resolved in 100 µl of 0.1 % FA in H_2O and protein concentration was determined using a Nanodrop 2000 Spectrophotometer (Thermo Fisher Scientific). Samples were equalized to a final peptide concentration of 0.2 µg/ µl with 0.1 % FA in H_2O.

The peptides were then analyzed via LC-MS/MS on a nanoLC-Ultra 1D+ (Eksigent Technologies) coupled to a Q Exactive HF mass spectrometer (Thermo Fisher Scientific). Peptides were delivered to a trap column (75 µm x 2 cm, packed in house with Reprosil-Pur C18 ODS3 5 µm resin, Dr. Maisch HPLC) for 10 min at a flow rate of 5 µl/ min in 100 % solvent A0 (0.1 % FA in HPLC grade water). Peptides were separated on an analytical column (75 µm x 40 cm, packed in-house with Reprosil-Gold C18 120, 3 µm resin, Dr. Maisch HPLC) using a 120 min gradient ranging from 4 – 32 % solvent B (0.1 % FA and 5 % DMSO in acetonitrile) in A (0.1 % FA and 5 % DMSO in HPLC grade water) at a flow rate of 300 nl/ min. The MS was operated in data dependent mode, automatically switching between MS1 (resolution: 60,000) and MS2 spectra (resolution: 15,000). Up to 20 peptide precursors were subjected to fragmentation by higher energy collision-induced dissociation and analyzed in the Orbitrap. Dynamic exclusion was set to 20 sec.

Label free quantification was performed using MaxQuant (version 1.5.3.30) [239] by searching MS data against a mouse UniProt reference database (version 03.05.16, 24853 entries) using the search engine Andromeda [240]. Carbamidomethylated cysteine was used as fixed modification; variable modifications included oxidation of methionine and N-terminal protein acetylation. Trypsin/P was specified as proteolytic enzyme with up to two or respectively five allowed miscleavage sites. Precursor tolerance was set to 10 ppm and fragment ion tolerance to 0.05 Da. Label-free quantification [241] and match-between-runs options were enabled (matching time window: 2 min, alignment time window: 20 min) and results were filtered for a minimal length of seven amino acids, 1 % peptide and protein false discovery rate as well as common contaminants and reverse identifications.

Functional annotations were carried out with Perseus 1.5.4.1. The unique proteins were annotated with lipid metabolism related terms (filter: lipid metabolism, lipid synthesis, lipid catabolic

processes). Information about proteins was gathered via uniprot.org, http://www.ncbi.nlm.nih.gov/pubmed and KEGG database. A Venn diagram was generated using the proteome data received by mass spectrometry for each housing group (cutoff: detected in 4 out of 5 samples for SPF mice; detected in 5 out of 6 in GF and *CORIO* mice). The Venn diagram itself was compiled using the webtool of bioinformatics and evolutionary genomics.

The histone masses received from proteome analysis were used to calculate the cell volume of eWAT of the three colonization groups. For this approach, the proteomic ruler plugin 0.1.6 [242] for Perseus 1.5.5.3 was used, following the instructions on http://www.coxdocs.org/doku.php?id=perseus:user:plugins:proteomicruler. The proteomic ruler approach is based on the assumption that the number of histones is constant in each cell, whereas the amount of protein depends on the cell volume. Therefore, the ratio of histone and protein mass can be a measure of the cell volume.

3.14 RNA isolation

3.14.1 Liver and ileum

Distal ileum and liver were stored in RNAlater (Sigma Aldrich) at -80 °C. After thawing, the tissue was taken out of the RNAlater and added to RA1 buffer (Macherey Nagel) and β-Mercapthoethanol (Sigma Aldrich). One piece of liver (ca. 30 mg) was smashed with a plastic pastille. Ileal tissue was opened longitudinal, smashed and passed through a 0.9 mm syringe needle. Then the smashed samples were loaded on QIAshredder columns (QIAGEN). The flow through, which contains the RNA, was used for RNA isolation following manufacturer's instructions (NucleoSpin® RNAII kit; Macherey-Nagel). Quantity and purity of the RNA was measured using NanoDrop® (Thermo Fisher Scientific).

3.14.2 White adipose tissue (WAT)

Samples of epididymal (e) and mesenterial (m) WAT were stored in RNAlater at -80 °C. One piece of the sample (ca. 50 mg) was used for RNA Isolation. 1 ml Isol-RNA lysis reagent (5Prime/ VWR) was added to the sample. The samples were then homogenized using Ultra-Turrax (Art-Miccra D-1, ART modern Labortechnik) for 20 sec and incubated 5 min at RT. After centrifugation, the homogenates were taken off through the fat phase. 200 µl ice cold chloroform (Carl Roth) was added, mixed for 15 sec by hand shaking and incubated for 3 min at RT. The samples were then centrifuged for 15 min at 12,000 x g and 4 °C to receive the aqueous RNA containing phase which was afterwards transferred in a new eppendorf tube. The RNA was then isolated following manufacturer's instructions (Direct-zol RNA MiniPrep, Zymo Research). Quantity and purity of the RNA was measured using NanoDrop® (Thermo Fisher Scientific).

3.14.3 Reverse transcription (RT) PCR and qPCR

Complementary DNA (cDNA) was synthesized from 500 ng (ileum and WAT) and 1000 ng (liver) RNA in 13 µl PCR-grade H_2O using random hexamers and M-MLV RT Point Mutant Synthesis System (Promega) (**Table 10**). qPCR was performed using the LightCycler® 480 from Roche with 10 µM UPL-Probe, 20 µM forward and reverse primer, ca. 125 ng/ µl cDNA and 2x Probe or SYBR Master Mix. For the reaction, either Brilliant III Ultra-Fast QPCR Master Mix from Agilent Technologies or SensiFAST™ SYBR No-ROX Mix 2x from Bioline was used. The used temperature settings for qPCR are displayed in **Table 11**. The used primer and probe combinations for the target genes are shown in **Table 12**. The expression of hepatic *Il1*β, *Ppar*α and γ, *Mlxipl, Acaca, Tnf*α and *Cd*36 were analyzed via TaqMan™ approach at INRA, France. Calculations were done using the 2-ΔΔCt method [243].

Table 10: cDNA synthesis

Components	Volume per sample [µl]
Random-Hexamer [200ng/µl]	1
5 min. 70°C	
5 min. 4°C	
5x 1. Strang Puffer (Promega)	5µl
PCR grade H_2O	3,1 µl
rRNasin® (Promega)	0.65
dNTP Mix 10mM	1,25µl
M-MLV (200U/µl) (Promega)	1µl
10 min. 25°C	
50 min. 48°C	

Table 11: Temperature settings used for UPL and SYBR green based qPCR

	UPL Probe based		SYBR Green based		
Step	**Temperature [°C]**	**Time**	**Temperature [°C]**	**Time**	**Number of cycles**
Denaturation	95	3 min.	95	5 min.	1
2 step cycle:					
Denaturation	95	5 sec.	95	10 sec.	45
Annealing & Elongation	60	10 sec.	60	20 sec.	
Melting curve			95	5 sec.	
			65	1 min.	
			97	continuous	
cooling	40	30 sec	40	10 sec	

Table 12: Primer and UPL probe combinations for the analyzed genes as well as their uniprot accession number

Protein name	Gene name (Mouse)	Accession number	Forward primer	Reverse primer	UPL Probe
ASBT	*Slc10a2, Ntcp2*	P70172	gactagctggtcaaccctggta	gggggagaaggagagctgta	22
BSEP	*Abcb11, Bsep, Spgp*	Q9QY30	accaggacactgatccaga	gaagatgcattgccaatattca	6
CYP7A1	*Cyp7a1, Cyp7*	Q64505	caccattcctgcaaccttct	ttggccagcactctgtaatg	92
FGF15	*Fgf15*	O35622	ggcaagatatacgggctgat	tccatttcctccctgaaggt	69
FXR	*Fxr, Nr1h4*	Q60641	agaaatggcaaccagtcatgta	gcaaagcaatctgatcttcgt	47
HMG CoA reductase	*Hmgcr*	Q01237	tgcgtaagcgcagttcct	ttgtagcctcacagtccttgg	19
Leptin	*Lep, Ob*	P41160	caggatcaatgacatttcacaca	gctggtgaggacctgttgat	93
LXR [a]	*Nr1h3*	Q9Z0Y9	agctctgcctacatcgtggt	tcatggcccagcatcttc	
NPC1L1	*Npc1l1*	Q6T3U4	caacatcttcatctttgttcttgag	gccaatgtgagcctctcg	110
SCD1 [a]	*Scd1*	Q9Z0R9	tgcctcttcgggattttctactac	tggaacgccatggtgttggc	
SHP	*Nr0b2, Shp*	Q62227	cgatcctcttcaacccagat	ggtaccagggctccaagact	104
Srebp1c	*Srebf1, Srebp1*	Q9WTN3	atggattgcacatttgaagacatg	agaggaggccagagaagcag	
TGR5	*Tgr5, Gpbar1*	Q80SS6	attcccatgggggttctg	gagcaggttggcgatgac	81
Housekeeper					
60S ribosomal protein L13a	Rpl13a	P19253	atccctccaccctatgacaa	gccccaggtaagcaaactt	108
GAPDH	Gapdh	P16858	gggttcctataaatacggactgc	ccattttgtctacgggacga	52
HPRT	Hprt1	P00493	tcctcctcagaccgctttt	cctggttcatcatcgctaatc	95

[a] these targets were measured by SYBR green based qPCR

3.15 Histology and immunohistochemistry (IHC) of liver and WAT

Histology: Formalin-fixed paraffin embedded liver and adipose tissue samples were cut into 3.5 (liver) and 5 µm (WAT) thick sections using the Leica rotary microtome RM2255, mounted on SuperFrost® microscope slides and dried overnight. On the next day the sections were heat treated for 15 min at 60 °C to melt the paraffin. Afterwards, the sections were automatically stained with hematoxylin (H) and eosin (E) with the multistainer station LeicaST5020 and covered with embedding medium (Carl Roth GmbH). Stained sections were then scanned using a M8 digital microscope (PreciPoint GmbH). The sections were examined in a blinded manner.

Histopathological evaluation of the liver: Due to their functions, *CORIO* might have an impact on the development of NAFLD. Therefore, blinded histopathological evaluation of liver tissue section was performed at INRA, Micalis, AMIPEM, France to analyze NAFLD activity score. This was done using a semi-quantitative scoring system. Briefly, steatosis (0–3 points), lobular inflammation (0–3 points and ballooning (0–2 points) of hepatocytes was evaluated in a blinded manner. The points were then summed up to the total NAFLD activity score, which ranges from 0-8.

Adipocyte size: HF feeding leads to an increase in fat mass. This increase can be either due to an increase in cell volume (hypertrophy) and in cell number (hyperplasia) [244]. Therefore, adipocyte

sizes were measured in six 10-fold pictures of different, not overlapping areas of H & E stained sections and analyzed using Image J software. The threshold was set once and kept for all pictures of one feeding group and WAT. The size was analyzed using the following settings: size (600-infinity), circularity (0.4-1), choose Outlines, exclude on edges and remove default option. Afterwards, analysis was done using GraphPad Prism version 7.00.

IHC staining: IHC staining of liver sections (3.5 µm and mounted on SuperFrost® plus microscope slides) was used to identify the impact of *CORIO* and diet on infiltration of immune cell in the liver. Liver sections were stained at the Institute of Virology, Helmholtz Zentrum, Technical University Munich with antibodies for MHCII, F4/80, Ki67, B220 and CD3. The procedure was performed as described in Wolf *et al.* (2014) [245]. Stained sections were then scanned using a M8 digital microscope (PreciPoint GmbH). The sections were examined in a blinded manner.

3.16 Immunofluorescence staining of FXR

FXR, key regulator of bile acid metabolism, was analyzed on protein level by immunofluorescence (IF) staining. Therefore, frozen TissueTec® O.C.T.-embedded liver tissues were cut into 5 µm thick cryosections using a cryostat Microm HM560 (Thermo Fisher Scientific), mounted onto SuperFrost® Plus microscope slides (Thermo Fisher Scientific) and stored at -20 °C until further use. After thawing, cryosections were immediately fixed in 4 % formalin for 15 min at RT and washed 3 times with 0.1 M PBS for 5 min each. For permeabilization, liver sections were incubated for 5 min in 1x PBS containing 0.3 % Triton-X-100 (AppliChem) [246].

Following the permeabilization step sections were blocked in goat blocking buffer (1x PBS, 5 % goat serum) for 1.5 hours. After blocking, sections were incubated with the polyclonal rabbit anti-FXR antibody (H-130, Santa Cruz Biotechnology) diluted 1:75 in antibody dilution buffer (1x PBS, 10 mg/ ml BSA 0.3 % Triton X-100) at 4 °C overnight. At the next day sections were washed three times 5 min with 1x PBS and incubated with the secondary antibody (goat anti-rabbit Alexa Fluor 594, Life Technologies) diluted 1:200 in antibody dilution buffer for 1.5 hours at RT. After rinsing three times in 1x PBS containing DAPI (1:1000) for 5 min, each tissue sections were cover slipped using Aquatex mounting medium. At least three images were taken at 60-fold magnification from randomly chosen areas using an Olympus FluoView FV10i confocal microscope.

Volocity 3D image analysis software (Perkin Elmer Inc.) was used to quantify immunofluorescence intensities. By using the measurement tool of the software, in each image a certain area (representing as most of the tissue as possible) was selected for which the software automatically calculated the surface area in µm². In the next step, for each staining round a minimum threshold intensity was set based on the images of the control group (SPF fed CD). Thresholds were defined by

obtaining the best signal sensitivity as possible while minimizing measurements of background intensity. Based on this threshold, which was used for all images of one staining round, all intensities within one image that were above this threshold were calculated by the software and all intensity measurements were summed up to a total intensity. Based on the total intensity and surface area, the intensity per µm² was calculated for each image. Finally, the mean was calculated from all images of one mouse and graphs were made using GraphPad Prism version 7.00.

3.17 Statistics

Statistical analyses were performed with R or GraphPad Prism version 7.00 using one- or two-way ANOVA followed by pairwise comparison testing (Holm-Sidak Significance is indicated through the thesis as follows: ●, one-way ANOVA; * two-way ANOVA; *, ●, $p < 0.05$; **, ●●, $p < 0.01$; ***, ●●●, $p < 0.001$.

Regression analysis was done by ANCOVA using Microsoft Office Excel 2016 with pairwise comparison based on a Students t-test adjusted for the mean of WAT mass and corrected for the error term from the ANOVA using the following calculation:

$$t = \frac{\bar{y}_i^t - \bar{y}_j^t}{\sqrt{MS_{Res(y,x,t)}\left[\frac{1}{n_i} + \frac{1}{n_j} + \frac{(\bar{x}_i - \bar{x}_j)^2}{SS_{Res(x,t)}}\right]}}$$

Principal component analyses (PCA) were performed in R. ANOVA analysis of proteome data were carried out using R scripts of the RHEA package [232]. Graphics were created using GraphPad Prism version 7.00. Unless otherwise stated, data are presented as mean ± SD.

4 Results

Coriobacteriaceae are dominant mammalian gut commensals able to convert bile salts and steroids. Hence, they may influence host health by modulating bile acid and lipid metabolism. First, it was important to characterize the four *Coriobacteriaceae* strains selected for *in vivo* experiments in greater detail. We thus tested their ability to deconjugate bile acids and to degrade lipids *in vitro*. In addition, their occurrence in human populations was investigated to assess possible links to metabolic diseases. These data are presented in section **4.1**. Second, *in vivo* effects of *Coriobacteriaceae* in combination with bile acids were analyzed using a gnotobiotic mouse model, as detailed in section **4.2**. Finally, the impact of dietary lipids and bile acids on host metabolism were investigated in section **4.3**.

4.1 Metabolic functions and occurrence of *Coriobacteriaceae*

The host produces primary bile acids from cholesterol in the liver, which are then conjugated to the amino acids glycine or taurine to increase solubility and reduce toxicity prior to secretion into bile. Upon ingestion of food, bile acids are released into the duodenum to support the digestion of lipids and liposoluble dietary compounds in the small intestine. It is known that some *Coriobacteriaceae* strains can dehydrogenate bile acids via the action of hydroxysteroid dehydrogenase (HSDHs). However, this transformation is only possible under the condition that bile acids are present in unconjugated forms. The enzyme responsible for deconjugation is called bile salt hydrolase (BSH) (also referred to as choloylglycine hydrolase). Until now, no study focused on BSH activity in *Coriobacteriaceae*.

The presence of BSH protein sequences in each of the four strains selected for *in vivo* experiments was tested by screening protein databases, which showed that *C. aerofaciens* and *E. mucosicola* have the ability to deconjugate bile acids (protein accession no. CUO91292.1 and WP_028027311.1, respectively). In contrast, no protein sequences annotated as BSH were found in the genome of *Egg. lenta* and *A. parvulum*.

These results were confirmed *in vitro* by testing the ability of the strains to produce active BSH using an agar plate assay, in which deconjugation of bile acids results either in visible precipitates around colonies or induces whitening (see section 3.3.1 for technical details). *C. aerofaciens* was the only strain able to deconjugate TDCA *in vitro* resulting in formation of a halo around colonies (**Figure 11A**). *Egg. lenta* as well as *A. parvulum* grew on TDCA-supplemented agar plates, but neither precipitation nor difference in the appearance of colonies were observed. *E. mucosicola* did not grow on TDCA-supplemented agar plates under the experimental conditions used. In addition to BSH, HSDHs, which

catalyze the dehydrogenation of bile acids, have been reported in *Coriobacteriaceae*. *Egg. lenta* and *C. aerofaciens* are known to possess 3α- and 12α-HSDH as well as 7β-HSDH, respectively [158, 162]. By performing fermentation experiments with primary bile acids and each of the *Coriobacteriaceae* strains, followed by quantification of single bile acids (in cooperation with AG Rohn at the University of Hamburg), we reported for the first time that *E. mucosicola* and *C. aerofaciens* are able to oxidize α-hydroxyl groups at position C3 and C12 to generate 3- and 12-oxo-bile acids [115].
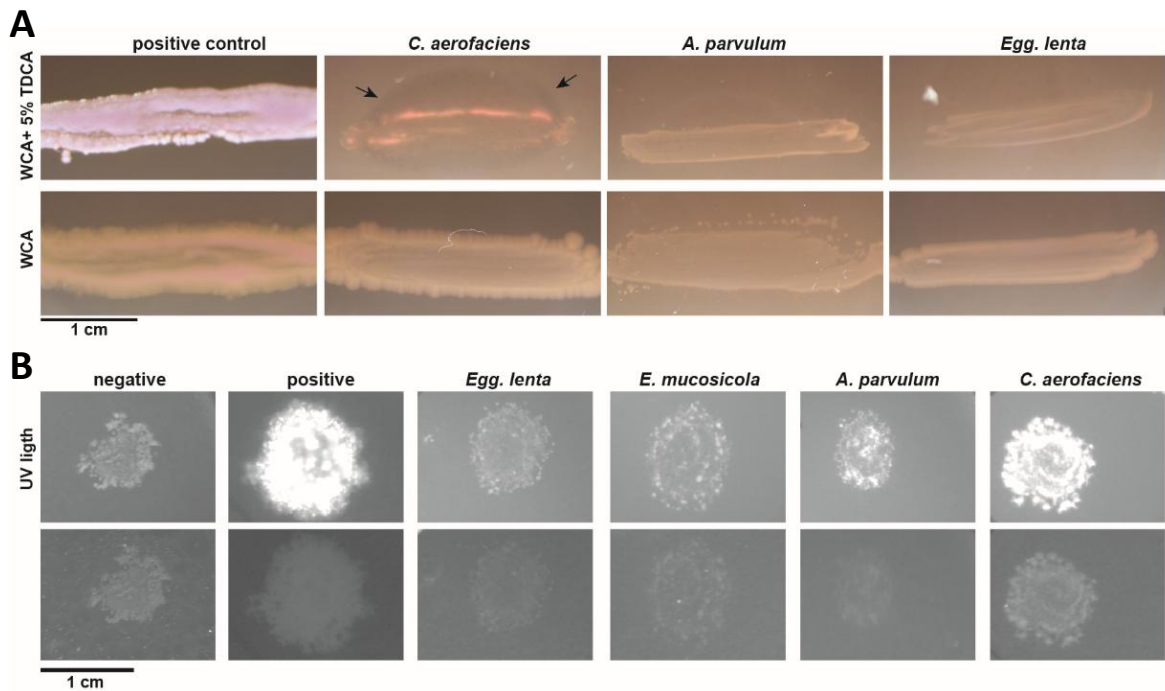
Figure 11: *Coriobacteriaceae* strains have the ability deconjugate bile acids and to cleave dietary triglycerides.
(**A**) BSH activity was tested *in vitro* using WCA agar supplemented with 5 % TDCA. Active BSH results in precipitates, which either lead to formation of a halo surrounding colonies or induce their whitening. *Clostridium* sp. strain FSA-380-WT-2B was used as positive control (whitening). *E. mucosicola* did not grow on WCA agar plates supplemented with 5% TDCA and could thus not be tested. (**B**) Lipase activity was analyzed using olive oil-rhodamin B WCA agar plates. Lipase activity leads to the formation of a rhodamin B-fatty acid complex which can be visualized by UV light (360nm). *E. coli* and *Acinetobacter johnsonii* MG844 were used as negative and positive control, respectively.

Since certain bacteria can catalyze lipolysis and thereby contribute to lipid metabolism, we tested the ability of *Coriobacteriaceae* to cleave triglycerides. Therefore, a lipase activity assay using rhodamin B olive oil agar was performed (see section 3.3.2 for technical details). This assay revealed that colonies of *C. aerofaciens* and *A. parvulum* were fluorescent upon exposure to UV light (**Figure 11B**), meaning that these strains are able to cleave triglycerides.

With respect to the occurrence of *Coriobacteriaceae* in metabolic diseases, literature data proposed that their presence is associated with disturbed host metabolism and type-2 diabetes. To clarify whether the prevalence of the four strains used in our animal experiments is associated with

metabolic disorders in human subjects, we searched for matches between coding sequences in their genomes and shotgun sequencing data of the Integrated Gene Catalogue of [217] (see section 3.1 for technical details). This reference dataset consists of metagenomic sequences from feces from normal weight, underweight, overweight, obese and morbid obese individuals of three different nationalities (185 Chinese, 177 Danish, and 59 Spanish). Diabetic patients were excluded from the analysis due to missing information about medications. The BLAST search (similarity and query length coverage $\geq 90\%$; $p < 0.05$) identified 2110 *C. aerofaciens*-related coding sequences from which 79 were enriched in obese and morbid obese individuals (**Figure 12A**). In contrast, out of 3212 *Egg. lenta*-related coding sequences 59 were less abundant in feces from obese and morbid obese individuals (**Figure 12B**). Sequences related to *A. parvulum* and *E. mucosicola* were not detected in this metagenomic dataset.
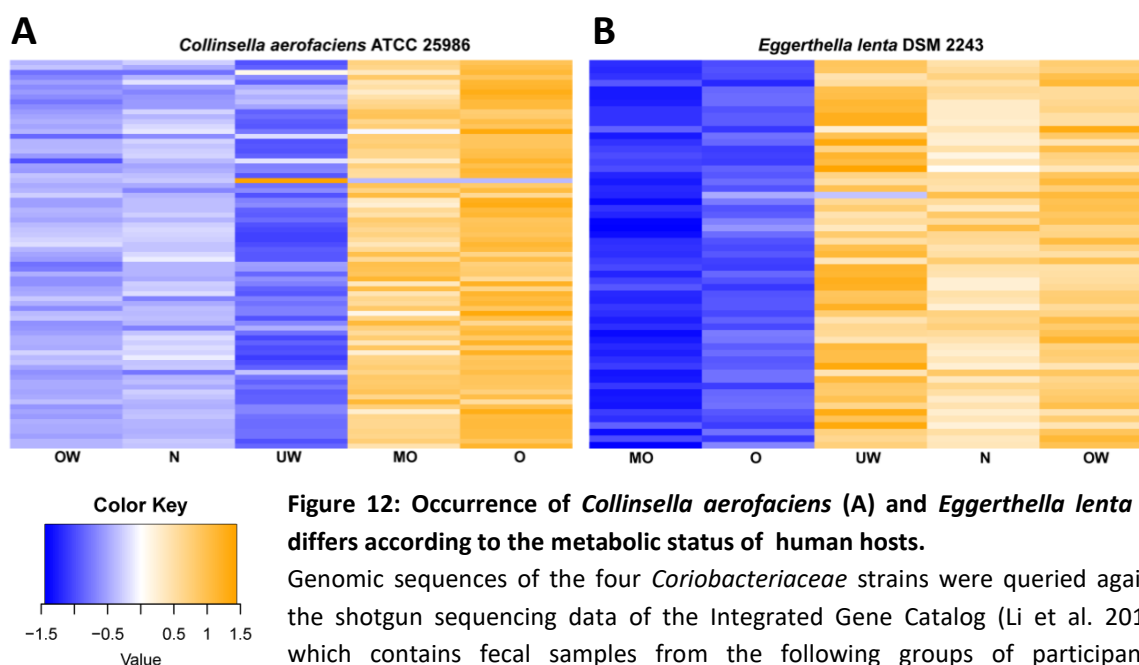
Figure 12: Occurrence of *Collinsella aerofaciens* (A) and *Eggerthella lenta* (B) differs according to the metabolic status of human hosts.
Genomic sequences of the four *Coriobacteriaceae* strains were queried against the shotgun sequencing data of the Integrated Gene Catalog (Li et al. 2014), which contains fecal samples from the following groups of participant's: underweight (UW, n = 19), normal weight (N, n = 194), overweight (OW, n = 102), obese (O, n = 76) and morbid obese (MO, n = 30). Sequence similarity and query length coverage was $\geq 90\%$. **Courtesy of Stanislas Mondot.**

In combination with literature evidence, the data aforementioned support a link between the presence of *Coriobacteriaceae* and metabolic diseases, highlighting the importance of investigating the functions of this bacterial family and their mechanistic role in host physiology.

4.2   *Coriobacteriaceae* modulate host metabolism

To test whether *Coriobacteriaceae* can influence host metabolism, in particular lipid, bile acid, and cholesterol metabolism *in vivo*, GF mice were associated with four *Coriobacteriaceae* strains (*CORIO* mice) and fed CD, palm oil based high-fat diet (P-HFD), or control diet supplemented with primary bile acids (BA) diet for 16 weeks (see experimental details in section 3.5). GF and SPF mice were used as controls.

4.2.1   Colonization of GF mice with the *Coriobacteriaceae* consortium

Before assessing in detail diet- and bacteria-driven effects on the host, we tested the efficacy of gut colonization by the *Coriobacteriaceae*. GF mice were associated with four strains at the age of five weeks, and fecal samples were collected one and two weeks after association for cultivation and 16S rRNA gene-targeted qPCR. In addition, luminal content was collected from different gut locations at the end of the trial (26 weeks of age) (see experimental details of 16S rRNA gene-targeted qPCR in section 3.4). DNA isolation protocols, which differed between feces, caecal and luminal content are described in section 3.7.

Cultivation of fecal samples showed that *CORIO* mice were colonized at a mean cell density of approximately 5×10^{11} cfu/ g feces at one and two weeks after colonization (**Figure 13A**). Because cultivation does not allow testing of individual strains, and growth on agar plates was dominated by two of the four strains (*C. aerofaciens* and *Egg. lenta*; data not shown), 16S rRNA gene-targeted qPCR assays specific for each of the strains was established and applied to DNA extracted from fecal samples. Results clearly indicated the presence of all four *Coriobacteriaceae* strains (**Figure 13B**). One week after colonization, *C. aerofaciens* ($\log_{10} 7.0 \pm 0.5$ gene copy numbers per 1 µg fecal DNA) and *Egg. lenta* ($\log_{10} 6.2 \pm 0.5$ copies/µg) colonized mice more efficiently than *A. parvulum* ($\log_{10} 3.7 \pm 0.9$ copies/µg) and *E. mucosicola* ($\log_{10} 5.0 \pm 0.7$ copies/µg). After two weeks of colonization, *C. aerofaciens*, *Egg. lenta*, and *E. mucosicola* showed unchanged colonization densities, whereas that of *A. parvulum* increased to 5.1 ± 0.3/ µg.

In general, one main difference between GF and SPF mice is caecum volume: GF mice have a highly enlarged caecum with smoother content than SPF mice, and association of GF mice with a complex microbiota is known to restore normal caecum size. *CORIO* and GF mice had a 5.2- to 15.4-fold higher caecum to body weight ratio compared to SPF mice regardless of diet (**Figure 13C**). Hence, colonization with *Coriobacteriaceae* was not efficient in restoring caecum size. In contrast, *CORIO* mice on CD had significantly heavier caeca compared to GF (123.5 ± 31.6 vs. 97.9 ± 31.3 mg/ g body weight; $p = 0.029$). In addition to colonization, diet can also modulate caecum mass. Diets with a high content of fat are known to reduce caecum volume, which was also observed in our study (SPF mice: CD: 273.3 ± 50.2 vs. P-HFD: 234.8 ± 67.1 mg/ g body weight; $p < 0.0001$). A novel observation is that

BA diet resulted as well in a significant decrease in caecum size in GF and *CORIO* mice compared to CD feeding (p < 0.001), whereas this effect was not significant in SPF mice (CD: 273.3 ± 50.2; BA: 228.7 ± 42.2 mg/ g body weight; p = 0.249).
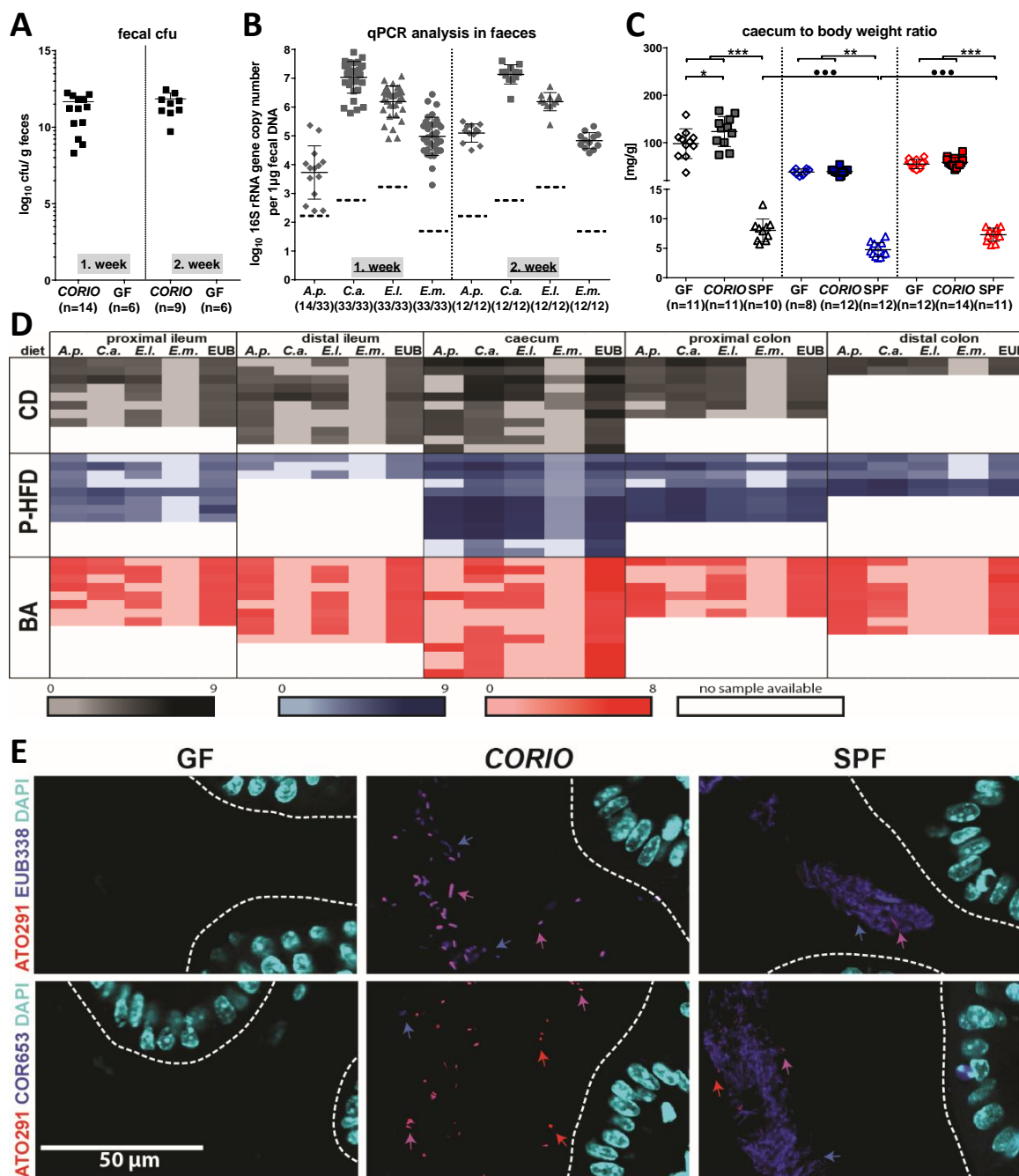
Figure 13: *Coriobacteriaceae* colonized GF mice at relatively low population densities.
(**A**) Colonization efficacy was analyzed by anaerobic cultivation of fecal pellets, one and two weeks after association. (**B**) Strain-specific 16S rRNA gene-based qPCR analysis of fecal DNA to quantify the abundance of all four individual strains. Grey dotted lines indicate the detection limits of each qPCR assay. (**C**) Caecum to body weight ratios revealed diet and colonization effects. (**D**) Heat map of 16S rRNA gene-based qPCR quantifications in ileal, caecal, and colonic contents 21 weeks after colonization. EUB primers were used to analyze total bacterial counts. (**E**) FISH analysis in proximal colon from P-HFD-fed *CORIO* mice (**Panel B**) using the 16S rRNA-specific probes **ATO291**, **COR653** or **EUB338.** GF (**Panel A**) and SPF mice (**Panel C**) were used as controls. Bacterial cells stained with two probes appear **purple**. Arrows indicate stained bacteria. **CD; P-HFD; BA;** Abbreviations: *A.p., A. parvulum; C.a., C. aerofaciens; E.l., Egg. lenta; E.m., E. mucosicola;*

For detailed description of the statistical analysis see section 3.17; In panel A-C, the number of mice in each group is indicated below the x-axis (n = number of mice measured).

At the end of the study (21 weeks after colonization and 16 weeks of feeding), lower densities of the four strains were detected in all gut compartments from proximal ileum through distal colon: values ranged from $\log_{10}$ 0 to 9 16S rRNA gene copies/ µg and marked inter-individual variations were observed (**Figure 13D** and **Suppl. Fig. S2**). *Coriobacteriaceae* seemed to colonize distal parts of the gut (caecum and colon) at higher population densities than proximal parts, especially in the case of *C. aerofaciens*. Comparing colonization efficiency between strains, *E. mucosicola* was poorly detected, but its abundance was significantly higher when mice were fed P-HFD. This diet effect was also observed for the other three strains. In contrast, feeding of the BA diet resulted in a slight to strong reduction in bacterial gene counts (23 and 100 % compared to CD depending on the strain and gut location considered).

Moreover, the colonization of mice with *Coriobacteriaceae* was confirmed by FISH staining of colonic tissue sections using two different combinations of nucleotide probes (ATO29 + EUB338 and ATO29 + COR653) (see experimental details in section 3.12) (**Figure 13E**). In tissue sections of *CORIO* mice, bacterial cells were mainly observed in P-HFD fed mice. CD- and BA-fed mice were only sparsely populated. In all tissue sections of SPF mice, bacteria could be detected and ATO291- as well as COR653-positive cells were also found. No bacteria were detected in gut sections from GF mice.

In conclusion, assessment of the colonization by *Coriobacteriaceae* showed that the strains were able to colonize the gut of GF mice, but at relatively low population densities. Furthermore, the abundance of *Coriobacteriaceae* was generally higher in mice fed P-HFD.

4.2.2   *CORIO* mice fed BA diet were characterized by increased fat mass

The primary aim of the mouse experiments was to assess the impact of *Coriobacteriaceae* in combination with diet on the host metabolism. Body weight measurement showed that 16-week P-HFD feeding triggered a 1.4-fold increase in body weight compared to CD in all three colonization groups (*CORIO*: 44.9 ± 3.9 vs. 31.0 ± 2.7 g; GF: 42.5 ± 3.1 vs. 31.4 ± 2.3 g; SPF: 49.0 ± 4.9 vs. 34.4 ± 2.9 g) (**Figure 14A**). Body weight development throughout the experiment showed that all P-HFD-fed mice constantly gained weight overtime (**Suppl. Fig. S3**). Within the P-HFD group, SPF mice were characterized by a body weight significantly higher than that of GF and *CORIO* mice. No significant colonization differences in body weight were observed within CD and BA groups.

The most striking observation in this experiment was that *CORIO* mice fed the BA diet had a two-fold increase in white adipose tissue (WAT) mass (2120.1 ± 623.2 mg) compared to GF

(1127.4 ± 530.8 mg) and SPF mice (841.7 ± 549.3 mg) (**Figure 14B**), in spite of similar body weight. Regression analysis of WAT and body weight within the BA group confirmed this significant difference between the three colonization groups (**Figure 14C**) (*CORIO* vs. SPF p = 0.00006; *CORIO* vs. GF p = 0.0273; GF vs. SPF p = 0.0465; t-Test). P-HFD feeding significantly increased WAT mass by approximately four-fold compared to CD and BA diet (**Figure 14B**), albeit no *CORIO*-specific effects were observed.
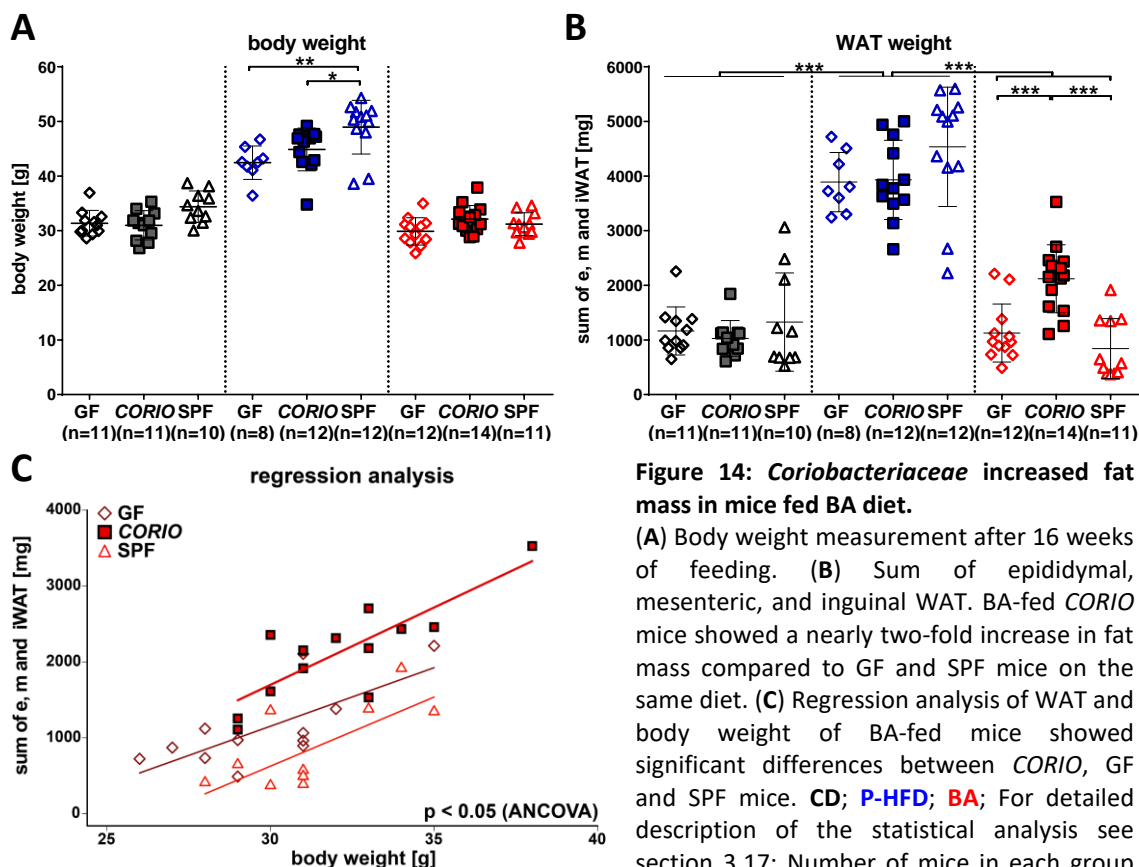

Figure 14: *Coriobacteriaceae* increased fat mass in mice fed BA diet.

(**A**) Body weight measurement after 16 weeks of feeding. (**B**) Sum of epididymal, mesenteric, and inguinal WAT. BA-fed *CORIO* mice showed a nearly two-fold increase in fat mass compared to GF and SPF mice on the same diet. (**C**) Regression analysis of WAT and body weight of BA-fed mice showed significant differences between *CORIO*, GF and SPF mice. **CD**; **P-HFD**; **BA**; For detailed description of the statistical analysis see section 3.17; Number of mice in each group are indicated below the x-axis (n = number of

4.2.3 BA feeding induced metabolic disturbances in *CORIO* mice

Diet-induced obesity via HF feeding is usually associated with comorbidities such as insulin resistance and eventually diabetes. In SPF mice, measurement of fasting glucose in blood revealed a significant increase in glucose levels by 26 to 39 % after P-HFD compared to CD and BA feeding, despite high inter-individual differences (**Figure 15A**). In GF and *CORIO* mice, P-HFD did not significantly increase fasting glucose levels compared to CD and BA diet. No effect of the colonization status of mice was observed in any of the diet groups. Another indicator of diabetes is the circulating concentration of insulin, which was five- to seven-fold higher in all P-HFD mice, independent of the colonization status (**Figure 15B**). In line with the aforementioned increased fat mass, BA feeding was associated with 50 % increased plasma insulin levels in *CORIO* mice (1.8 ± 1 ng/ ml) compared to GF controls

(0.8 ± 0.3 ng/ ml). Levels in *CORIO* mice were higher than in SPF, but results did not reach significance (1.8 ± 1.0 vs. 1.2 ± 1.0 ng/ ml; p = 0.2380).
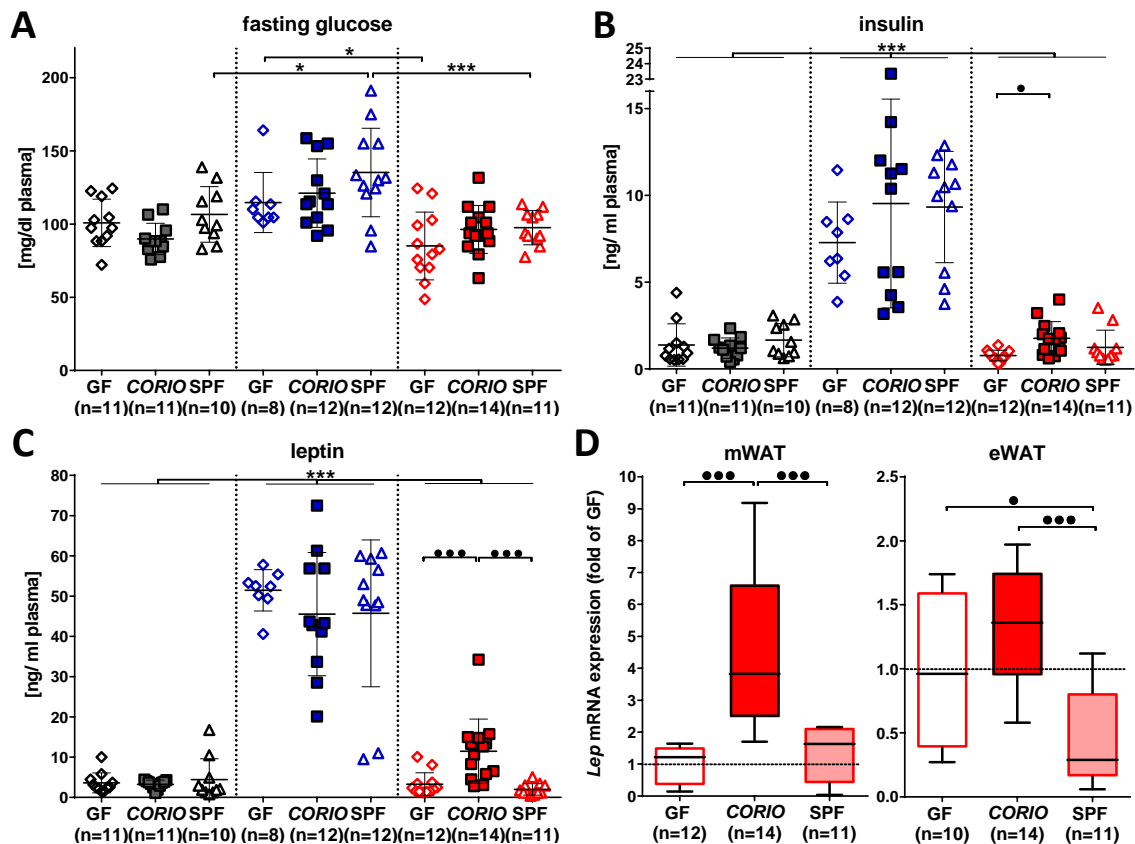
Figure 15: *CORIO* mice fed BA diet showed signs of metabolic disturbances.
(**A**) Fasting blood glucose measured in all mice after a 6 h fasting period. Measurement of systemic insulin (**B**) and leptin (**C**) levels. (**D**) Transcription analysis of *leptin* in mWAT and eWAT revealed increased expression in BA-fed *CORIO* mice. **CD**; **P-HFD**; **BA**; For detailed description of the statistical analysis see section 3.17; Number of mice in each group are indicated below the x-axis (n = number of mice measured).

WAT produces and secrets adipokines, including leptin, which has signaling functions of importance for host metabolism (e.g. leptin reduces hunger feeling and is also referred to as the satiety hormone). It is reported that obese patients have higher circulating levels of leptin due to increased fat mass, which can eventually lead to leptin resistance and thereby to uncontrolled hunger feeling. As expected, P-HFD feeding significantly increased systemic levels of leptin compared to CD and BA diet, a phenomenon that was independent of colonization (**Figure 15C**). Interestingly, *CORIO* mice fed BA diet had 3.5- to 5.8-fold higher circulating levels of leptin compared to both GF and SPF mice (11.5 ± 8.0 vs. 3.3 ± 2.9 and 2.0 ± 1.4 ng/ ml, respectively). In line with this observation, a four-fold increased *Lep* (gene of leptin) expression was observed in mWAT from *CORIO* compared to GF and SPF mice fed BA diet (**Figure 15D**). In eWAT, BA-fed *CORIO* mice had three-fold higher *Lep* expression levels compared to SPF mice, but difference with GF mice did not reach significance.

Altogether, the data presented in section 4.2.1 to 4.2.3 indicate that *Coriobacteriaceae* in combination with dietary supplementation of primary bile acid modulated host metabolism. The phenotype included increased fat mass and signs of metabolic disturbances (high insulin and leptin levels). To assess mechanisms behind the observed effects in greater detail, further characterization of adipose tissues was carried out.

4.2.4 Shifts in WAT mass were accompanied by functional changes

The *Coriobacteriaceae*-induced increase in WAT mass under BA feeding can either be due to increased fat cell size (hypertrophy) or increased fat cell number (hyperplasia). Therefore, WAT sections were H & E stained and adipocyte areas were measured in mice fed BA or P-HFD. P-HFD feeding led in all colonization groups to a higher abundance of larger adipocytes compared to BA diet (**Figure 16A**). No statistically significant differences in adipocyte size between the three colonization statuses could be observed, neither in the BA (**Figure 16B**) nor in the P-HFD (**Suppl. Fig. S4**) feeding groups. In the case of BA feeding, these results were confirmed by cell volume estimation in eWAT based on histone mass as obtained by proteome analysis (**see below**) (**Figure 16C**). These data hint at hyperplasia and the possible involvement of cell proliferation pathways as no obvious signs of hypertrophy were observed in *CORIO* mice with increased WAT mass.
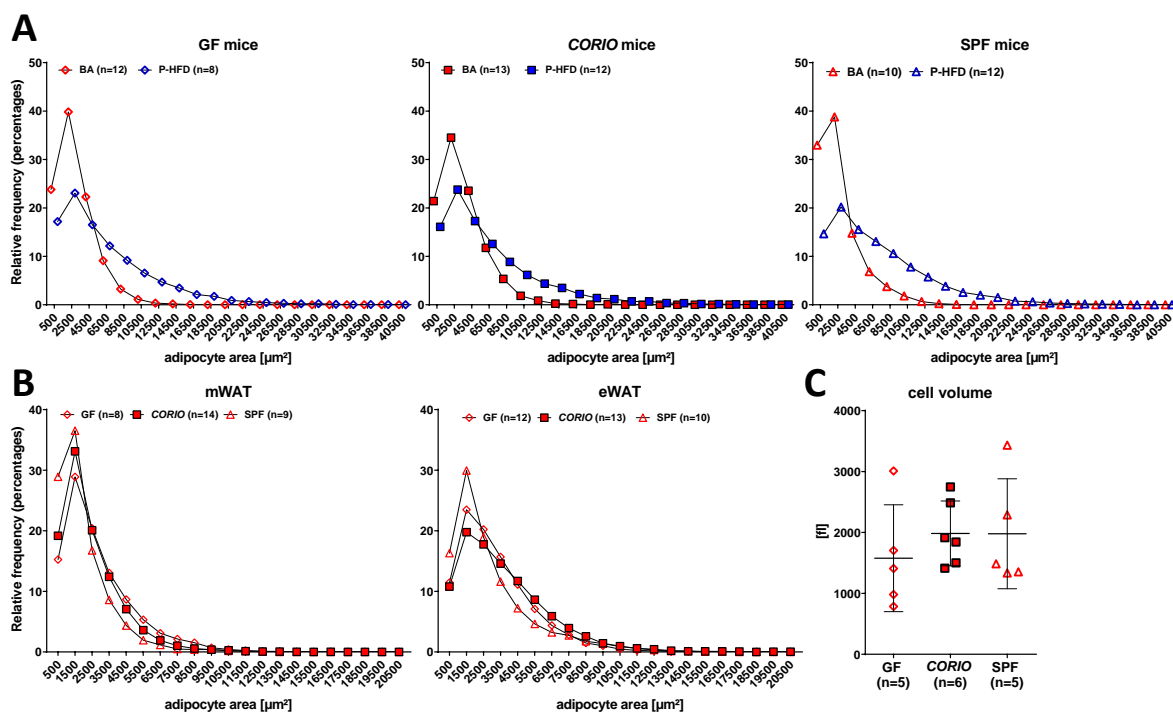

Figure 16: P-HFD, but not the combination of *CORIO* and BA diet, induced hypertrophy of adipocytes.
(**A**) Adipocyte sizes distribution in eWAT of P-HFD- and BA-fed mice of all three colonization groups revealed diet-induced changes. (**B**) Adipocyte sizes were measured in mWAT and eWAT from BA-fed mice to assess differences related to colonization. No differences were observed, which speaks in favor of a hyperplasia and not hypertrophy of adipocytes. (**C**) This observation was confirmed by calculation of cell volume using histone

mass based on proteome analysis of eWAT. **P-HFD**; **BA**; Number of mice measured in each group are indicated in brackets (n = number of mice measured).

To obtain detailed information about possible pathophysiological cellular mechanisms associated with increased WAT mass, non-targeted proteome analysis of eWAT collected from BA-fed mice was performed (n = 5-6 per colonization group). Principle component analysis (PCA) analysis of eWAT proteomes based on label-free quantification intensity of individual proteins clustered according to colonization status, despite marked inter-individual differences (**Figure 17A**).
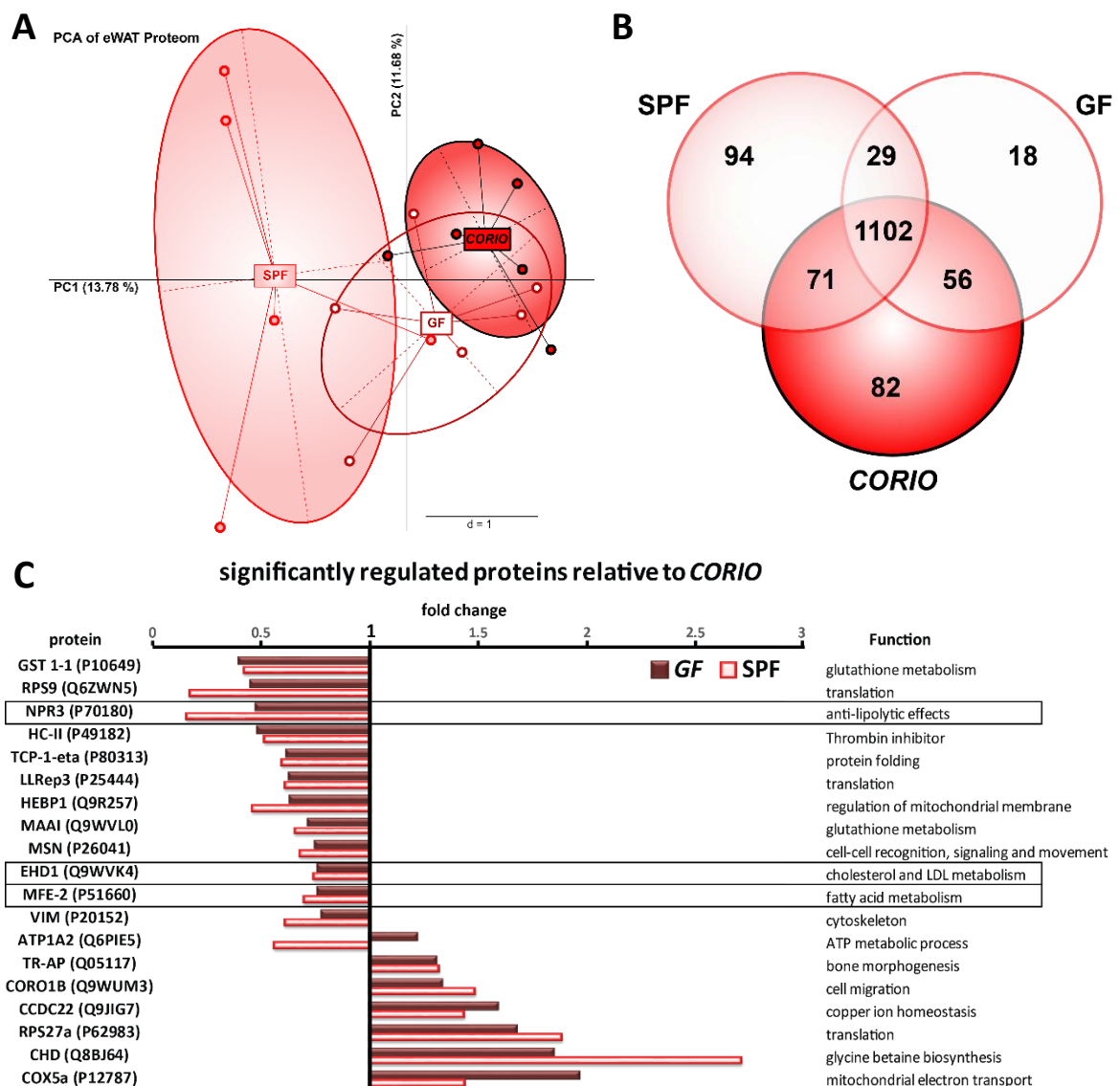
Figure 17: *Coriobacteriaceae* **modulated eWAT proteome in BA-fed mice.**
(**A**) PCA analysis of eWAT proteomes revealed that protein landscape separated according to colonization status. (**B**) Venn diagram showing shared and unique proteins. (**C**) *CORIO* mice (n = 6) were characterized by 19 proteins with significantly different signal intensities compared to SPF (n = 5) and GF mice (n = 6). Of those 19 proteins, 3 were related to lipid metabolism (black boxes). All values are fold changes relative to *CORIO* mice: < 1, lower intensity than *CORIO*; > 1, higher than *CORIO*; ATP1A2, sodium/potassium-transporting ATPase subunit alpha-2; TR-AP, tartrate-resistant acid phosphatase type 5; CCDC22, coiled-coil domain-containing protein 22; TCP-1-eta, t-complex protein 1 subunit eta; CHD, mitochondrial choline

dehydrogenase; CORO1b, coronin-1B; COX5a, mitochondrial cytochrome c oxidase subunit 5A; EHD1, EH domain-containing protein 1; GST 1-1, glutathione S-transferase Mu 1; MAAI, maleylacetoacetate isomerase; HEBP1, heme-binding protein 1; MFE-2, peroxisomal multifunctional enzyme type 2; NPR3, natriuretic peptide receptor 3; LLRep3, 40S ribosomal protein S2, RPS27a, ubiquitin-40S ribosomal protein S27a; RPS9, 40S ribosomal protein S9; HC-II, Heparin cofactor 2; VIM, vimentin; MSN, Moesin.

Venn diagram analysis was performed to identify shared and unique proteins according to bacterial colonization status and revealed that the three groups of mice shared 1102 proteins, whereas 94 proteins were unique to SPF, 18 to GF, and 82 to *CORIO* mice (**Figure 17B**). Of the 82 *CORIO*-specific proteins, 12 (14.6 %) were related to lipid metabolism, against 2 of 18 in GF (11.1 %) and 5 of 94 (5.3 %) in SPF mice (**Table 13**). These differences in the prevalence of lipid metabolism-related proteins between *CORIO* and GF/ SPF mice were not statistically significant (p > 0.05; Chi-squared test). One *CORIO*-specific protein caught our attention: cell death activator 3 (CIDEC; FSP27). CIDEC is localized at the membranes of lipid droplets in adipocytes and liver and favors lipid storage [247]. Serial comparison of proteomics data revealed 19 proteins which were significantly different comparing CORIO to GF and SPF mice. Of those, three were related to lipid metabolism (**Figure 17C**).

Table 13: Lipid metabolism-related proteins unique to the respective colonization group*

	Protein name	Gene name	Accession number
CORIO mice	Acyl-CoA dehydrogenase family member 11	Acad11	Q80XL6
	Acyl-CoA:lysophosphatidylglycerol acyltransferase 1	Lpgat1	Q91YX5
	3-ketoacyl-CoA thiolase B, peroxisomal	Acaa1b, Acaa1	Q8VCH0
	Phosphatidylinositol-glycan-specific phospholipase D	Gpld1	O70362
	STIP1 homology and U box-containing protein 1	Stub1, Chip	Q9WUD1
	Extended synaptotagmin-2	Esyt2, Fam62b	Q3TZZ7
	Cell death-inducing DFFA-like effector protein C	Cidec, Fsp27	P56198
	Sulfotransferase 1A1	Sult1a1 , St1a1, Stp, Stp1	P52840
	Beta-2-glycoprotein 1	Apoh,	Q01339
	Protein VAC14 homolog	Vac14	Q80WQ2
	Cholinephosphotransferase 1	Chpt1, Cpt1, Dn4	Q8C025
	Lambda-crystallin homolog	Cryl1, Cry	Q99KP3
GF mice	Selenocysteine lyase	Scly, Scl	Q9JLI6
	Ferrochelatase, mitochondrial	Fech	P22315
SPF mice	Serine protease HTRA2, mitochondrial	Htra2, Omi, Prss25	Q9JIY5
	Apolipoprotein C-III	Apoc3	P33622
	Lysophosphatidic acid phosphatase type 6	Acp6, Acpl1, Lpap	Q8BP40
	Retinol-binding protein 1	Rbp1, Crbpi, Rbp-1	Q00915
	Isopentenyl-diphosphate Delta-isomerase 1	Idi1	P58044

* Proteins were found in at least 5 of 6 *CORIO* or GF mice and 4 of 5 SPF mice

Measurement of free fatty acids in mWAT of mice from the BA group revealed that *CORIO* mice had significantly lower levels of lauric, myristic, palmitic, palmitoleic, stearic, oleic, linoleic, arachidic, eicosenoic and eicotrienoic acid compared to GF and SPF mice fed the same diet (**Table 14**).

Table 14: *CORIO* mice fed BA had lower levels of long-chain free fatty acids in mWAT

	GF	*CORIO*	SPF
lauric acid (C12:0)	10.8 ± 4.3	5.8 ± 1.8 [a, b]	13.2 ± 7.8
myristic acid (C14:0)	145.8 ± 61.5	77.2 ± 14.7 [a, b]	188.2 ± 113.2
palmitic acid (C16:0)	1694.0 ± 687.6	930.0 ± 262.8 [a, b]	2202.6 ± 1261.2
palmitoleic acid (C16:1)	816.8 ± 414.2	513.3 ± 110.9 [a, b]	763.2 ± 431.2
stearic acid (C18:0)	293.9 ± 107.9	170.2 ± 94.6 [a, b]	395.8 ± 211.9
oleic acid (C18:1)	2643.2 ± 961.0	1533.5 ± 478.3 [a, b]	3001.2 ± 1655.4
linoleic acid (C18:2)	1185.8 ± 485.5	767.3 ± 282.5 [a, b]	1904.7 ± 1037.9
arachidic acid (C20:0)	74.9 ± 34.6	48.1 ± 13.6 [b]	112.2 ± 63.3
eicosenoic acid (C20:1)	50.8 ± 22.5	27.5 ± 11.8 [a, b]	97.6 ± 62.2
eicotrienoic acid (C20:3)	14.8 ± 7.5	9.3 ± 5.2 [a, b]	17.1 ± 10.0
C20:3 n6/C20:4n6	41.6 ± 27.3	20.1 ± 7.8 [a, b]	68.1 ± 55.3

Data are expressed as µg free fatty acids/g mWAT (mean ± standard deviation); Significance ($p < 0.05$; one-way ANOVA and Holm-Sidak for pairwise tests) is indicated by superscript letters: [a] between *CORIO* (n = 13) and GF (n = 12) mice; [b] between *CORIO* and SPF (n = 9) mice.

In summary, *CORIO* mice fed BA diet had significantly higher WAT mass than GF and SPF mice fed the same diet, which might be due to an increase in the number of adipocytes. This increased fat mass led to metabolic disturbances as well as changes in eWAT proteome, including proteins involved in lipid metabolism. Since the liver is a master regulator of host lipid metabolism, we assessed hepatic physiology in greater detail.

4.2.5 *Coriobacteriaceae* modulated liver physiology

The liver is the central organ for metabolism of nutrients and metabolites absorbed in the intestine and transported via portal blood and for lipid, bile acid, and cholesterol homeostasis. The fact that *Coriobacteriaceae* modulate lipid homeostasis in WAT hints at possible effects on liver physiology. *Coriobacteriaceae* are involved in the metabolism of bile acids, synthesized from cholesterol in the liver. Moreover, Martinez *et al*. (2013) showed that the occurrence of *Coriobacteriaceae* was associated with cholesterol absorption and synthesis [116]. Hence, we first analyzed in detail cholesterol homeostasis in the mice.

CORIO mice were characterized by cholesterol levels of approximately 150 to 210 µM in systemic plasma, which was significantly elevated compared to GF (ca. 1.5-fold) and SPF mice (ca. 2.5-fold) (**Figure 18A**). Strikingly, this *CORIO*-associated hypercholesterolemia was observed in all diet groups.

Levels in GF mice were generally 1.7-fold higher than in SPF, with concentrations of 55 to 205 µM depending on diet. Moreover, in agreement with the interesting WAT phenotype described above, higher levels of cholesterol were also observed in iWAT of BA-fed *CORIO* mice (*CORIO*, 110.6 ± 107.2 µg/ g iWAT; GF, 47.7 ± 33.1; SPF, 74.6 ± 49.7) (**Figure 18B**).

The observed systemic hypercholesterolemia raised the question whether *CORIO* mice have altered secretion, absorption or *de novo* synthesis of cholesterol. Therefore, cholesterol levels were measured in caecal content, but *CORIO* mice did not show any changes, regardless of the diet (**Figure 18C**). Interestingly, significantly higher cholesterol levels were observed in the caeca of GF mice fed P-HFD (2.6 ± 0.3 vs *CORIO*: 1.9 ± 0.7 and SPF: 1.7 ± 0.2 mg/ g content). In portal plasma, CD-fed *CORIO* mice had two-fold higher cholesterol levels compared to GF and SPF mice (**Figure 18D**). No *CORIO*-specific differences were found in the other two dietary groups in portal blood, indicating that cholesterol absorption was not increased in those mice. Accordingly, the mRNA expression of the ileal cholesterol transporter Niemann Pick C1 like protein 1 (NPC1L1) was not affected (**Figure 18E**). Expression of the key enzyme for cholesterol *de novo* synthesis, HMG CoA reductase, did not show significant differences regarding colonization status or diets either (**Figure 18F**).
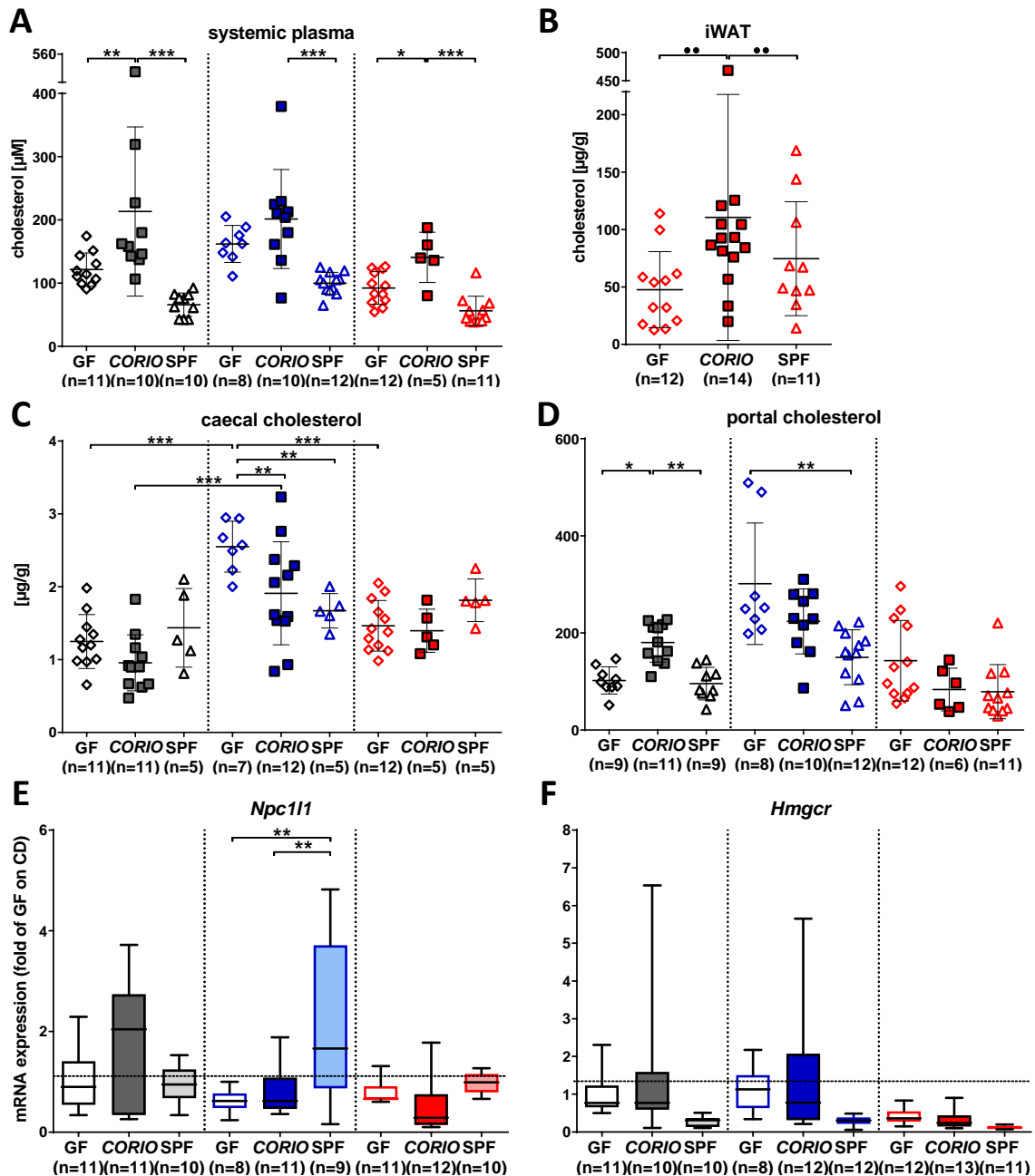
Figure 18: *Coriobacteriaceae* induced hypercholesterolemia.
(**A**) Measurement of systemic cholesterol levels revealed hypercholesterolemia in *CORIO* mice regardless of the diet. Cholesterol levels in iWAT (**B**), caecal content (**C**), and portal plasma (**D**). (**E**) Transcription analysis of the cholesterol transporter *Npc1l1* in total ileal tissue. (**F**) Hepatic expression of *Hmgcr*, the key enzyme in cholesterol *de novo* synthesis. **CD**; **P-HFD**; **BA**; For detailed description of the statistical analysis see section 3.17; Number of mice in each group are indicated below the x-axis (n = number of mice measured).

A common liver dysfunction associated with dietary and microbial factors is non-alcoholic fatty liver disease (NAFLD), which is characterized by steatosis (fat accumulation), changes in bile acid composition, and is also associated with hypercholesterolemia. Therefore, *Coriobacteriaceae* might influence the development of NALFD via their metabolic functions.

Measurement of liver weight showed that P-HFD triggered a significant increase in all three colonization groups, accompanied by increased NAFLD activity score (**Figure 19A** and **B**). No differences in liver weight or NAFLD score were observed between CD and BA fed mice. Another marker for NAFLD is an increased hepatic triglyceride content. P-HFD-fed mice had 3.4- to 11.3-fold higher triglyceride load compared to CD- and BA-fed mice (**Figure 19C**). Interestingly, hepatic triglyceride content was higher in *CORIO* mice fed the BA diet compared to GF and SPF on the same diet (12.0 ± 4.3 vs. 10.2 ± 3.3 and 4.3 ± 3.2 mg/ g, respectively), but results did not reach significance in GF mice.
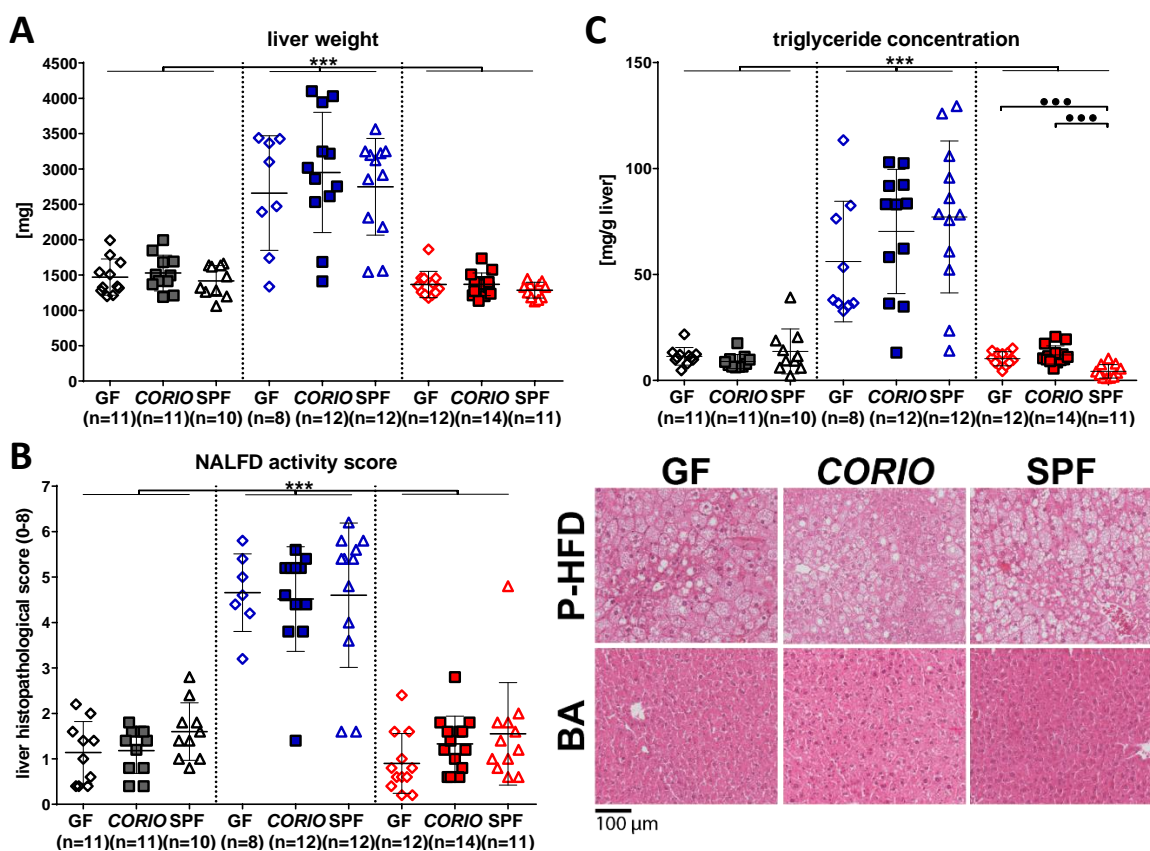
Figure 19: P-HFD induced NAFLD and *CORIO* mice fed BA had higher hepatic triglyceride levels.
(**A**) Liver weight measurement after 21 weeks of feeding. (**B**) Histopathological evaluation and representative pictures for P-HFD and BA diet of H&E stained liver sections. (**C**) Hepatic triglyceride concentrations. **CD**; **P-HFD**; **BA**; For detailed description of the statistical analysis see section 3.17; Number of mice in each group are indicated below the x-axis (n = number of mice measured).

This increase in hepatic triglycerides and the increased fat mass observed in BA-fed *CORIO* mice might be due to changes in the endogenous hepatic lipid metabolism (**Figure 20A**). Lipidomics of liver tissue revealed that BA-fed *CORIO* mice had a 1.6-fold higher amount of total fatty acids than SPF mice (152.6 ± 56 vs. 95.3 ± 26.5 nmol/ mg; p = 0.002), but differences in GF mice were not significant (131.2 ± 23.8 nmol/ mg; p = 0.383) (**Figure 20B**). Looking at fatty acid composition, a shift from polyunsaturated fatty acids (PUFAs) to monounsaturated fatty acids (MUFAs) was found in BA-fed

CORIO mice (**Figure 20C**). In line with this, *CORIO* mice had 2.5 to 12.6 % higher levels of C18:1(n-9) and 2.9 to 6.7 % lower levels of C18:2 (n-6) compared to GF and SPF mice (**Figure 20D**).

Next, we asked whether the observed different proportions of MUFAs were due to differences in fatty acid desaturation capacities. Therefore, the desaturation index was calculated for C16:0 and C18:0. In BA-fed *CORIO* mice, the C16:0 desaturation index was 1.3- to 2.1-fold higher compared to GF and SPF mice, respectively (**Figure 20E**). Furthermore, the C18:0 desaturation index was 2.2- to 2.6-fold higher in GF and *CORIO* than SPF mice. This increases desaturation capacity would imply a higher activity of hepatic SCD1, the key enzyme for fatty acid desaturation. However, measurement of hepatic Scd1 mRNA expression did not show any differences (**Suppl. Fig. S5**). As SCD1 is beside others regulated by SREBP1c, the mRNA expression of *Srebf1c* was measured. Interestingly, *CORIO* mice fed BA diet showed a 1.9-fold higher expression compared to SPF mice (**Figure 20F**).
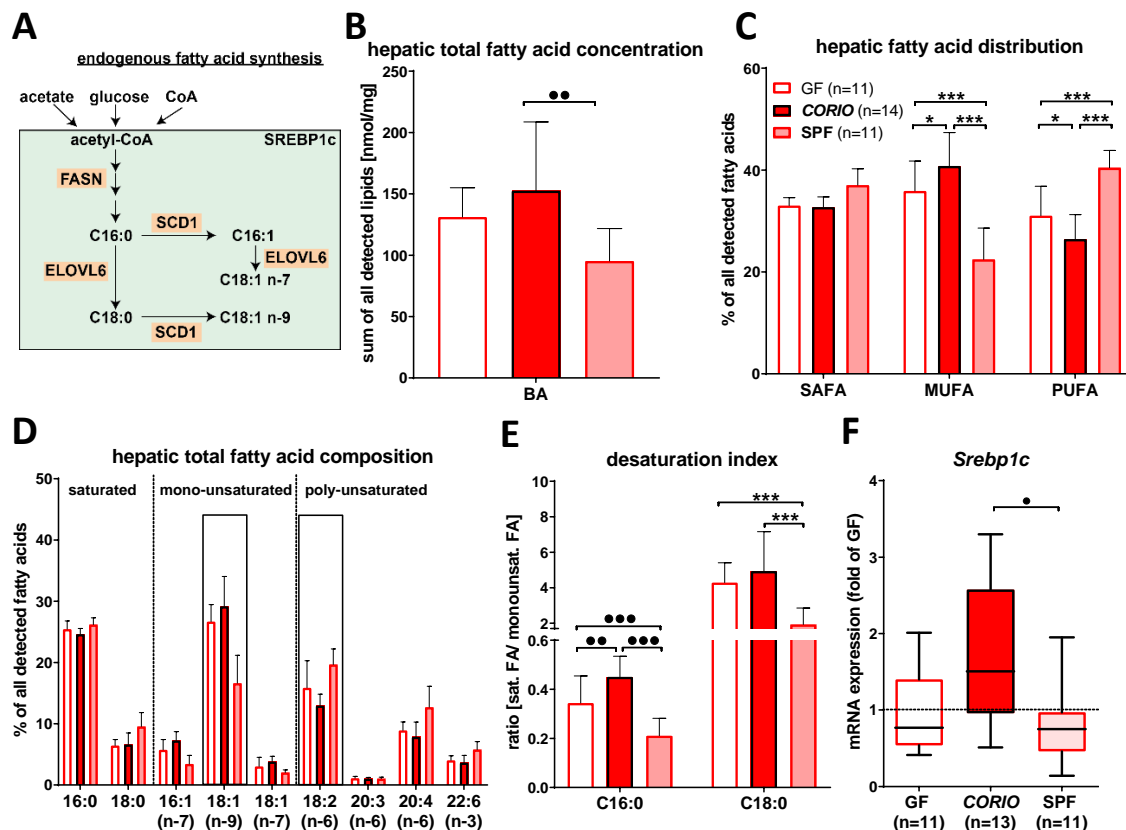
Figure 20: *Coriobacteriaceae* modulated hepatic fatty acid amount and composition in BA-fed mice.
(**A**) Overview of endogenous fatty acid synthesis [248]. (**B**) Calculation of the total amounts of detected fatty acids (FA). (**C**) Amounts of total saturated (SA), monounsaturated (MU) and polyunsaturated fatty acids (PUFA). (**D**) Hepatic total FA composition. Black boxes indicate significant differences. (**E**) Desaturation index, which is the ratio of monounsaturated to saturated FA, was used to analyze the activity of the hepatic enzyme Stearoyl-CoA desaturase (SCD1). (**F**) Hepatic expression of sterol regulatory binding protein 1c (Srebp1c), which controls fatty acid *de novo* synthesis. **BA**; For detailed description of the statistical analysis see section 3.17. Number of mice in each group are indicated in brackets (n = number of mice measured); FASN, fatty acid synthase; ELOVL, elongation of very long chain fatty acids protein

The lipidomics results aforementioned showed that *Coriobacteriaceae* interfere with hepatic lipid metabolism. The gut microbiota in SPF mice triggered down-regulation of the fatty acid transporter CD36 (also referred to as FAT) when fed CD and BA but not P-HFD diet. (**Figure 21A**). However, no *Coriobacteriaceae*-specific effects were observed. Interestingly, expression analysis of hepatic *Pparγ*, a key modulator of glucose and lipid homeostasis, revealed 2.7- to 6.9-fold higher levels in *CORIO* than GF and SPF mice fed BA diet (**Figure 21B**) Furthermore, *Pparγ* expression was 2.9- to 45-fold induced by P-HFD, depending on the colonization and diet with the highest induction in SPF mice. Furthermore, the expression of *Nr1h3*, which codes for liver X receptor (LXR), a key regulator of lipid and cholesterol homeostasis, was reduced by 20 % in *CORIO* than SPF mice which is a minor but significant difference (**Figure 21C**).
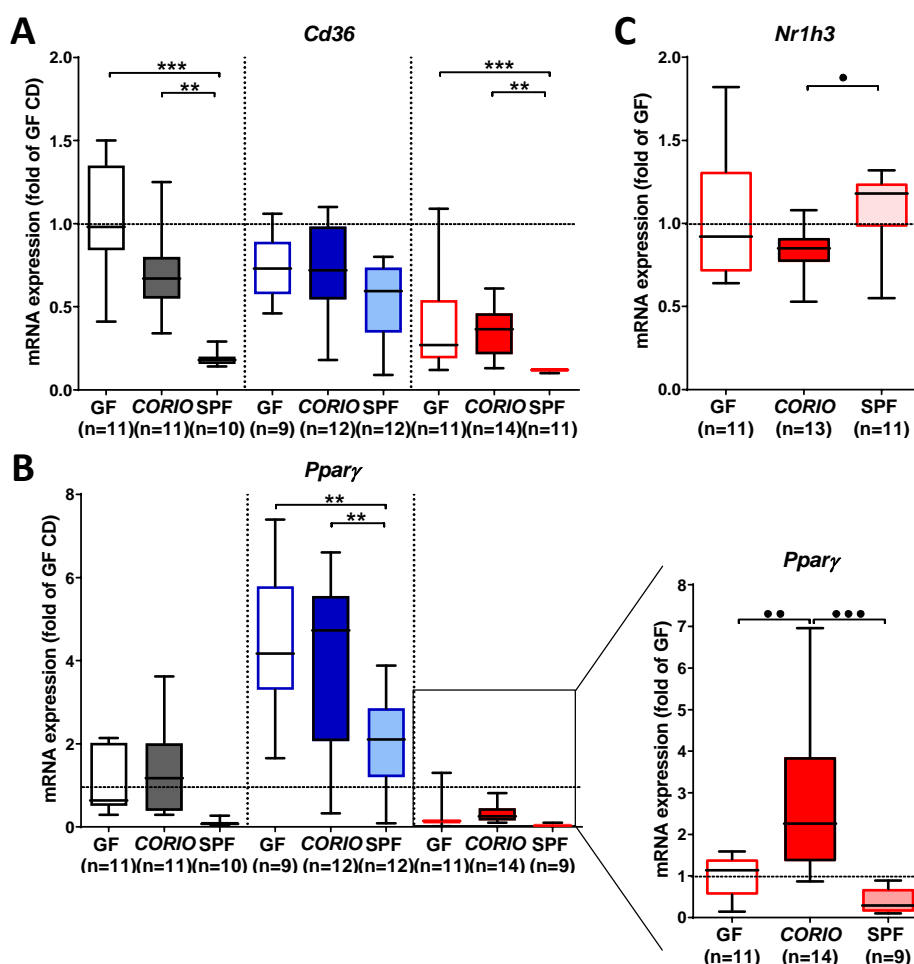
Figure 21: Diet and colonization status modulated expression of genes involved in hepatic lipid metabolism.
Hepatic mRNA expression of *Cd36* (**A**), a fatty acid transporter, and *Pparγ* (**B**), a modulator of lipid and glucose homeostasis as well as *Nr1h3* (**C**), a regulator of bile acid, cholesterol and lipid metabolism **CD**; **P-HFD**; **BA**; For detailed description of the statistical analysis see section 3.17; Number of mice in each group are indicated below the x-axis (n = number of mice measured).

In summary, all *CORIO* mice were characterized by systemic hypercholesterolemia and increased cholesterol levels in iWAT when fed BA diet. Additionally, BA-fed *CORIO* mice had higher hepatic triglyceride levels, accompanied by increased fatty acids content and shifts in their composition.

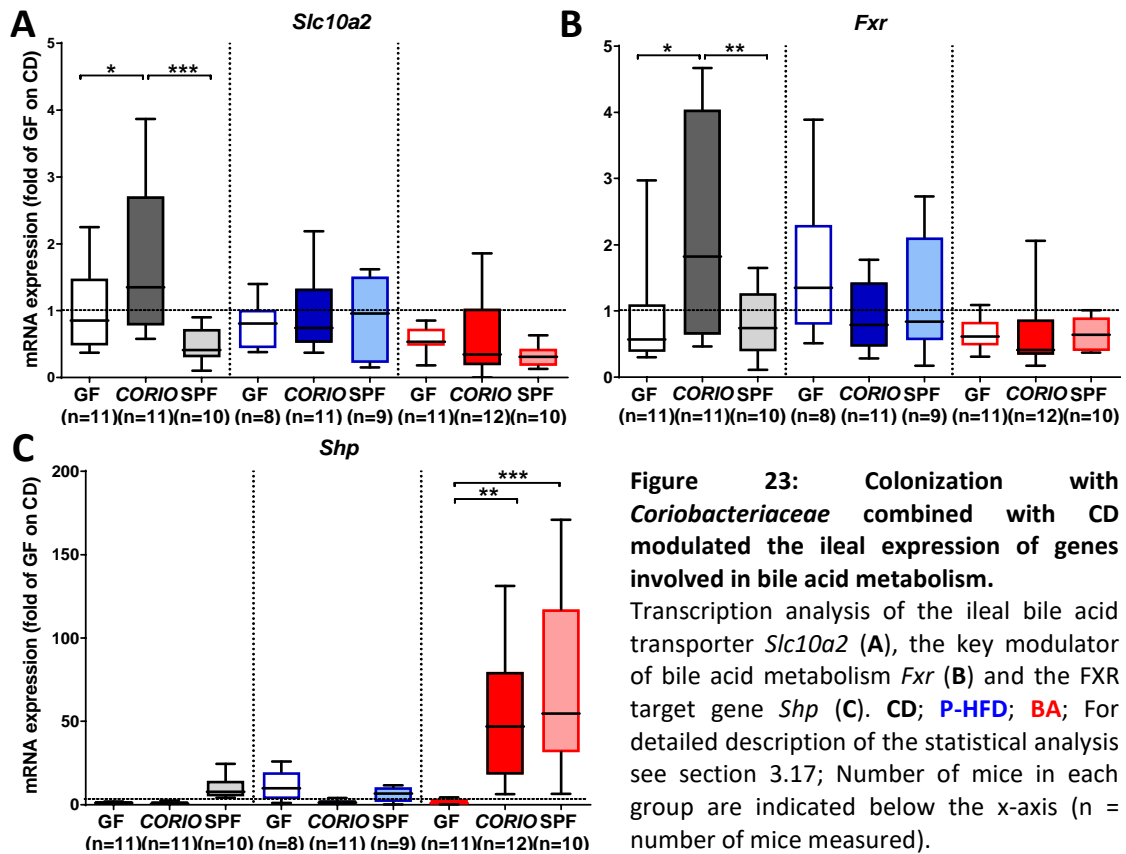### 4.2.6 Colonization with *Coriobacteriaceae* resulted in slight modulation of host bile acid metabolism

Coriobacteriaceae are capable of deconjugating bile acids and can further oxidize them via HSDH activity *in vitro*. Whether *Coriobacteriaceae* possess these functions *in vivo* has not been investigated yet. Therefore, bile acid composition of systemic and portal plasma as well as caecal content was analyzed in all dietary and colonization groups. Within the BA feeding groups, results for *CORIO* mice have to be handled carefully, due to low animal numbers.

PCA analysis of bile acid composition in systemic plasma revealed that SPF mice were most distant from *CORIO* and GF mice (**Figure 22A**). Only minor differences in bile acid composition were observed when comparing *CORIO* to GF and SPF mice. Calculation of total systemic bile acid concentration did not reveal significant differences in either of the groups (data not shown). In portal plasma, colonization with *Coriobacteriaceae* or a complex microbiota (SPF mice) was associated with decreased total bile acid amounts compared with GF, in mice fed P-HFD (**Figure 22B**). Within the BA group, *CORIO* mice had the highest amount of total bile acids ($253.1 \pm 138.8\ \mu M$). However, results reached significance only when compared with SPF mice ($88.5 \pm 50\ \mu M$), not with GF ($190.3 \pm 73.4\ \mu M$). A closer look at single bile acids in portal plasma of BA-fed mice showed that TCDCA levels were significantly higher in *CORIO* mice ($8.0 \pm 4.2\ \mu M$) compared to GF ($2.2 \pm 1.7\ \mu M$) and SPF mice ($1.2 \pm 0.6\ \mu M$).
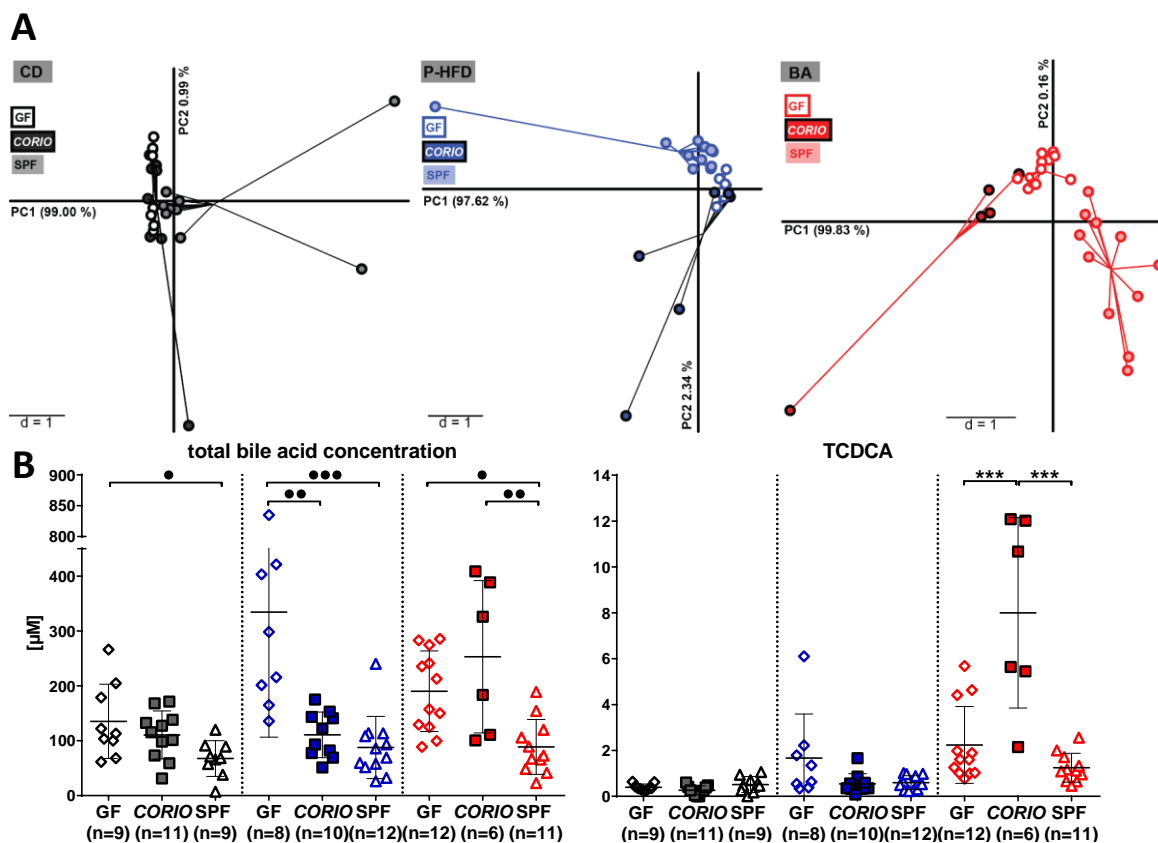
Figure 22: Bile acid composition in systemic and portal plasma is modulated by colonization and diet. (**A**) PCA analysis of the systemic bile acid composition within the three feeding groups. (**B**) Total bile acids and TCDCA concentration were measured in portal plasma. **CD**; **P-HFD**; **BA**; For detailed description of the statistical analysis see section 3.17; Number of mice in each group are indicated below the x-axis (n = number of mice measured).

Bile acids are re-absorbed in the intestine (primarily the ileum) as part of the enterohepatic cycle. Therefore, we measured mRNA levels of the ileal bile acid transporter ASBT (gene: *Slc10a2*) and observed a three-fold higher expression in *CORIO* mice fed CD compared to SPF mice (**Figure 23A**). In line with this, mRNA expression of *Fxr*, a key nuclear receptor for bile acids, was 2.4- to 2.9-fold higher in *CORIO* mice fed CD (**Figure 23B**). BA feeding strongly increased ileal *Shp* expression by 11- to 60-fold in all colonization groups compared to CD (**Figure 23C**). This effect was more pronounced in *CORIO* and SPF mice which showed 4.4- to 6.1-fold higher levels than GF mice. No differences in the expression of the FXR target gene *Fgf15/19* and the bile acid receptor *Tgr5* could be observed between the colonization groups (**Suppl. Fig. S6**).

Figure 23: Colonization with Coriobacteriaceae combined with CD modulated the ileal expression of genes involved in bile acid metabolism.
Transcription analysis of the ileal bile acid transporter *Slc10a2* (**A**), the key modulator of bile acid metabolism *Fxr* (**B**) and the FXR target gene *Shp* (**C**). **CD**; **P-HFD**; **BA**; For detailed description of the statistical analysis see section 3.17; Number of mice in each group are indicated below the x-axis (n = number of mice measured).

Next, bile acid composition in caecal content was analyzed. Levels of total bile acids were 7.7- to 11.5-fold higher in SPF mice compared to the other colonization groups when fed CD or P-HFD (**Figure 24A**). In GF and *CORIO* mice, BA feeding resulted in an increase of total ceacal bile acids concentrations up to SPF levels. Interestingly, BA feeding in SPF mice was not associated with increased caecal concentrations of bile acids when compared to the other diets. GF and *CORIO* mice fed P-HFD and especially BA diet showed much higher levels of conjugated bile acids than SPF mice (mostly tauro-conjugates) (**Figure 24B** and **C**). Levels of unconjugated bile acids were 39- to 651-fold lower in *CORIO* and GF compared to SPF mice, regardless of diet (**Figure 24D**). Oxo-bile acids were only detected in SPF mice (**Figure 24E**).
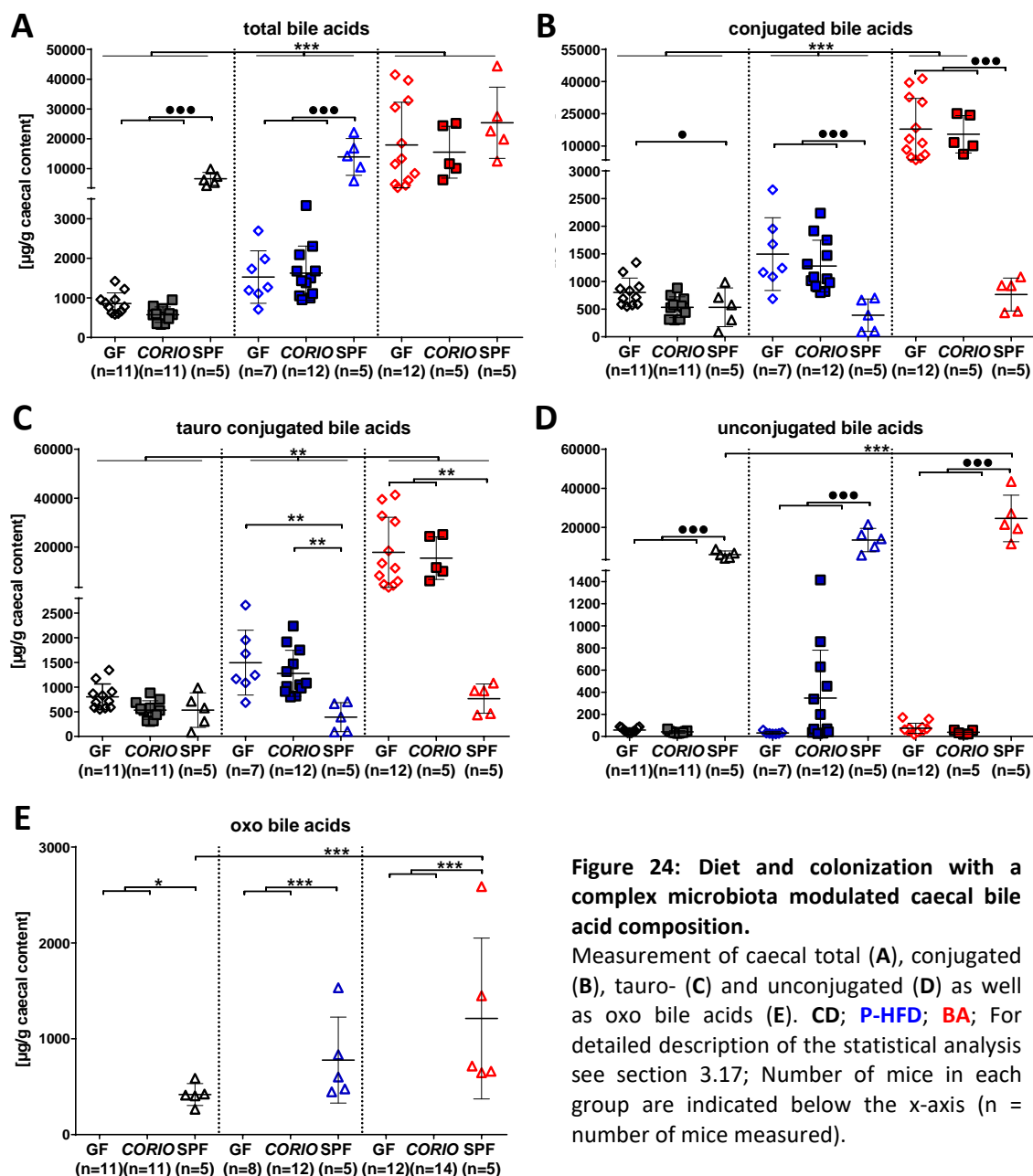
Figure 24: Diet and colonization with a complex microbiota modulated caecal bile acid composition.
Measurement of caecal total (**A**), conjugated (**B**), tauro- (**C**) and unconjugated (**D**) as well as oxo bile acids (**E**). **CD**; **P-HFD**; **BA**; For detailed description of the statistical analysis see section 3.17; Number of mice in each group are indicated below the x-axis (n = number of mice measured).

Absorbed bile acids can directly or indirectly modulate hepatic bile acid metabolism including *de novo* synthesis via FXR. Hence, hepatic *Fxr* expression was analyzed, which revealed that CD-fed *CORIO* mice had significantly higher expression levels compared to GF mice (1.6 ± 0.3-fold increase) (**Figure 25A**). To clarify whether FXR protein levels were as well higher in CD-fed *CORIO* mice, liver tissue sections were stained for FXR (**Figure 25B**). Calculation of the intensity/ µm² showed no differences for CD- and P-HFD-fed mice. However, *CORIO* (1122 ± 358 intensity/ µm²) and SPF mice (985 ± 385 intensity/ µm²) fed BA diet had significantly higher levels than GF mice (586 ± 271 intensity/ µm²).
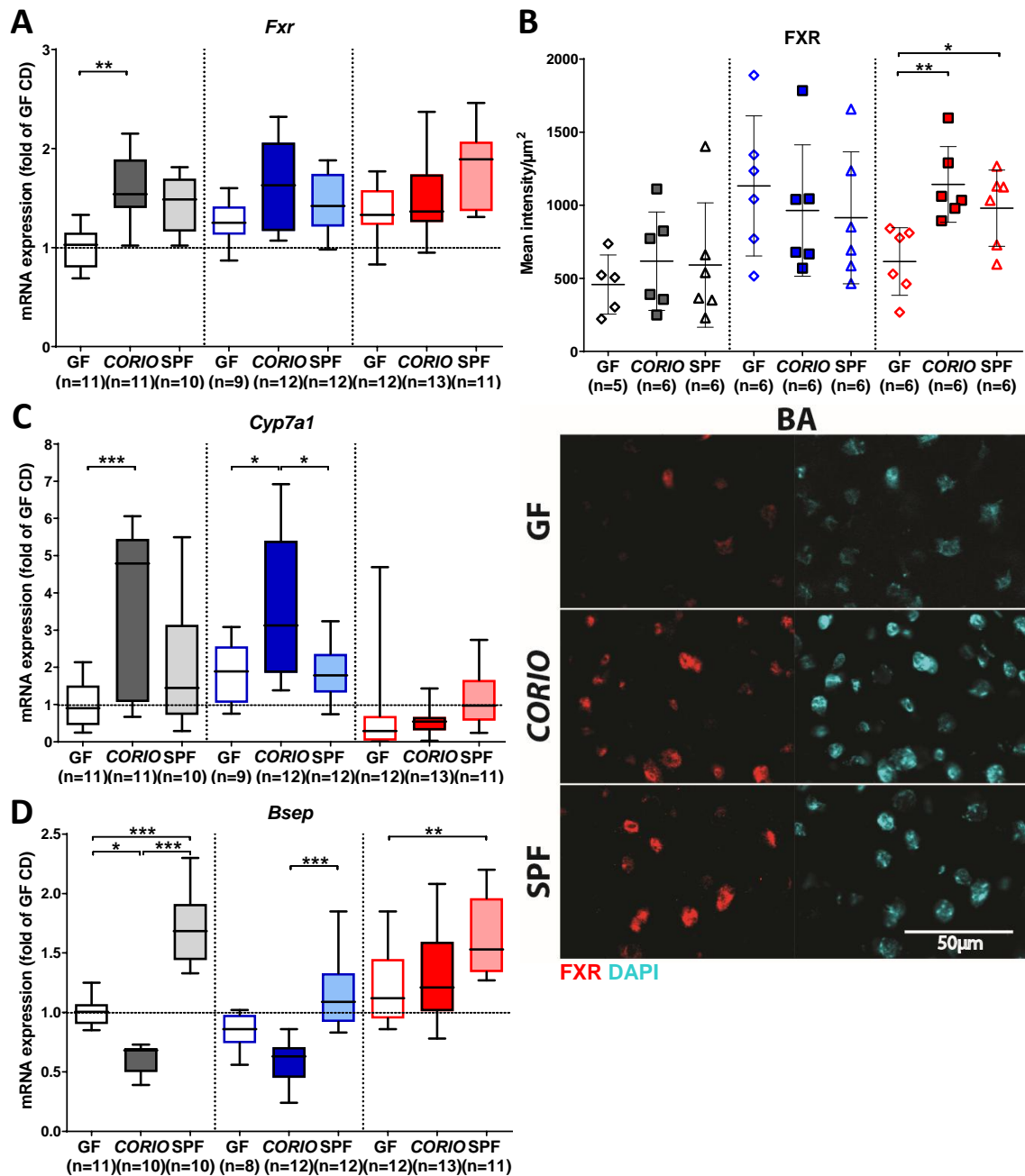
Figure 25: *Coriobacteriaceae* modulated hepatic bile acid metabolism.
(**A**) Hepatic mRNA expression of *Fxr*. (**B**) Quantification of hepatic FXR stained by IF. (**C**) Expression of hepatic *Cyp7a1*, which is one target gene of FXR and key modulator of bile acid *de novo* synthesis. (**D**) Transcriptional analysis of *Bsep*, which is responsible for the secretion of bile salts into the canaliculus of hepatocytes. CD; **P-HFD**; **BA**; For detailed description of the statistical analysis see section 3.17; Number of mice in each group are indicated below the x-axis (n = number of mice measured).

One target gene of FXR is *Shp*, which usually leads to the repression of bile acid *de novo* synthesis via *Cyp7a1*. Analysis of hepatic *Shp* expression did not show any differences within the feeding groups but its expression was increased after BA feeding (**Suppl. Fig. S7**). Transcriptional analysis of *Cyp7a1* showed that CD- and P-HFD-fed *CORIO* mice had three- to two-fold higher levels than GF mice (**Figure 25C**). Furthermore, FXR activates the hepatic bile acid transporter BSEP, involved in trafficking of bile

acids from hepatocytes to the gallbladder. However, *Bsep* expression was reduced by 35 % in CD- and P-HFD-fed *CORIO* compared to SPF mice (**Figure 25D**).

Beside the liver, bile acids can also modulate metabolism in WAT. *Fxr* as well as *Tgr5* expression in eWAT was two-times lower in *CORIO* mice fed BA diet compared to SFP mice (**Figure 26A**). In mWAT, *Tgr5* was significantly lower expressed in *CORIO* and GF than in SPF mice fed BA diet (**Figure 26B**), whereas no differences were observed for *Fxr* expression (**Suppl. Fig. S8**). To see whether these expression levels were associated with changes in bile acid concentrations, total bile acid amounts were measured in eWAT, mWAT and iWAT of BA-fed mice (**Figure 26C**). In general, the highest amounts of bile acids were found in mWAT (10-fold higher vs. iWAT and eWAT). In mWAT, *CORIO* (7732 ± 4345 ng/ g tissue) and GF mice (5431 ± 4761) had significantly higher bile acid levels than SPF mice (1453 ± 1020 ng/ g tissue). Furthermore, GF mice (316 ± 216 ng/ g tissue) had four-fold higher bile acid levels compared to SPF mice (79 ± 56) in iWAT. No differences were observed in eWAT.
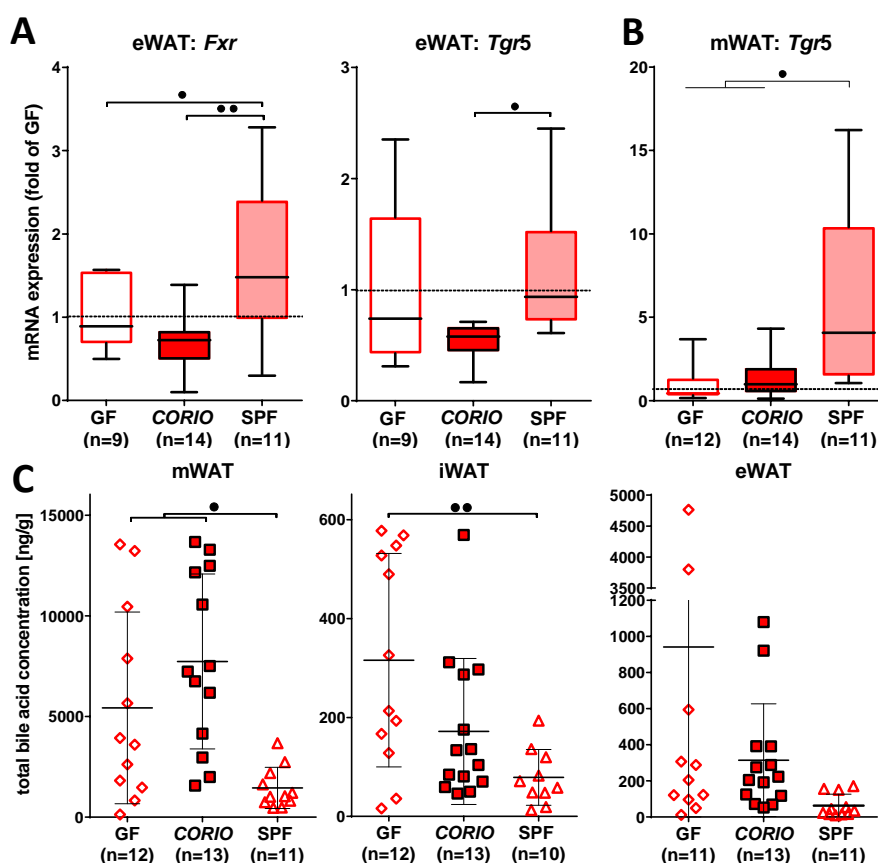

Figure 26: Total bile acid concentration was highest in mWAT of GF and *CORIO* mice.
(**A**) mRNA Expression of *Fxr* and *Tgr5* in eWAT. (**B**) Transcription analysis of T*gr5* in mWAT. (**C**) Total bile acid concentration in mWAT, iWAT and eWAT. **BA**; For detailed description of the statistical analysis see section 3.17; Number of mice in each group are indicated below the x-axis (n = number of mice measured).

Metabolic dysregulation can be associated with alterations of immune responses, and bile acids are known to regulate inflammatory pathways. Hence, we assessed whether *Coriobacteriaceae* modulate immune infiltration in the liver. Therefore, IHC staining of hepatic MHCII-, F4/80-, Ki67-, CD3- and B220-positive cells was performed. *CORIO* mice fed BA diet were characterized by 55 % lower amounts of MHCII-positive cells compared to GF and SPF mice (**Figure 27**). Regarding F4/80-positive

cells (including mostly macrophages like Kupffer cells in the liver), BA-fed *CORIO* and GF mice had two-fold less positive cells than SPF mice. No differences were observed regarding MHCII- and F4/80-positve cells in CD- and P-HFD-fed mice as well as in Ki67-, CD- and B220-positive cells in neither of the groups (data not shown). Furthermore, hepatic inflammation was assed via *Tnf-α* and *Il*-1β expression (**Suppl. Fig. S9**). However, no differences were found.
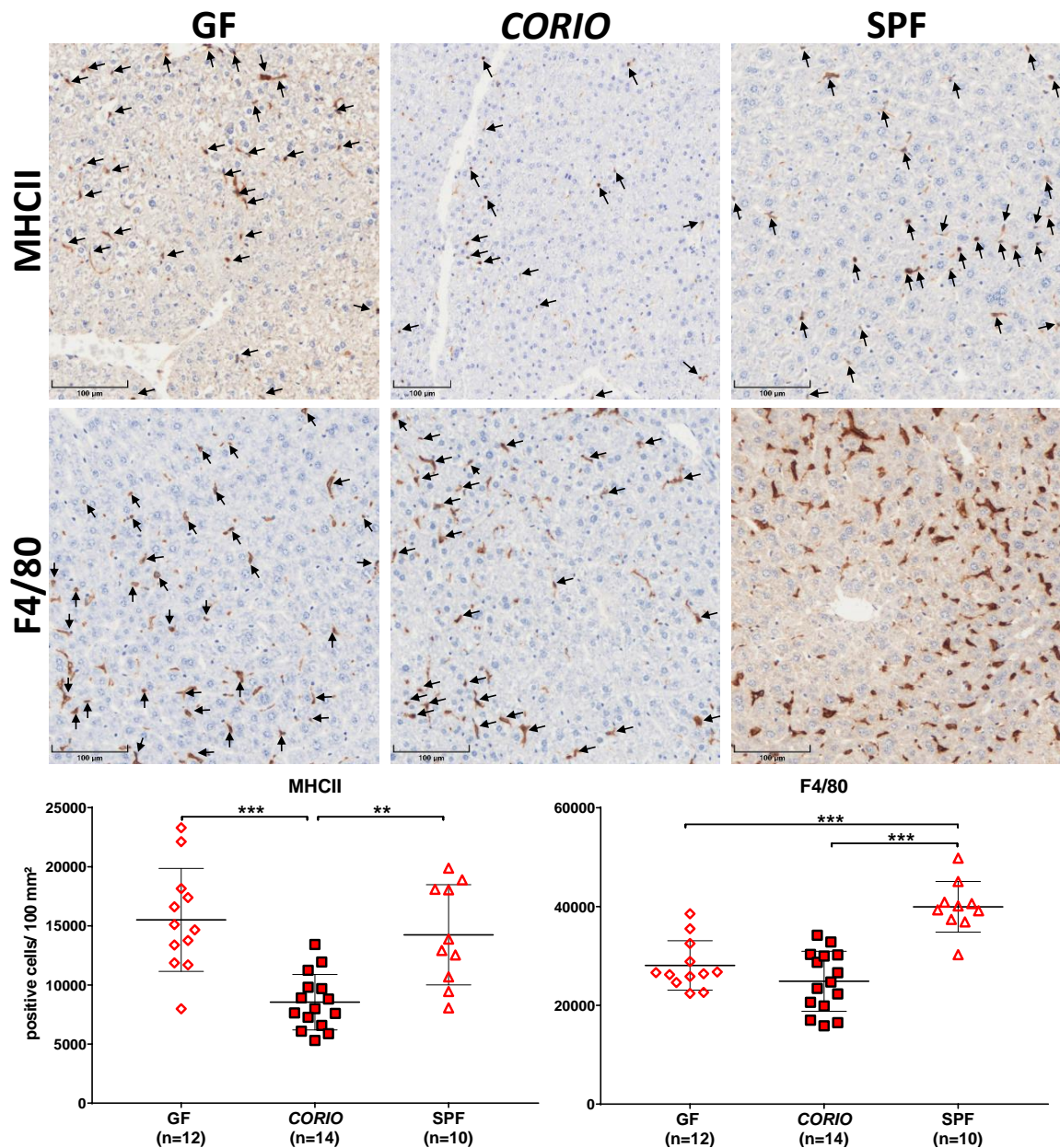
Figure 27: *CORIO* **mice fed BA diet had lower hepatic infiltration with MHCII positive cells.**
(**A**) IHC staining of liver tissue with MHCII (**upper panel**) and F4/80 (**lower panel**) antibodies was performed to reveal differences in hepatic immune cell in filtration within BA fed mice. (**B**) Quantification of hepatic MHCII and F4/80 positive cells. **BA**; Arrows indicate counted cells; For detailed description of the statistical analysis see section 3.17; Number of mice in each group are indicated below the x-axis (n = number of mice measured).

All the data aforementioned prove that intestinal *Coriobacteriaceae* can modulate host metabolism - in particular lipid homeostasis. In order to characterize the effects of these gut bacteria in more detail, we aimed at assessing the impact of fat source (plant or animal) in combination with BA feeding.

Unfortunately, these experiments were completed with GF and SPF mice only, because the isolator hosting *CORIO* mice became contaminated towards the end of the trial. The experiments with *CORIO* mice could not be repeated at a later time point because of the sake of comparison and due to the fact that the breeding isolator of C57BL/6N mice was contaminated as well. Hence, the next section focuses on the impact of different dietary fat source in combination with BA on host metabolism in GF and SPF mice.

4.3 The impact of dietary fat source on host metabolism depends on the gut microbiota

To test the influence of a combination of different fat sources and bile acids, mice were fed either CD, BA, palm oil- or lard-based HFD supplemented with bile acids (P- or L-HFD-BA) for 8 weeks (see experimental details in section 3.5).

4.3.1 Bile acid supplementation prevented diet-induced obesity in GF but not in SPF mice

Feeding two different HF-BA diets for 8 weeks resulted in increased body weight in SPF mice by 1.1- to 1.2-fold (**Figure 28A**). Although mean body weight was higher in the L-HFD-BA (36.3 ± 2.6 g) vs. P-HFD-BA group (34.6 ± 4.1 g), results did not reach significance ($p = 0.234$). Interestingly, GF mice did not gain weight when fed any of the two HF-BA diets. Of note, GF mice were characterized by lower body weight compared to SPF mice from start and throughout the whole trial, regardless of diet (**Suppl. Fig. S10**).

Inspection of WAT revealed higher fat mass in SPF mice fed both HFD-BA compared to CD and BA (**Figure 28B**). Interestingly, SPF mice on L-HFD-BA had 1.5-fold higher WAT mass than those fed P-HFD-BA (3145 ± 880 vs. 2049 ± 1332 mg; $p < 0.01$). In GF mice, no significant diet-induced changes in total WAT weight were observed. Regression analysis confirmed the significant differences in WAT mass between SPF mice fed the P- or L-HFD-BA (**Figure 28C**).
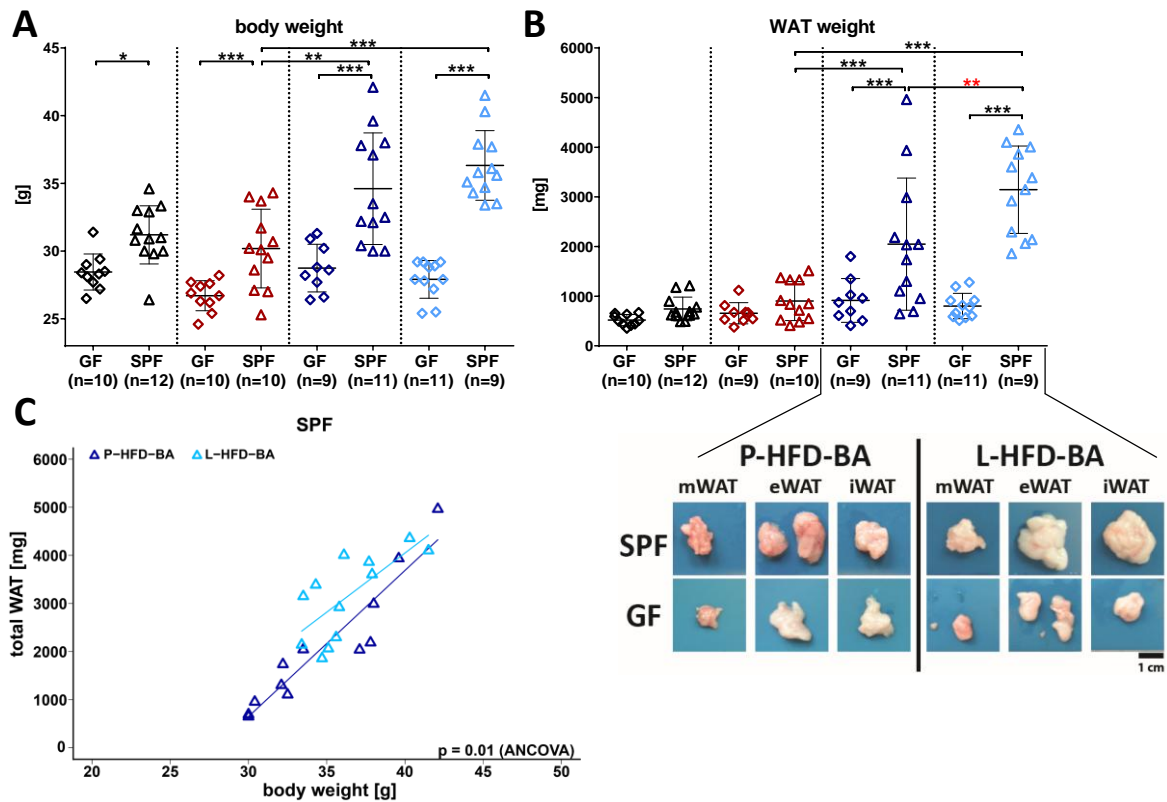
Figure 28: Bile acid supplementation prevented body weight gain in GF mice fed HFD.
(**A**) Body and (**B**) total WAT mass after 8 weeks of feeding. (**C**) Regression analysis of total WAT and body weight. **CD**; **BA**; **P-HFD-BA**; **L-HFD-BA**; For detailed description of the statistical analysis see section 3.17; Number of mice in each group are indicated below the x-axis (n = number of mice measured).

Next, we assessed whether the WAT mass differences observed had any pathophysiological consequences on the metabolic status of mice. Fasting blood glucose levels were generally higher in SPF vs. GF mice; this difference reached significance in the case of L-HFD-BA feeding (154 ± 21.8 vs. 88.5 ± 11.9 mg/ dl), indicating possible detrimental effects on glucose homeostasis in these mice (**Figure 29A**). Half of the fasted mice were challenged with an OGTT, which showed that L-HFD but not P-HFD in combination with BA triggered glucose intolerance (**Figure 29B**). Statistical comparison of areas under the curve (AUC) confirmed the significance of this observation with 30771 ± 4156 mg/ dl x min for L-HFD-BA vs. 23195 ± 2599 for P-HFD-BA (p = 0.0034) (**Suppl. Fig. S11**). Besides obesity, HF feeding is usually associated with comorbidities like insulin resistance. Measurement of circulating levels of insulin and leptin revealed higher levels in mice on both HF-BA diets under SPF but not GF conditions (**Figure 29C**). However, no differences were observed between the two HFDs. Measurement of the plasma cytokines TNFα, IL-6, IL-27, INFβ, INFγ, IL-1α, IL-1β, IL.23, IL-17a, IL-12p70, IL-10 and MCP1 did not show any diet or colonization dependent changes (data not shown).

In summary, differences between the two HF-BA diets were observed in SPF but not GF mice. The most striking result was the increased WAT mass and impaired glucose tolerance in SPF mice fed L-HFD-BA.
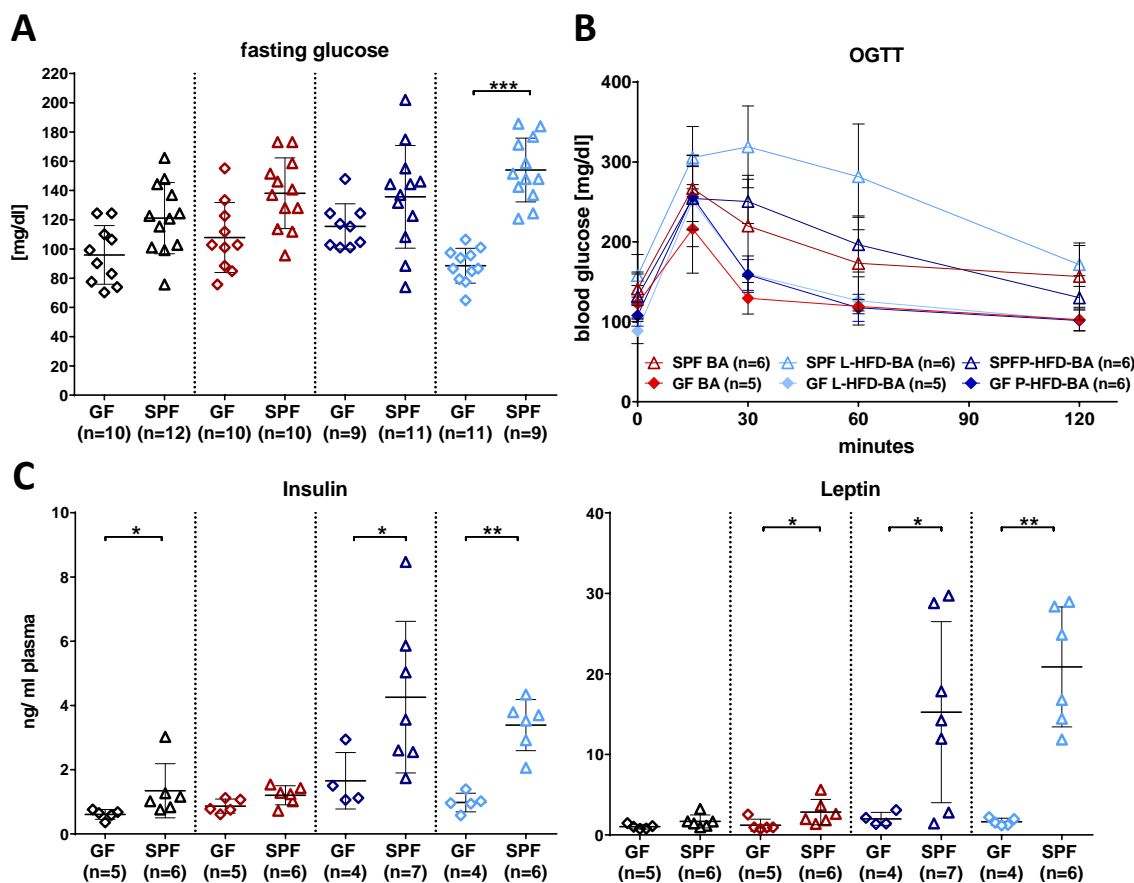

Figure 29: L-HFD-BA but not P-HFD-BA altered glucose tolerance in SPF mice.
(**A**) Measurement of glucose levels after 6h of fasting. (**B**) OGTT showed that SPF mice fed L-HFD-BA diet had impaired glucose tolerance. (**C**) Levels of insulin and leptin were measured in systemic plasma by Milliplex MAP mouse serum adipokine panel kit. **CD**; **BA**; **P-HFD-BA**; **L-HFD-BA**; For detailed description of the statistical analysis see section 3.17; Number of mice in each group are indicated below the x-axis (n = number of mice measured).

4.3.2 Diet and colonization status modulated hepatic lipid and bile acid metabolism

The liver is the central organ for lipid, bile acid, and cholesterol metabolism. Long-term HFD feeding is known to increase liver weight and induce NALFD, and these effects can be counteracted by the addition of BA in the diet. HFD-BA feeding for 8 weeks reduced liver to body weight ratios in GF mice by 10 to 13 % and in SPF mice by 20 to 26 % when compared to BA diet alone (**Figure 30A**). No statistically significant differences between the colonization groups were seen. Histological observation of liver sections revealed no, or only mild signs of steatosis in HFD-BA fed SPF but not GF mice (data not shown). Next, we wanted to identify whether this phenotype resulted in changes in liver physiology. Therefore, hepatic lipid metabolism was analyzed in fasted animals (n = 4 – 7). Gene

expression analysis of *Acaca*, which encodes the rate-limiting enzyme in long-chain fatty acid synthesis, showed a two-fold higher expression in SPF mice fed CD compared to all diets containing BA (**Figure 30B**). Expression of other lipid metabolism-related genes, including *Cd36*, *Srebf1c*, *Mlxipl*, *Pparα,* and *Pparγ*, did not show differences related to colonization or diet (**Suppl. Fig. S12**).
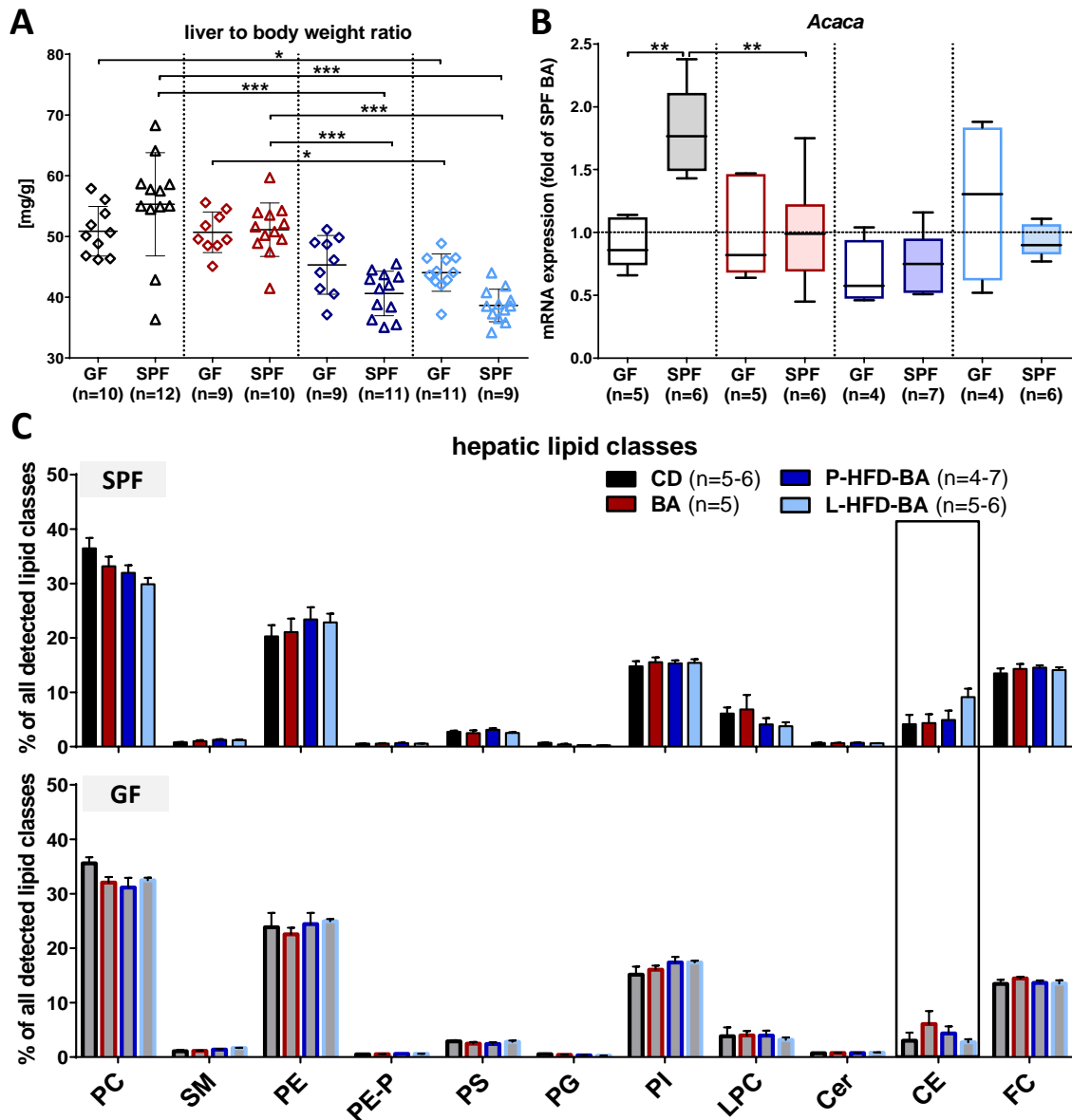

Figure 30: Short-term HFD-BA feeding reduced liver to body weight ratio.
(**A**) Liver to body weight ratio. (**B**) mRNA expression of *Acaca*, the rate-limiting enzyme of long-chain fatty acid biosynthesis. (**C**) Measurement of lipid classes in the liver of SPF (**upper panel**) and GF mice (**lower panel**) fed the four different diets. The black box indicates the major and significant finding. PC, phosphatidylcholine; SM, sphingomyelin; PE, phosphatidylethanolamine; PE-P, plasmalogen; PS, phosphatidylserine; PG, phosphatidylgcerol; PI, phosphatidylinositol; LPC, lyso-PC; Cer, ceramide; CE, cholesterol ester; FC, free cholesterol; **CD**; **BA**; **P-HFD-BA**; **L-HFD-BA**; For detailed description of the statistical analysis see section 3.17; Number of mice in each group are indicated below the x-axis or in brackets (n = number of mice measured).

Thereafter, hepatic lipid classes in fasted mice were measured. The major finding was that the amounts of cholesterol esters (CEs) were influenced by diet and colonization status (**Figure 30C**). BA feeding of GF mice increased the levels of CEs by 50 % compared to CD feeding. In SPF mice, L-HFD-BA-fed mice had a two-fold higher concentration of CEs than mice fed with CD, BA and P-HFD-BA. This was not observed in GF mice.

A closer look at phosphatidycholine (PC), which is the major component of cell membranes, showed that HFD-BA feeding regardless of the fat source significantly reduced the concentrations of PC 34:1 by 3 to 3.5 % in SPF but not GF mice (**Figure 31**). Additionally, the concentration of PC 36:4 was increased by 2.6 % in P-HFD-BA-fed compared to L-HFD-BA SPF mice.
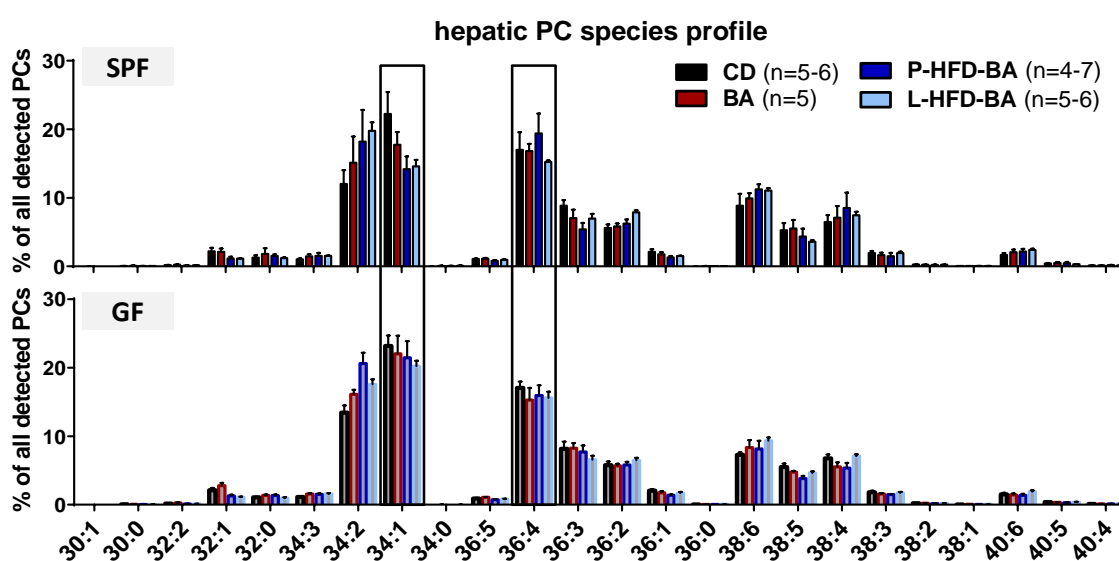
Figure 31: Diet and colonization status modulated hepatic PC species.
Measurement of hepatic PCs in the liver of SPF (**upper panel**) and GF mice (**lower panel**) fed the four different diets. Black boxes indicate the major and significant findings. **CD**; **BA**; **P-HFD-BA**; **L-HFD-BA**; For detailed description of the statistical analysis see section 3.17. Number of mice in each group are indicated in brackets (n = number of mice measured).

The next lipid class we looked at was lyso-PC (LPC), which is formed from PC (**Figure 32**). In SPF mice, BA-supplementation alone and in combination with HFD reduced the levels of LPC 16:0 by 5.5 to 6.2 %. However, only L-HFD-BA feeding reduced LPC 16:0 levels in GF mice by 5 %. The levels of LPC 18:1 were significantly reduced by BA-supplementation in GF and SPF mice. In contrast, in both colonization groups P- and L-HFD-BA feeding increased the concentration of LPC 18:2 by 3.5 to 6.4 %. Furthermore, P-HFD-BA-fed SPF but not GF mice had 2 % higher levels of LPC 20:4 compared to BA-fed mice.
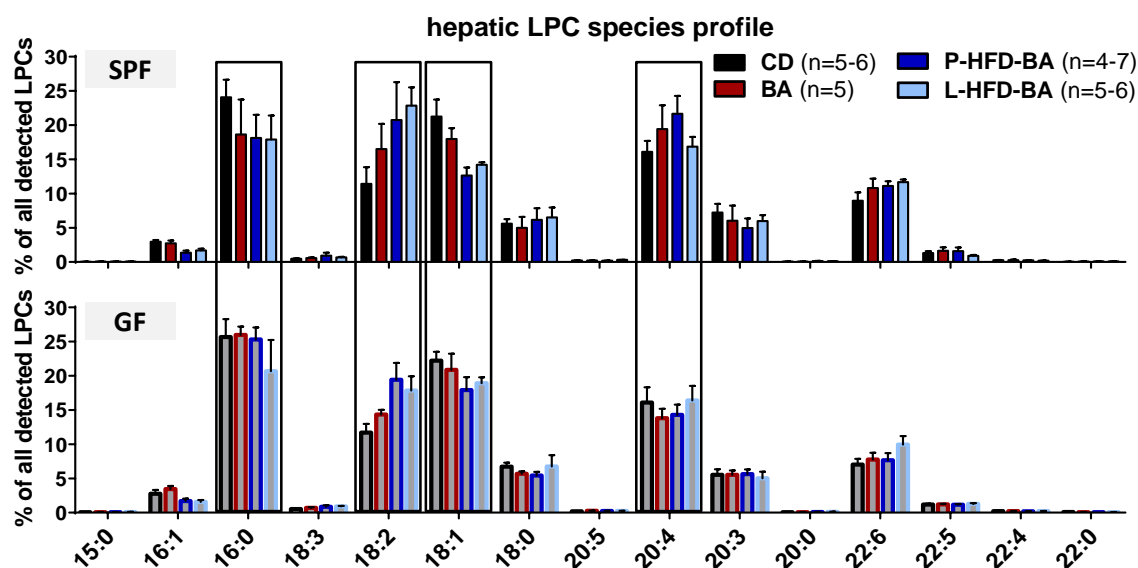
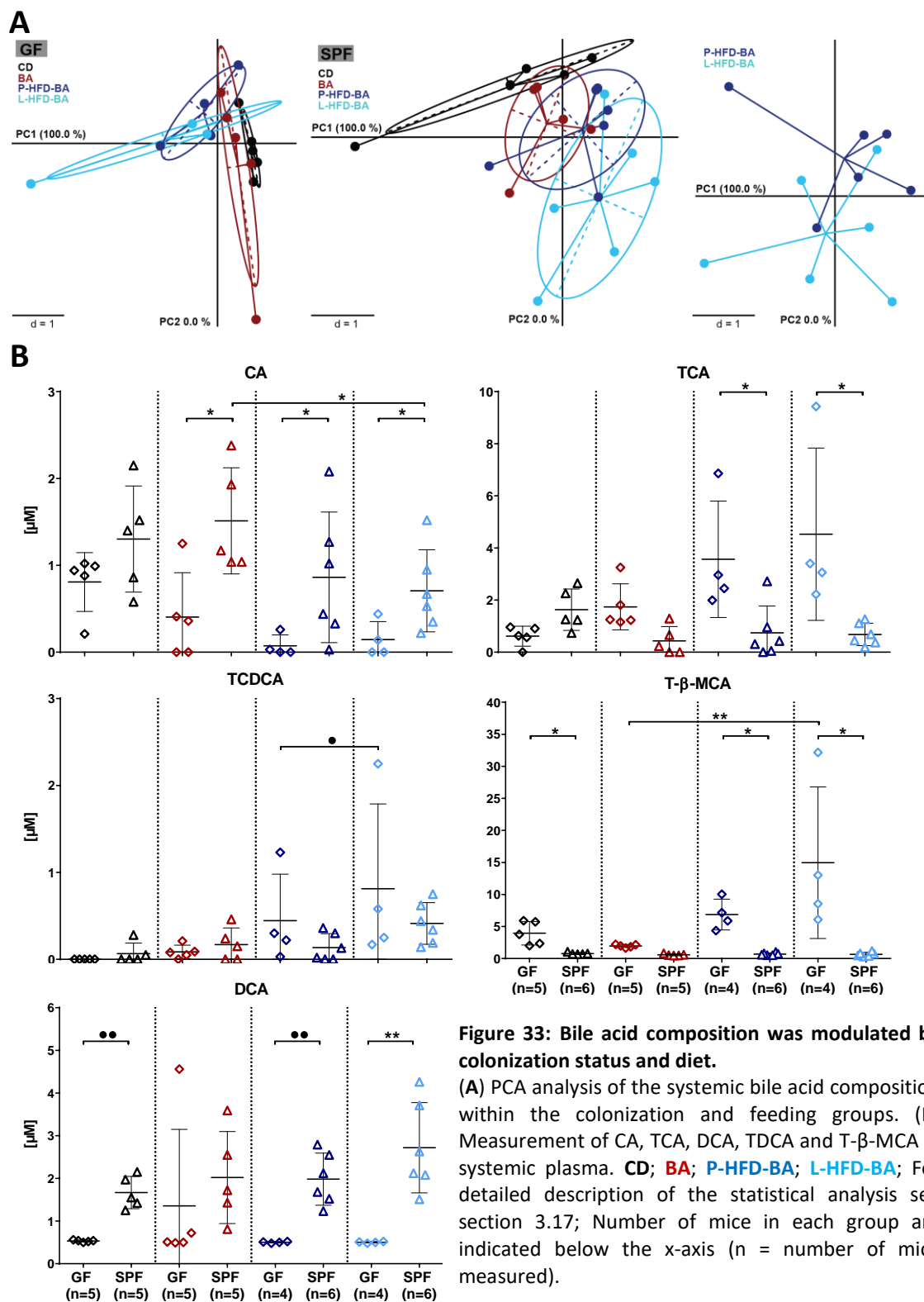**Figure 32: Diet and colonization status modulated hepatic LPC species.**
Measurement of lipid classes in the liver of SPF (**upper panel**) and GF mice (**lower panel**) fed the four different diets. Black boxes indicate significant differences. **CD**; **BA**; **P-HFD-BA**; **L-HFD-BA**; For detailed description of the statistical analysis see section 3.17. Number of mice in each group are indicated in brackets (n = number of mice measured).

As the liver is also responsible for bile acid and cholesterol homeostasis, we analyzed bile acid composition in systemic plasma of fasted mice. PCA plots were generated for the different colonization and feeding groups to identify diet and colonization induced changes in bile acid composition (**Figure 33A**). This analysis showed that the different diets had a stronger effect on bile acid composition in SPF compared to GF mice.

Additionally, the compositions of SPF and GF mice are clearly separated within each diet group. Looking closer at the single bile acids, we found over 3.4-fold higher concentrations of CA, DCA and TDCA in SPF mice compared to GF mice (**Figure 33B**). Additionally, CA concentration was 50 % higher in BA- than in L-HFD-BA-fed SPF mice. For the bile acids TCA and T-β-MCA, at least 4.8-fold higher levels were observed in GF compared to SPF mice. Surprisingly, no differences in circulating cholesterol levels were observed (**Suppl. Fig. S13**).

Summed up, the results indicate that the colonization status, the dietary supplementation of primary bile acid and the dietary fat source change hepatic lipid profile as well as bile acid metabolism.

Figure 33: Bile acid composition was modulated by colonization status and diet.
(**A**) PCA analysis of the systemic bile acid composition within the colonization and feeding groups. (**B**) Measurement of CA, TCA, DCA, TDCA and T-β-MCA in systemic plasma. **CD**; **BA**; **P-HFD-BA**; **L-HFD-BA**; For detailed description of the statistical analysis see section 3.17; Number of mice in each group are indicated below the x-axis (n = number of mice measured).

4.3.3 Dietary fat source modulates gut microbiota profiles

As described above, one main difference between GF and SPF mice is caecum weight. Therefore, the caecum to body weight ratio was calculated. BA, P- and L-HFD-BA feeding of GF reduced the caecum weight by over 1.5-fold (**Figure 34A**). As in the literature described, we also observed reduced

caecum weight in SPF mice fed HFD. Measurement of viable bacteria in caecal content of SPF mice by anaerobic cultivation revealed no differences between diets (**Figure 34B**). No viable bacteria were observed in GF mice, which was also confirmed by gram staining (data not shown).

High-throughput sequencing of 16S rRNA gene amplicon libraries was performed to identify diet-induced shifts in caecal microbiota profiles from SPF mice. Beta-diversity analysis revealed a significant clustering of samples according to diet. (**Figure 34C**). A clear separation induced by the diet was also observed in the 16 weeks feeding experiment (**Suppl. Fig. S14A**). Analysis of alpha-diversity, assessed by Shannon effective counts, was 1.2-fold lower in BA- than in CD-fed mice (**Figure 34D**). However, dietary intervention did not change microbial richness. In contrast, no differences in alpha-diversity were observed in the long-term feeding experiment (**Suppl. Fig. S14B**).

Diet-induced shifts in caecal microbiota composition were already visible at the phylum level (**Figure 34D**). The relative abundance of Firmicutes was 1.2-fold higher in CD- and P-HFD-BA- than in BA-fed mice. BA feeding increased the relative abundance of Deferribacteres by 32 % and of Proteobacteria by 41 % compared to CD feeding. In the first feeding experiment, the abundance of Firmicutes was also 1.2-fold lower and the abundance of Proteobacteria 40 % higher in BA than CD mice (**Suppl. Fig. S14C**). The relative abundance of *Coriobacteriaceae* was reduced in BA-fed groups but this difference did not reach significance (**Figure 34F**).

A deeper look at the level of single molecular species showed that the four dietary interventions were characterized by the presence of specific OTUs (**Figure 34G**). Most of the OTUs characteristic for CD mice belonged to the families *Ruminococcaceae* and *Rikenellaceae*, whereas BA feeding increased the relative abundance of OTUs belonging to *Oscillospiraceae* spp. and *Alistipes* spp. Interestingly, P-HFD-BA as well as the long-term P-HFD feeding increased the relative abundance of an OTU with closest match to *Acetatifactor muris*. L-HFD-BA feeding was characterized by the OTUs with was closest to *Clostridium lactatifermentans.*

As the duration of dietary intervention is also important for modulating the gut microbiota, we looked at changes in the gut microbiota induced by CD and BA diet fed 8 or 16 weeks (**Figure 35**). A clear separation of the feeding groups and duration was found when looking at beta-diversity (**Figure 35A**). Of note, different DNA isolation protocols were used for these two studies (see section 3.7 for technical details). Therefore, the results have to be handled with caution.

Alpha diversity analysis revealed a moderate but significant reduction in Shannon effective score induced by 8 weeks BA feeding (**Figure 35B**). No differences were observed in richness of molecular species. Interestingly, the relative abundance of Proteobacteria and the corresponding family *Desulfovibrionaceae* were significantly reduced by the longer feeding period of both diets (**Figure 35C**

and **D**). Moreover, BA diet increased the abundance of *Desulfovibrionaceae* independent of duration. In the CD-fed groups, long-term feeding resulted in a reduced relative abundance of *Deferribacteraceae* whereas *Rikenellaceae* were increased in their relative abundance. In contrast, long-term BA feeding decreased the relative abundance of *Lachnospiraceae* and increased the one of *Bacteroidaceae*. With respect to *Coriobacteriaceae*, BA feeding reduced their relative abundance compared to CD regardless of the feeding duration (**Figure 35E**). However, this difference did not reach significance. Furthermore, each diet as well as feeding duration was characterized by specific OTUs (**Figure 35F**). Interestingly, short-term CD feeding was characterized by one OTU with a 100 % sequence similarity to *Faecalibaculum rodentium*.

Summarizing all aforementioned results, the dietary fat source had important effects on host metabolism like glucose tolerance and hepatic lipid metabolism which then seems to modulate WAT mass. Furthermore, it changed caecal microbiota composition which may consequently affect the host. Further investigation is needed to dissect these differences in more detail.
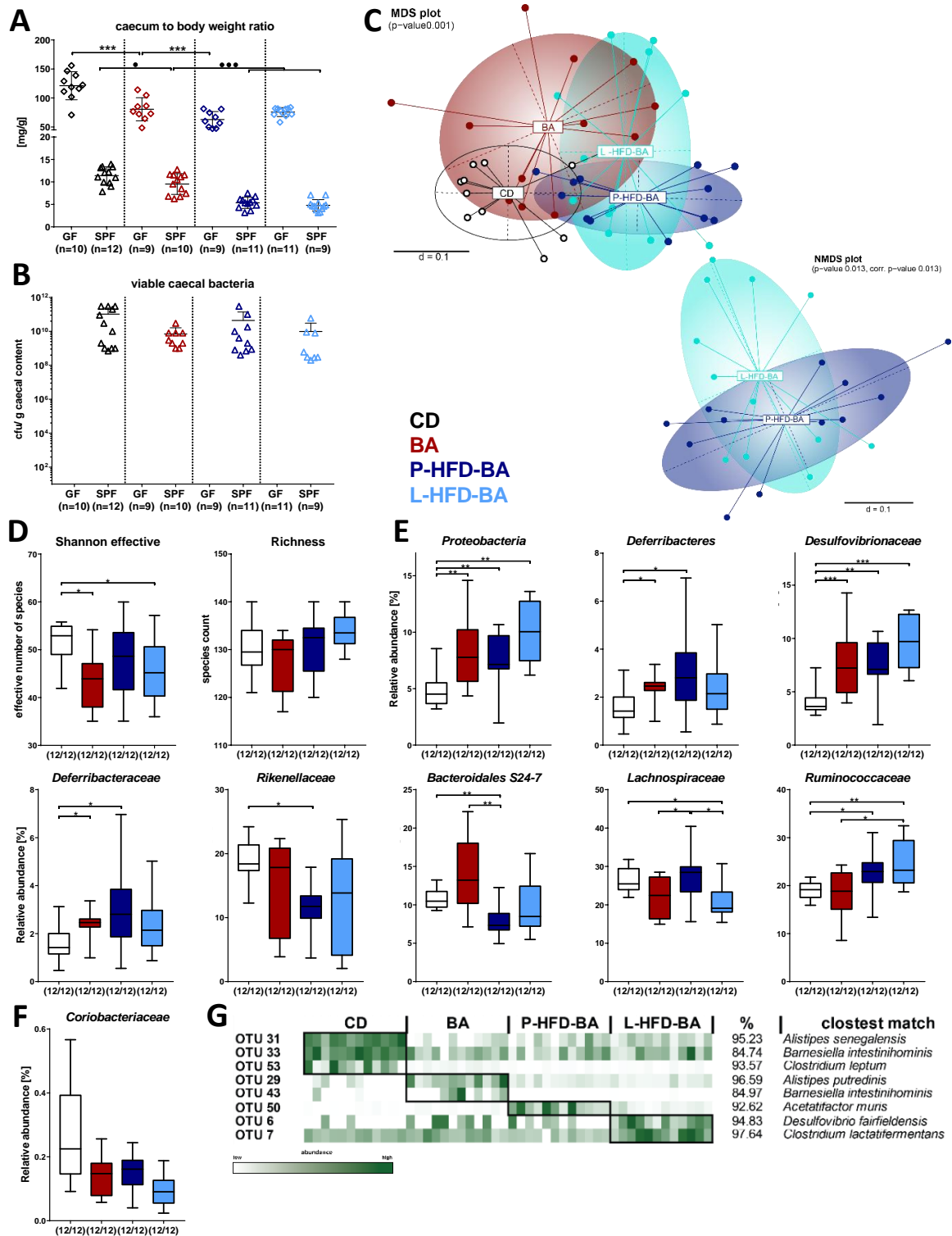
Figure 34: Diet modulated caecal microbiota profile of SPF mice.
(**A**) Measurement of caecum to body weight ratio showed colonization status and diet induced changes. (**B**) Viable bacterial cell counts were assessed by anaerobic cultivation of caecal content. (**C**) Analysis of β-diversity revealed significant differences in bacterial composition induced by the diet. (**D**) Shannon effective species counts and richness. (**E**) At phylum level, significant differences between the four feeding groups could be observed. (**F**) The relative abundance of the family *Coriobactericeae*. (**G**) Relative abundance heat map of OTUs characteristic for the different diets (classification was done with EzTaxon). **CD**; **BA**; **P-HFD-BA**; **L-HFD-BA**; *p<0.05; **p<0.01; ***p<0.001 (serial comparison was performed with the Rhea R package [232]). NGS was performed on the 16S ribosomal RNA gene amplicons of the V3/V4 region (450bp) of caecal content using MiSeq platform. IMNGS and Rhea were used for sequence analysis. Number of mice in each group are indicated below the x-axis (n = number of mice measured, or positive mice per total number of mice).
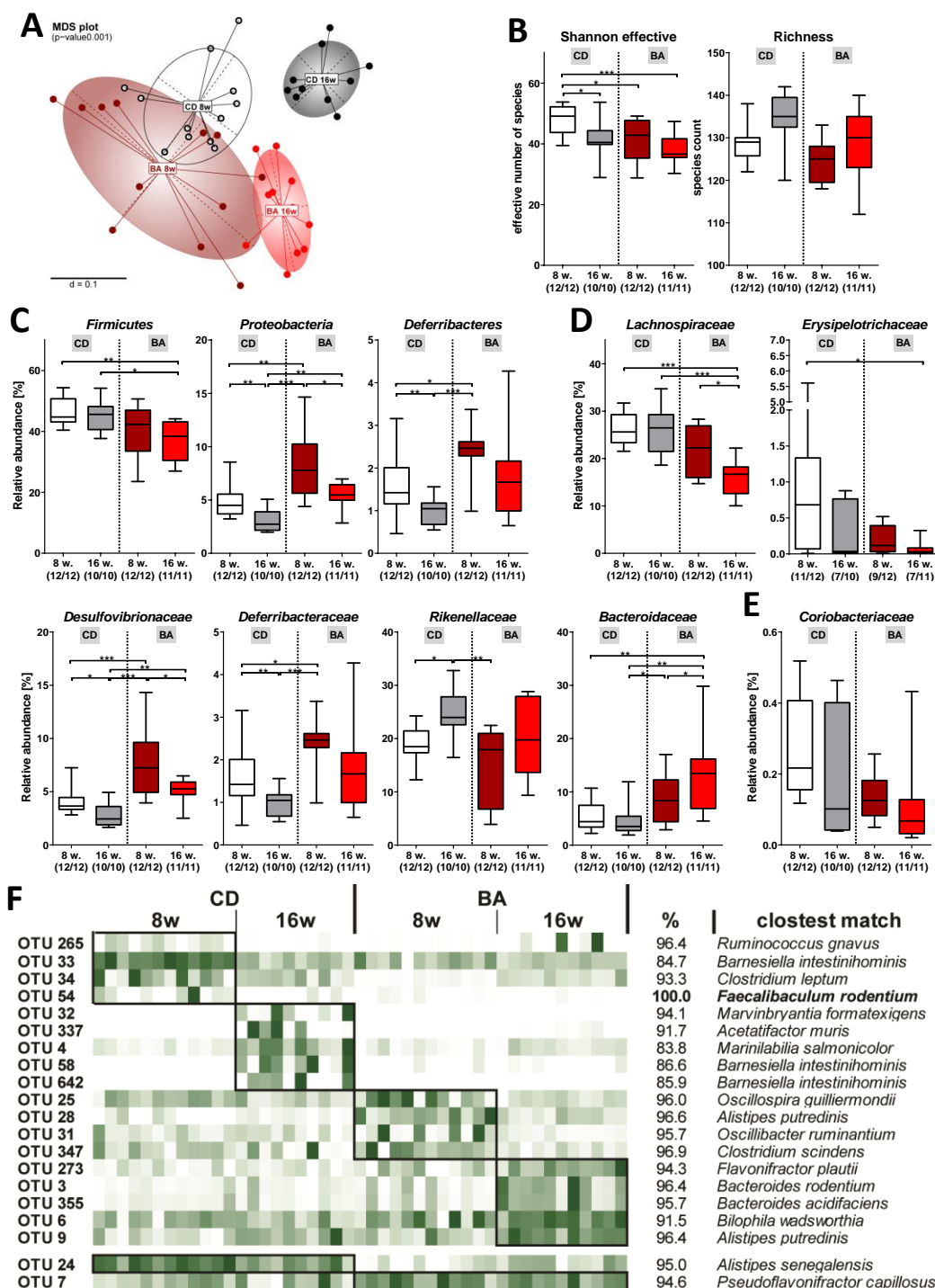
Figure 35: Caecal microbiome is modulated by diet.
(**A**) Analysis of β-diversity via MDS plot. (**B**) Shannon effective and richness species counts. At phylum (**C**) and family level (**D**), changes were observed between the two diets as well as the two feeding periods. (**E**) The relative abundance of *Coriobacteriaceae*. (**F**) Relative abundance heat maps of OTUs characteristic for the different groups, diets and feeding times (classification was done with EZBioCloud). **CD**; **BA**; w., weeks; *p<0.05; **p<0.01; ***p<0.001; NGS was performed on the 16S ribosomal RNA gene amplicons of the V3/V4 region (450bp) of caecal content using the MiSeq platform. Sequence analysis was done using IMNGS and Rhea. Number of mice in each group are indicated below the x-axis (n = positive mice per total number of mice).

5 Discussion

Coriobacteriaceae are prevalent and dominant members of the human gut microbiota and are able to metabolize bile acids, steroid hormones, and lipids. Furthermore, several studies associated their occurrence with increased cholesterol and lipid metabolism as well as T2D and obesity. However, no mechanistic study about the role of *Coriobacteriaceae* on host metabolism is currently available.

5.1 Gut-derived *Coriobacteriaceae* modulate host metabolism

To confirm the association between *Coriobacteriaceae* and host metabolism in human, the genomes of the four *Coriobacteriaceae* strains used in our experiments were mapped against the human fecal integrated gene catalogue of Li *et al*. (2014) [217]. This analysis revealed that the relative abundance of *C. aerofaciens*-like sequences was enriched in obese and morbid obese subjects and reduced in underweight, normal and overweight. In line with these result, the occurrence of *C. aerofaciens* or the family *Coriobacteriaceae* in general was found to be higher abundant in obese patients [26, 249, 250]. Interestingly, Forslund *et al.* (2015) found a lower relative abundance of *C. aerofaciens* in non-diabetic controls compared to metformin treated and non-treated diabetic subjects in the Danish MetaHIT study [28]. With respect to *Egg. lenta*, our analysis revealed a strong correlation with overweight but not with obesity. Additional work is required to obtain a clearer consensus in results. Nevertheless, evidence is there that *Coriobacteriaceae* might affect host metabolism and health as several publications showed a positive correlation between the occurrence of this family and host cholesterol, lipid and energy metabolism [117, 118].

Our animal study is the first that provides experimental evidence that gut-derived *Coriobacteriaceae* influence host metabolism. Until now, only a few specific bacterial species were shown to induce body weight changes and shifts in associated metabolic phenotypes. *Clostridium ramosum* and *Lactobacillus ingluviei* increased body weight after colonization of mice [87, 251]. Additionally, HFD-fed GF mice associated with *Enterobacter cloacae* B29, isolated from a morbid obese patient, developed obesity which was accompanied by massive increase in fat mass and insulin resistance [90]. Moreover, *Prevotella copri* increased systemic levels of branch chain amino acids (BCAA), induced insulin resistance and impaired glucose tolerance in mice [55]. Also in humans, increased circulating levels of various amino acids are increased in obesity and BCAA and aromatic amino acid levels positively correlated with insulin resistance [56, 252, 253]. Interestingly, *Coriobacteriaceae* possess various aminopeptidases influencing amino acid availability, nitrogen cycling processes and ammonia production which could be an additional function of this family to interact with host metabolism [107].

In other studies, the occurrence of *Akkermansia muciniphila* was negatively correlated with obesity and T2D in mice [88, 254]. In human, the abundance of this species was inversely correlated with adipocyte diameter [89]. Moreover, *Bacteroides uniformis* and some bifidobacteria and lactobacilli exhibit anti-obesity effects in mice [255–259]. With respect to *Coriobacteriaceae*, another study showed that Tempol, a synthetic antioxidant, was successful in lowering obesity in high-fat diet-fed mice and decreased the relative abundance of *Lactobacillaceae*, *Coriobacteriaceae*, and *Clostridiales*. The treatment also lowered BSH activity, changed bile acid composition (e.g. increased intestinal T-β-MCA concentrations), and reduced activation of intestinal FXR [260].

The most striking phenotype in gnotobiotic mice colonized with *Coriobacteriaceae* and fed BA diet was a doubling of eWAT, mWAT and iWAT mass beside no increase in body weight. This massive increase in total WAT weight was accompanied by changes in eWAT proteome. Three proteins involved in lipid metabolism were characterized by significantly higher occurrence in *CORIO* mice compared to GF and SPF controls. One of these proteins was the natriuretic peptide receptor 3 (NPR3), which was already shown to be positively associated with obesity and diabetes [261, 262]. NPR3 is highly expressed in adipose tissue and kidney and is involved in the clearance of active atrial natriuretic peptide (ANP), which induces lipolysis in adipocytes via NPRA [263–267]. Additionally, insulin increases NPR3 levels in WAT of rodents and humans and represses the lipolytic action of ANP [268–270]. In our study, *CORIO* mice fed BA diet displayed signs of metabolic disturbances including increased insulin and leptin levels compared to GF and SPF mice, which might explain the increased abundance of NPR3 in the WAT of these mice. In our experiments, insulin levels were generally higher compared to literature [37, 48, 271, 272]. This might be explained by the fact that insulin levels were measured in the systemic plasma of already dead mice [273]. As NPR3 is regulated by insulin and induces the clearance of the pro-lipolytic protein ANP, this could be a hint towards reduced lipolysis in adipose tissue of BA-fed *CORIO* mice. To strengthen the hypothesis of lower lipolysis and to identify a possible disturbance in glucose tolerance in BA-fed *CORIO* mice, further measurement such as total lipid composition in adipose tissues, plasma lipid profiling, and protein levels of ANP are necessary.

Proteome analysis of eWAT also led to the identification of 12 proteins unique for *CORIO* mice and related to lipid metabolism. One of these proteins is Acyl-CoA dehydrogenase family member 11 (ACAD11), which is involved in fatty acid oxidation. ACAD11 was increased in mice with higher body weight following colonization with *Lactobacillus ingluviei* [251, 274]. Another unique protein in BA-fed *CORIO* mice was apolipoprotein H (APOH), which is bound to VLDL and HDL and increases LPL activity [275–277]. APOH is known to be positively correlated with fasting glucose, lipids and lipoprotein levels, as well as metabolic syndrome via retinol binding protein 4 [278–280]. The most

interesting protein unique for BA-fed *CORIO* mice is CIDEC (also referred to as FSP27). CIDEC is a protein involved in lipid droplet formation in adipocytes. CIDEC is directly upregulated by insulin and fatty acids via the FAT/CD36 transporter. It inhibits lipolysis via inhibition of adipose triglyceride lipase and increases the size of lipid droplets [247, 281–283]. CIDEC is a target gene of PPARα in hepatic steatosis and PPARγ in adipose tissue, which are among several signaling pathways regulated by FXR [170, 171, 284, 285]. CIDEC-knockout mice exhibit increased insulin sensitivity and energy expenditure as well as decreased fat mass. Additionally, they are protected from diet-induced obesity [283, 286, 287]. Furthermore, the abundance of CIDEC is reduced in visceral adipose tissue of obese patients [288]. Interestingly, obese patients are characterized by increased lipolysis, which might due to insulin-resistance and increasing inflammatory status in these patients. This could in turn lead to reduced CIDEC levels and PPARγ activity as well as increased activity of the hormone sensitive lipase (HSL) [289]. The high abundance of CIDEC in eWAT of BA-fed *CORIO* mice might hint towards a lower lipolysis. More experiments like the measurement of HSL protein levels in eWAT or the usage of CIDEC knockout mice would help to further dissect the *in vivo* effects of gut-derived *Coriobacteriaceae*.

In addition to changes in eWAT proteome, we observed changes in hepatic lipid and bile acid metabolism as BA-fed *CORIO* mice showed higher levels of hepatic FXR. Interestingly, complete knockout of FXR (FXR$^{-/-}$) has been associated with low leptin levels, impaired glucose and insulin homeostasis, and lower fat mass possibly due to increased energy expenditure [70, 290]. Furthermore, complete and intestine-specific knockout or inhibition of FXR by glycine-β-MCA resulted in a reduction of weight and fat mass gain upon HFD feeding [291–293]. Surprisingly, liver-specific knockout of FXR did not prevent the development of DIO, which hints at a role of non-hepatic FXR in the regulation of body composition [291, 294]. In line with this observation, feeding of mice with HFD plus GW4064, a synthetic FXR agonist, increased their body weight and fat mass and reduced bile acid pool and energy expenditure compared to HFD alone [295]. In contrast, treatment of DIO C57BL/6J mice with the intestinal FXR agonist fexaramine (Fex) increased ileal FGF15 expression, leading to reduction of body weight due to increased browning of adipose tissues and thereby thermogenesis [296]. As FXR is a major modulator of fat storage in adipocytes and liver, the interplay between FXR and *Coriobacteriaceae*-specific effects should be analyzed in greater detail. One opportunity would be the usage of GF FXR$^{-/-}$ mice with the four *Coriobacteriaceae* strains or the application of FXR antagonists like glycine-β-MCA to assess whether the observed massive increase in WAT mass can be prevented.

In the liver of *CORIO* mice fed BA diet, we found a three-fold increase in hepatic *Pparγ* mRNA expression. As described above, PPARγ is one target gene of FXR, the expression of which was

induced in the liver of BA-fed *CORIO* mice. PPARγ was previously found to be induced in murine models of obesity and directly activated CIDEC, resulting in increased lipid storage in the liver [284, 297–300]. Furthermore, the desaturation enzyme SCD1 seemed to be more active in the liver of BA-fed *CORIO* mice as assessed by hepatic desaturation capacities. Interestingly, SCD1 is an indirect target gene of PPARγ via LXR [300, 301]. Therefore, the activation of FXR could induce PPARγ in BA-fed *CORIO* mice which further activates SCD1. This could then increase unsaturation of fatty acids and thereby induce shifts in fatty acid profiles. Targeted protein analysis is needed to specify whether hepatic protein levels of PPARγ and SCD1 as well as LXR and SREBP1c are higher abundant in these mice. Additionally, hepatic lipid class profiling could be helpful for the interpretation of the results.

Strikingly, all *CORIO* mice had a systemic hypercholesterolemia, regardless of diet. Furthermore, we found increased cholesterol levels in iWAT of BA-fed *CORIO* mice. This is in line with the literature, as a positive correlation between the relative abundance of *Coriobacteriaceae* and plasma total cholesterol, non-HDL cholesterol (VLDL and LDL), plasma and hepatic triglyceride concentrations and cholesterol absorption was observed in human and animal studies [116–118, 134]. Additionally, sequences assigned to the genus *Collinsella* were found to be enriched in patients with symptomatic atherosclerosis, even though plasma cholesterol levels did not differ from controls [41]. Further analysis of HDL, LDL and VLDL in systemic plasma would help dissecting the effects of *Coriobacteriaceae* on cholesterol metabolism and in line with this the development of atherosclerosis.

The measurement of free fatty acids (FFA) in adipose tissue revealed that BA-fed *CORIO* mice have lower abundance of lauric, myristic, plamitic, palmitoleic, stearic, oleic, linoleic, arachidic, eicosenoic and eicotirenoic acid in mWAT compared to GF and SPF mice. This could imply that these mice store FFA as triglycerides or export them into the circulation. Interestingly, mesenterial adipose tissue mass is negatively associated with its 18:0 content and positively with the desaturation index [302]. In contrast, Kunesova *et al.* (2012) described the higher abundance of some of those fatty acids in adipose tissue before weight loss in women [303]. Further analyses like total fatty acid and lipid class composition in WAT are needed to specify the influences of *Coriobacteriaceae* on lipid metabolism.

Interestingly, the regulation of lipid metabolism and adipocyte homeostasis by *Coriobacteriaceae* was only observed when diet was supplemented with primary bile acids, suggesting that *Coriobacteriaceae* modulate bile acid metabolism via BSH and HSDH activity. BA-fed *CORIO* mice were characterized by increased concentrations of TCDCA in portal plasma, which is a potent activator of FXR [304]. Increased FXR may contribute to increased triglyceride storage in the liver and WAT via PPARγ as discussed above. Furthermore, increased concentrations of bile acids in the gut of

BA-fed mice most likely favored emulsification of lipids [305–307]. This may in turn increase the contact surface for lipases from *C. aerofaciens* and *A. parvulum*, as we found that these two strains exhibited lipase activity *in vitro*. As a consequence, the concentration and absorption of fatty acids would increase and thereby contribute to the observed increase in WAT mass. Increased intestinal uptake of fatty acids could further result in increased uptake into adipocytes via FAT/CD36, with subsequent activation of CIDEC expression and thereby inhibition of lipolysis [247, 308]. To test this hypothesis, FAT/CD36 protein levels as well as free fatty acid concentrations in portal and systemic plasma should be analyzed. Additionally, fatty acid uptake could be investigated by using fluorescent fatty acids or ^{13}C-labeled fatty acids [309–311]. Furthermore, overexpression and knockout of active lipases in *Coriobacteriaceae* strains could be an option to investigate the effects of bacterial lipases on host metabolism in greater detail.

Although our data clearly hint at a substantial impact of *Coriobacteriaceae* on the metabolism of mice, population densities of the bacteria were relatively low in *gnotobiotic* mice. This may be a result of either incomplete DNA isolation from intestinal contents or the dependence of *Coriobacteriaceae* on other bacterial strains for effective colonization of the intestinal tract. Rey *et al*. (2013) associated mice with a minimal consortium of 8 species, including *C. aerofaciens,* alone or plus *Desulfovibrio* (*D*.) *piger*, a sulphate-reducing bacterium. They could show that *D. piger* increased the abundance of *C. aerofaciens* [312] and concluded that H$_2$ and formate produced by *C. aerofaciens* are substrates for *D. piger*. This indicates that the combination of *Coriobacteriaceae* with other bacterial strains might be necessary to improve colonization efficacy. Differences in colonization may also explain the marked inter-individual differences observed within groups, especially with respect to gene expression and bile acid composition in various tissues. Another reason may be the relatively low and variable fasting time before sacrification, ranging from 6 to 9 h.

5.2 The dietary fat source exhibits an important impact on host metabolism

In the second animal experiment of the present thesis, we wanted to investigate the combined effect of supplementing bile acids and fat to diets, including various fat types (animal or plant). Due to contamination of the isolator housing the *CORIO* mice, novel data pertaining to the main fatty phenotype described above could not be generated, and the interpretation of results was restricted to the impact of different fat sources in combination with bile acids on host metabolism in GF and SPF mice.

The impact of dietary fat source and amount on host metabolism and the development of metabolic diseases has already been pointed out by others. For instance, the response of GF mice to HFD, *i.e.*

their susceptibility to diet-induced obesity, was shown to be dependent on the type of high calorie diet given to the animals, with a particular importance of dietary fat source [22, 54]. Kübeck *et al.* (2016) revealed that lard-based HFD-fed GF mice were resistant to DIO, whereas palm oil-based HFD-fed mice were not. This resistance to DIO was due to a higher metabolic rate and a less efficient fat absorption. The main difference between these two diets was their cholesterol content, with lard-based HFD containing 10 % more than palm oil-based HFD. As cholesterol can modulate bile acid and lipid metabolism, these and other authors proposed that dietary cholesterol content drives the response of mice to high-fat diets [116, 313, 314]. Furthermore, the fatty acid composition of the diet can modulate body weight gain as well as host metabolism [268–270]. The two diets, L- vs. P-HFD-BA, used in our own studies, mainly differ in their amounts of C16:0 (5.37 vs. 9.18 %, respectively), C18:0 (2.88 vs. 1.11 %) and C16:1 (0.6 vs. 0.05 %).

In our study, bile acid supplementation (0.1 % CA and 0.1 % CDCA) to L- and P-HFD prevented body weight gain in GF mice. In contrast, SPF mice fed these diets gained weight with no statistically significant difference between the two groups. This combination of CA and CDCA in the diets has no precedent in the literature. Interestingly, L-HFD-BA feeding to SPF mice resulted in exacerbated increase in WAT mass and impairment of glucose tolerance. Moreover, supplementation of this bile acid combination to the diet suppressed the obese phenotype previously found to be associated with P-HFD feeding in GF mice [313]. Others reported that 0.5 % (w/w) CA in the diet induced weight loss in mice that had been previously fed a HFD for 17 weeks, and completely prevented weight gain in a mouse model for obesity and diabetes [190, 194]. This discrepancy in results between our own experiments and the studies by Watanabe *et al.* can be due to differences in the amount of CA in the diet.

The texture of diets can also be important for their effects on host metabolism. Powdered isocaloric diets were shown to induce a weight gain comparable to that of a high-fat feeding due to an increase in food intake, an effect that was less severe with HFDs [315–317]. Powder vs. pellet standard carbohydrate diet was associated with shifts in the gut microbiota of mice, with a reduction in Shannon effective counts and marked changes in β-diversity [318]. This effect might also be important in the present study, as the two HFDs used were slightly different in texture. Although both diets were administered as pellets, they were crumbly and the mice easily scattered them into cages. This was more pronounced in the L-HFD- than the P-HFD-BA groups. Hence, the effect of the two different diets on fat mass could also have been impacted by this difference in texture. Assessment of food intake, energy expenditure via indirect calorimetry, and fecal fat and energy content via Fourier transform-infrared spectroscopy (FT-IR) would be helpful for the interpretation of results.

We demonstrated that the gut microbiota as well as the diet can modulate hepatic lipid composition. The strongest effect was observed in cholesterol esters, which were highly increased in SPF mice fed L-HFD-BA compared to the other diets and to GF mice. Difference between SPF and GF mice had been previously observed by Caesar *et al.* (2016), but results comparing diets varying in fat type are novel. Despite the increase in hepatic cholesterol esters, no differences were observed in systemic cholesterol levels. Further analysis of WAT lipid as well as hepatic fatty acid composition should be performed to reveal possible differences between the two HFD-BA diets.

In the present study, analysis of bile acid composition revealed a strong impact of animal housing and a mild impact of diet. We observed that serum levels of TCA, T-β-MCA were increased by bile acid supplementation of CD- as well as L- and P-HFD in GF, but not SPF mice. In literature, strong differences between GF, which were characterized by the presence of only primary bile acids and their conjugates in intestinal content and serum, and conventional or SPF mice were also reported by others. Interestingly, GF mice had higher levels of T-MCAs, which are potent FXR antagonists [178, 313, 319]. Furthermore, higher levels of T-β-MCA were shown to reduce FXR activity and preventing weight gain in cold exposed mice [320]. This may partly explain the resistance of GF mice to weight gain under bile acid supplementation of HFD. Surprisingly, we detected low levels of DCA, a secondary bile acid, in the plasma of GF mice which was also reported by Sayin *et al.* (2013) [319].

Amplicon sequencing of 16S rRNA genes from the caecal content of SPF mice including both the long-term (16 weeks) and short-term (8 weeks) feeding trials revealed diet-induced changes in gut microbiota diversity and composition. Within the short-term feeding experiment, the main differences in abundances were found between CD and the other three diets. Interestingly, feeding of bile acids alone or in combination with HFDs did not reduce richness and only slightly reduced Shannon effective counts. Only few publications assessed differences in the intestinal microbiome induced by bile acid supplementation in mice. Isalm *et al.* (2011) observed that feeding of different CA concentrations to rats reduced alpha-diversity of the caecal microbiota with increased relative abundance of *Lachnospiraceae*, *Erysipelotrichaceae* and γ-*Proteobacteria* [321]. Moreover, feeding of 1 % CA to mice increased the relative abundance of phylogenetic groups that include 7-α-dehydroxylating bacteria (producing DCA from CA), such as *Clostridium* cluster XIVa [322].

When comparing the two types of HFDs used in our experiments, P-HFD-BA significantly increased the relative abundance of *Lachnospiraceae*, including one specific OTU with 92.6 % similarity to *Acetatifactor muris*. This was also the case for P-HFD in the long-term feeding trial. *Acetatifactor muris* was originally isolated from the caecum of an obese mouse [323]. This species is the closest relative, yet still distant (usually <94 % sequence identity), of numerous molecular species also found by others to have higher abundance in HFD-fed mice [51, 228, 313, 324].

In the recent study, the relative abundances of the family *Desulfovibrionaceae* (within the delta-*Proteobacteria*) was increased in response to bile acid supplementation of CD as well as the two HFD. One OTU belonging to the genus *Desulfovibrio* was characterized by higher relative abundances in L-HFD-BA mice. In line with this finding, relative abundances of *Desulfovibrionaceae*, which are sulphate-reducing and endotoxin-producing bacteria, were found to be significantly increased in obese and metabolically impaired mice fed HFD by others [324–326]. In contrast, the occurrence of *Desulfovibrionaceae* was increased in lean individuals from preschool children and Japanese study populations [19, 327].

Another OTU also characterized by higher relative abundance following L-HFD-BA-feeding could be identified at the species level as *Clostridium lactatifermentans*, a lactate-fermenting bacterium which produces the short-chain fatty acids (SCFA) acetate, propionate, butyrate and isovalerate [328]. Although this species is characteristic for L-HFD-BA feeding and produces SCFAs, an interpretation is difficult as the role of SCFAs in metabolic diseases is controversially discussed [20, 25, 52]. Therefore, measurement of fecal SCFA would be needed for interpretation of our results.

6 Conclusion and perspective

The first part of this thesis identified that *Coriobacteriaceae* are linked to hypercholesterolemia regardless of diet. Furthermore, the combination of *Coriobacteriaceae* and BA diet induced a doubling of WAT mass which was accompanied by modulation of hepatic lipid metabolism and increased plasma levels of insulin and leptin. NPR3 and CIDEC were abundant in eWAT of BA-fed *CORIO* mice, and the expression of these proteins might be induced via an insulin- and/ or FXR/PPARγ-dependent signaling pathway in adipocytes. This may finally result in reduced lipolysis and increased lipid storage. Furthermore, *C. aerofaciens* and *A. parvulum* possess active lipases *in vitro* which could, in combination with BA diet, increase fatty acid absorption.

Further research will be needed to confirm and strengthen the results of the present thesis. The use of knockout models or selective antagonists for FXR and PPARγ would help dissecting the influence of *Coriobacteriaceae in vivo*. Moreover, a longer feeding period of BA-fed *CORIO* mice or in combination with HFD could further aggravate the observed metabolic disturbances and eventually lead to the development of T2D, highlighting also the need to perform OGTT in these mice. Generation of genetically modified *Coriobacteriaceae*, which overexpress the target function, would be a potent method to unravel whether lipase activity or bile acid transformation of the used strains are responsible for the observed phenotype. With respect to the lipase activity, labeled fatty acids could be used to address the hypothesis of a higher absorption rate of dietary lipids in BA-fed *CORIO* mice. Colonization densities of *Coriobacteriaceae* at the end of the trial were relatively low, although

higher levels were found in P-HFD-fed mice. Different approaches could be followed to counteract this problem: (I) combine bile acids and HFD as in the second part of the thesis; (II) use of HFD alone for 8 weeks to support better colonization by *Coriobacteriaceae* followed by a combination of HFD and primary bile acids. Moreover, it is important to assess whether *Coriobacteriaceae* can induce the observed phenotype also in the presence of endogenous gut microbes, for instance by using mice colonized with a minimal consortium such as the Oligo-Mouse-Microbiota (Oligo-MM[12]) [329].

In the second part of this thesis, it could be clearly shown that the dietary fat source in combination with bile acids and the gut microbiota are major modulators of host lipid metabolism. Comparing the two HFD-BA diets, L-HFD-BA feeding more strongly increases WAT mass, impaired glucose tolerance and modulated hepatic lipid composition than P-HFD-BA. Further analyses are needed to investigate in greater detail mechanisms that may explain the differences in host metabolic phenotypes observed between the two HFD-BA diets. Measurement of SCFA, bile acids, cholesterol and lipid metabolism, and metatranscriptomics are ongoing. If marked phenotype and diet-driven changes are observed in the metatranscriptomics data and on this basis, minimal consortia could be designed. Association of mice with those consortia could then be used to assess whether similar phenotypes are observed as in the present trial. This could help to identify specific bacterial species which induce or prevent weight gain in mice and can further be tested in humans.

7 Supplementary Figures

A

| A. parvulum | C. aerofaciens | Egg. lenta | E. mucosicola |

B

qPCR for *A.parvulum*

DNA of	Ct value	DNA of	Ct value
Mix pure (2.5 ng per strain)	**15,00**	Mix + 1.25 ng E.l.	14,82
Mix + 1.25 ng A.p.	**13,62**	Mix + 2,5 ng E.l.	14,90
Mix + 2.5 ng A.p.	**12,53**	Mix + 5 ng E.l.	14,56
Mix + 5 ng A.p.	**11,40**	Mix + 1.25 ng E.m.	11,61
Mix + 1.25 ng C.a.	14,80	Mix + 2,5 ng E.m.	14,52
Mix + 2,5 ng Ca	14,88	Mix + 5 ng E.m.	14,82
Mix + 5 ng C.a.	14,44		

qPCR for *C. aerofaciens*

DNA of	Ct value	DNA of	Ct value
Mix pure (2.5 ng per strain)	**14,15**	Mix + 1.25 ng E.l.	14,36
Mix + 1.25 ng C.a.	**12,76**	Mix + 2,5 ng E.l.	14,13
Mix + 2,5 ng Ca	**11,64**	Mix + 5 ng E.l.	14,06
Mix + 5 ng C.a.	**10,80**	Mix + 1.25 ng E.m.	14,61
Mix + 1.25ng A.p.	14,26	Mix + 2,5 ng E.m.	14,27
Mix + 2.5 ng A.p.	14,19	Mix + 5 ng E.m.	14,33
Mix + 5 ng A.p.	14,38		

qPCR for *Egg. lenta*

DNA of	Ct value	DNA of	Ct value
Mix pure (2.5 ng per strain)	**17,67**	Mix + 1.25 ng C.a.	17,64
Mix + 1.25 ng E.l.	**16,51**	Mix + 2,5 ng Ca	17,45
Mix + 2,5 ng E.l.	**15,42**	Mix + 5 ng C.a.	17,95
Mix + 5 ng E.l.	**14,46**	Mix + 1.25 ng E.m.	17,68
Mix + 1.25ng A.p.	17,77	Mix + 2,5 ng E.m.	21,34
Mix + 2.5 ng A.p.	17,79	Mix + 5 ng E.m.	16,43
Mix + 5 ng A.p.	17,64		

qPCR for *E. mucosicola*

DNA of	Ct value	DNA of	Ct value
Mix pure (2.5 ng per strain)	**15,09**	Mix + 1.25 ng C.a.	20,01
Mix + 1.25 ng E.m.	**18,70**	Mix + 2,5 ng Ca	19,85
Mix + 2,5 ng E.m.	**17,25**	Mix + 5 ng C.a.	20,18
Mix + 5 ng E.m.	**16,47**	Mix + 1.25 ng E.l.	19,85
Mix + 1.25ng A.p.	20,21	Mix + 2,5 ng E.l.	19,67
Mix + 2.5 ng A.p.	20,00	Mix + 5 ng E.l.	20,06
Mix + 5 ng A.p.	20,22		

Suppl. Fig. S1: Validation of 16S rRNA gene-based qPCR.
(**A**) Graphical representation of 16S rRNA gene-based qPCR using UPL (Roche) approach with 2.5 ng target DNA of pure cultures of *A. parvulum* DSM 20469[T], *C. aerofaciens* DSM 3979[T], *Egg. lenta* DSM 2243[T] and *E. mucosicola* DSM 19490[T]. (**B**) Selectivity of the 16S rRNA gene based qPCR for the four strains was tested using a Mixture (Mix) of 2.5 ng DNA of each of the four strains spiked with three different concentrations of the target strain (in bold) and each of the three other strains. Decrease of Ct values with increasing concentrations of the target strain but not the three others confirmed the specificity of the qPCR assay. See section 3.4 for technical details. A.p., *A. parvulum*; C.a., *C. aerofaciens*; E.l., *Egg. lenta*; E.m., *E. mucosicola*.

Suppl. Fig. S2: *Coriobacteriaceae* **were capable to colonize GF mice.** Colonization efficacy for each diet of the single strains as well as total bacteria is visualized for proximal (n = 8) (**A**) and distal ileum (n= 3 – 10) (**B**), caecum (n = 11 – 14) (**C**), proximal (n = 7 – 8) (**D**) and distal colon (n = 2 – 9) (**E**). In addition to that, the colonization of all bacteria together (**F**) and the single strains (**G-J**) was analyzed. **CD**; **P-HFD**; **BA**; For detailed description of the statistical analysis see section 3.17. Abbreviations: *A.p., A. parvulum*; *C.a., C. aerofaciens*; *E.l., Egg. lenta*; *E.m., E. mucosicola*; pI, proximal ileum; dI, distal ileum; pC, proximal colon; dC, distal colon.

Suppl. Fig. S3: Body weight development over time.
CD; **P-HFD**; **BA.** Number of mice in each group are indicated in brackets (n = number of mice measured).

Suppl. Fig. S4: Adipocyte area distribution of eWAT and iWAT of P-HFD-fed mice.
Number of mice in each group are indicated in brackets (n = number of mice measured).
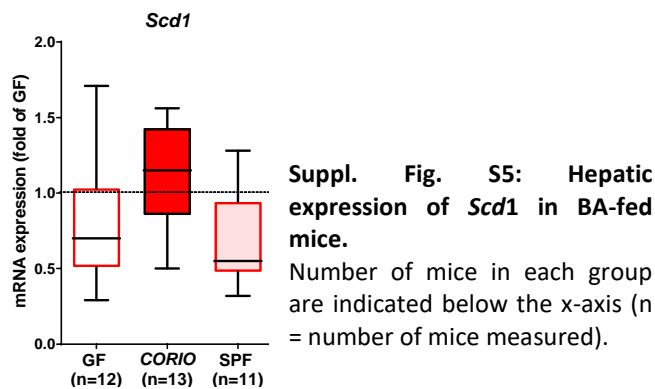
Suppl. Fig. S5: Hepatic expression of *Scd*1 in BA-fed mice.
Number of mice in each group are indicated below the x-axis (n = number of mice measured).
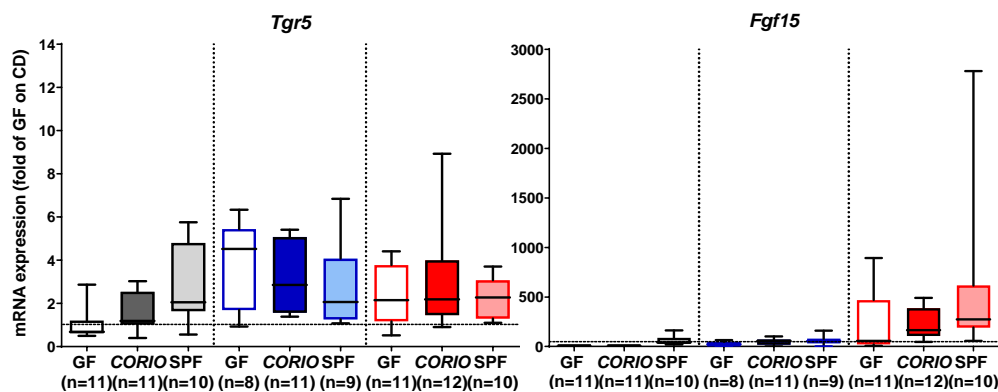
Suppl. Fig. S6: Ileal expression of bile acid and FXR target genes *Tgr5* and *Fgf15*.
CD; P-HFD; BA. Number of mice in each group are indicated below the x-axis (n = number of mice measured).
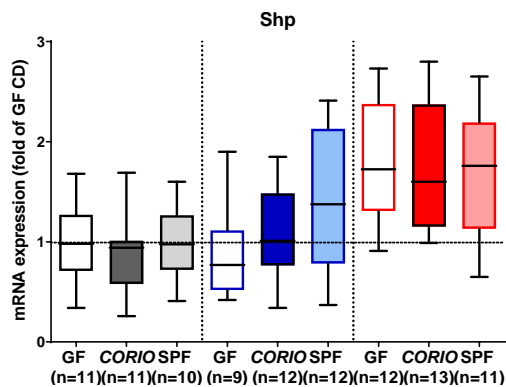
Suppl. Fig. S7: Hepatic expression of *Shp*.
CD; HFD; BA; For detailed description of the statistical analysis see section 3.17. Number of mice in each group are indicated below the x-axis (n = number of mice measured).
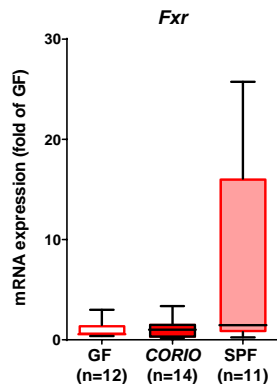
Suppl. Fig. S8: Expression of *Fxr* in mWAT of BA-fed mice.
BA; Number of mice in each group are indicated below the x-axis (n = number of mice measured).
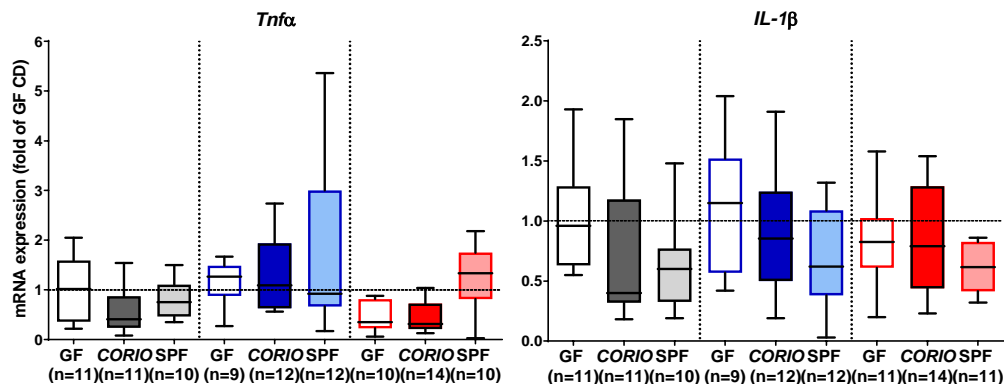
Suppl. Fig. S9: **Expression of hepatic *Tnfα* and *Il-1*β**.
CD; **P-HFD**; **BA**; For detailed description of the statistical analysis see section 3.17. Number of mice in each group are indicated below the x-axis (n = number of mice measured).
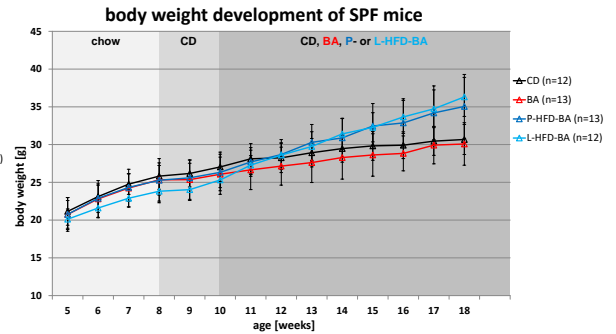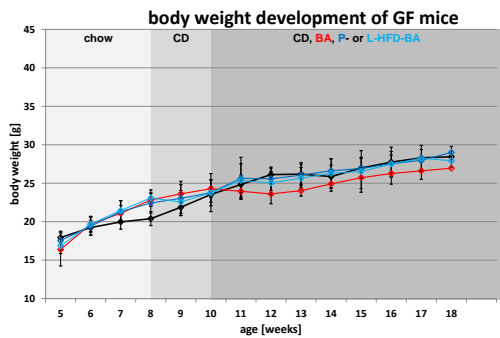
Suppl. Fig. S10: HFD-BA feeding induced body weight increase in SPF but not GF mice.
CD; **BA**; **P-HFD-BA**; **L-HFD-BA**.
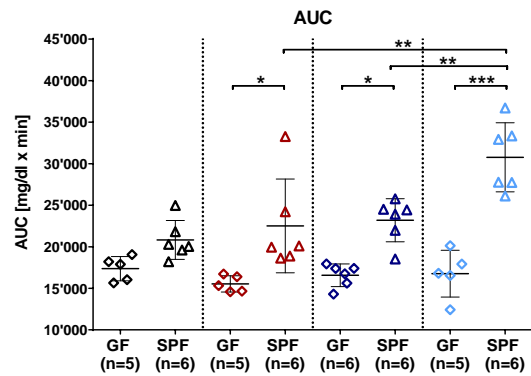
Suppl. Fig. S11: L-HFD-BA feeding reduced glucose tolerance.
AUC values of the OGTT of fasted mice. **CD**; **BA**; **P-HFD-BA**; **L-HFD-BA**. For detailed description of the statistical analysis see section 3.17. Number of mice in each group are indicated below the x-axis (n = number of mice measured).
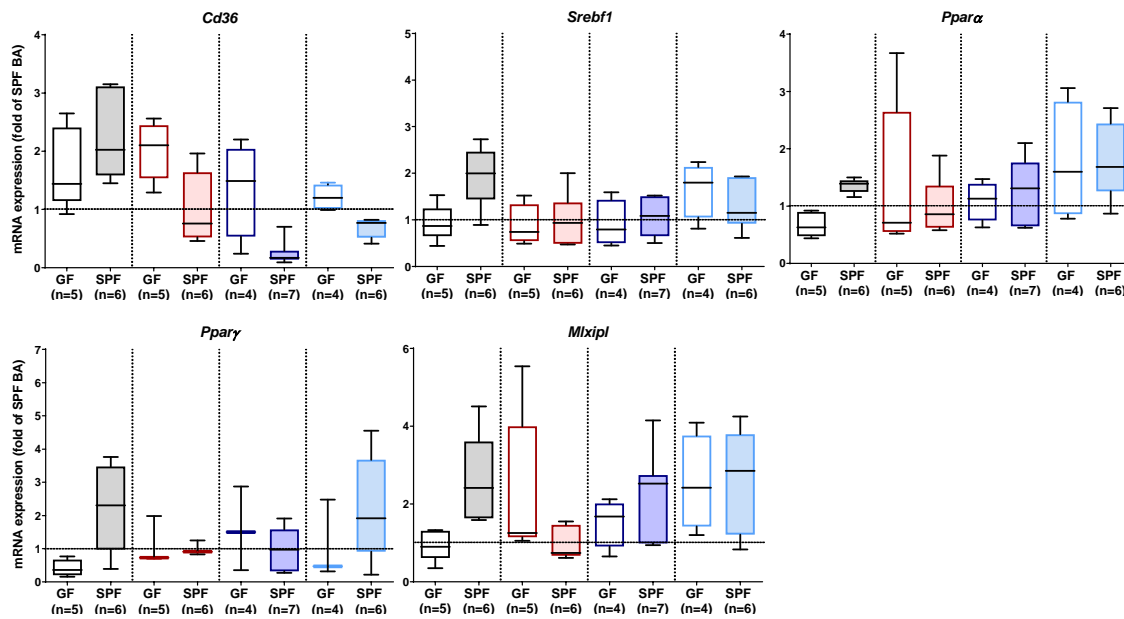
Suppl. Fig. S12: Expression analysis of genes involved in lipid homeostasis: *Cd36, Srefb1, Pparα, Pparγ* and *Mlxipl*.
CD; **BA**; **P-HFD-BA**; **L-HFD-BA**. Number of mice in each group are indicated below the x-axis (n = number of mice measured).
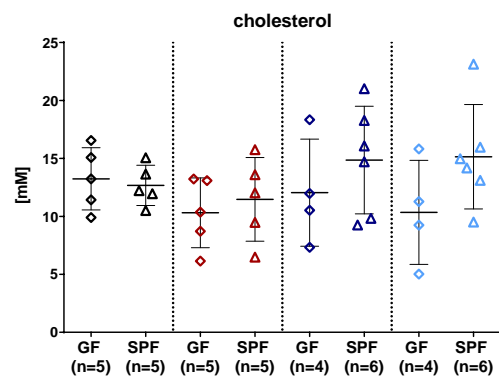
Suppl. Fig. S13: Diet did not influence systemic cholesterol levels after 8 weeks of feeding.
CD; **BA**; **P-HFD-BA**; **L-HFD-BA**. Number of mice in each group are indicated below the x-axis (n = number of mice measured).
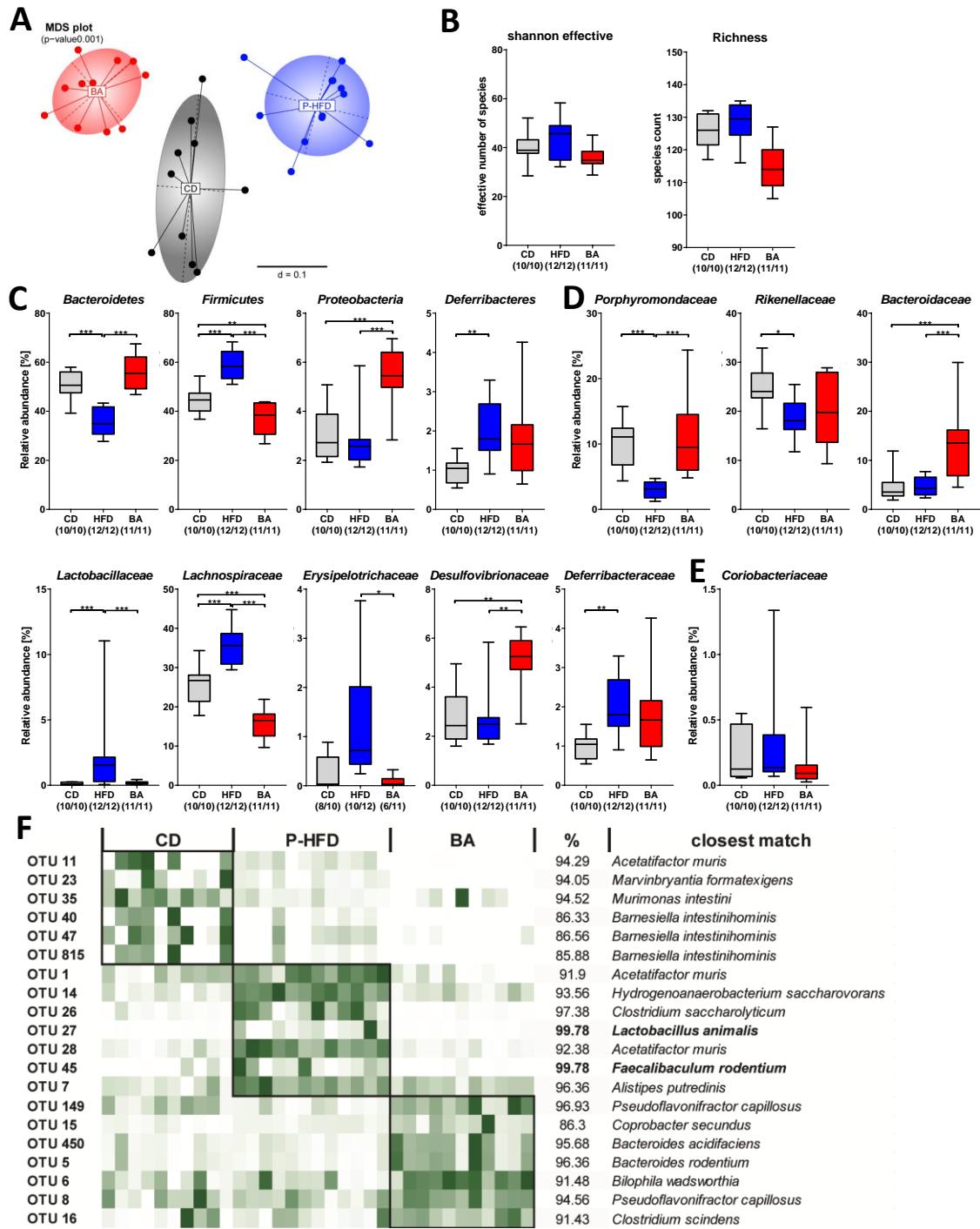
Suppl. Fig. S14: Long-term dietary intervention modulated microbiota composition of SPF mice.
(**A**) β-diversity via a MSD plot. (**B**) Shannon effective and richness. Analysis of the relative abundance revealed diet induced changes on phylum (**C**) and family level (**D**). (**E**) The relative abundance of the family *Coriobactericeae*. (**F**) Relative abundance heat map of OTUs characteristic for one diet and for CD- and BA-fed mice (identification was done using EZBioCloud); **CD**; **P-HFD**; **BA**; *p<0.05; **p<0.01; ***p<0.001; NGS was performed on the 16S ribosomal RNA gene amplicons of the V3/V4 region (450bp) of caecal content using the MiSeq platform. Sequence analysis was done using IMNGS and Rhea. Number of mice in each group are indicated below the x-axis (n = positive mice/total number of mice).

List of Figures

List of Tables

Abbreviations

A. parvulum; A.p.	*Atopobium parvulum*
Acaca	Acetyl-CoA carboxylase 1
ACAD11	Acyl-CoA dehydrogenase family member 11
ACN	Acetonitrile
Angptl4	Angiopoietin-like protein 4
ANP	Atrial natriuretic peptide
APO	Apolipoprotein
ASBT	Apical sodium bile acid transporter
AUC	Area under the curves
BA	Control diet supplemented with 0.1 % cholic and chenodeoxycholic acid
BAAT	Bile acid-CoA:amino acid n-acetyltransferase
BACS	Bile acid-CoA synthetase
bai	Bile acid inducible
BAT	Brown adipose tissue
BCAA	Branched-chain amino acids
BLASTN	Basic local alignment search tool for nucleotide sequences
bp	Base pairs
BSEP	Bile salt export pump
BSH	Bile salt hydrolase
C	Carbon
C. aerofaciens; C.a.	*Collinsella aerofaciens*
CA	Cholic acid
CAR	Constitutive androstane receptor
CCK	Cholecystokinin
CD	Control diet
CD3	Cluster of differentiation 3
CD36/FAT	Cluster of differentiation 36/ fatty acid translocase
CDCA	Chenodeoxycholic acid
cDNA	Complementary DNA
CDS	Coding sequences
CE	Cholesterol ester
Cer	Ceramide
ChREBP	Carbohydrate-responsive element-binding protein
CIDEC/ FSP27	Cell death inducing DFFA like effector C
CORIO	*Coriobacteriaceae*-associated mice
Cyp3a11	Cytochrome P450, family 3, subfamily a, polypeptide 11
Cyp7a1	Cholesterol 7α-hydroxylase
D2	Type 2 iodothyronine deiodinase
DAPI	4',6-Diamidin-2-phenylindo
DB	Data base
db/ db	Homozygous leptin receptor knockout mice
DCA	Deoxycholic acid
DGAT	Diacylglycerol acyltransferase
DIO	Diet-induced obesity
DNA	Deoxyribonucleic acid
DSM	Deutsche Sammlung von Mikroorganismen
DTT	Dithiothreitol
E. coli	*Escherichia coli*
E. mucosicola; E.m.	*Enterorhabdus mucosicola*

EDTA	Ethylenediaminetetraacetate
Egg. lenta; E.l.	*Eggerthella lenta*
EHD1	EH domain-containing protein 1
ELOVL	Elongation of very long chain fatty acids protein
EUB	Eubacterial
eWAT	Epididymal white adipose tissue
FA	Formic acid
FAME	Fatty acid methyl esters
FAS/ FASN	Fatty acid synthase
Fasta	Fasta format
FC	Free cholesterol
FFA	Free fatty acids
FFPE	Formalin-fixed paraffin-embedded
FGF	Fibroblast growth factor
Fiaf	Fasting-induced adipose factor
FISH	Fluorescence *In Situ* hybridization
FPR	Formyl-peptide receptors
FXR	Farnesoid X receptor
GAPDH	Glyceraldehyde 3-phosphate dehydrogenase
GC-FID	Gas chromatography flame ionization detector
GF	Germ-free
GLP-1	Glucagon like peptide 1
GPCR	G protein-coupled receptor
h	Hour
H & E	Hematoxylin and eosin staining
HCl	Hydrogen chloride
HDL	High density lipoprotein
HFD	High fat diet
HMG	Hydroxymethyl glutaryl
HPLC	High performance liquid chromatography
HPRT	Hypoxanthine-guanine phosphoribosyltransferase
HSDH	Hydroxysteroid dehydrogenases
IBABP	Intestinal bile acid-binding protein
IF	Immunofluorescence
IGC	Integrated gene catalogue
IL	Interleukin
INF	Interferon
iWAT	Inguinal white adipose tissue
KEGG	*Kyoto Encyclopedia of Genes and Genomes*
LB	Lysogeny broth
LCA	Lithocholic acid
LC-ESI-MS/MS	Liquid chromatography electrospray ionization tandem mass spectrometry
LDL	Low-density lipoprotein
Lep	Leptin gene
L-HFD	Lard based high-fat diet
L-HFD-BA	L-HFD plus 0.1 % cholic and chenodeoxycholic acid
LPC	Lyso-PC
LPGAT1	Acyl-CoA:lysophosphatidylglycerol acyltransferase 1
LPL	Lipoprotein lipases
LPS	Lipopolysaccharides

LXR (gene: Nr1h3)	Liver X receptor
MAG	Monoacylgylcerol
MCA	Muricholic acid
MCP	Monocyte chemoattractant protein
MeOH	Methanol
MFE-2	Peroxisomal multifunctional enzyme type 2
MGAT	Monoacylgylcerol acyltransferase
MHCII	Major histocompatibility complex II
min	Minutes
Mlxipl	MLX-interacting protein-like, gene of ChREBP
mRNA	Messenger RNA
MUFA	Monounsaturated fatty acid
mWAT	Mesenterial white adipose tissue
NaCl	Sodium chloride
NAFLD	Non-alcoholic fatty liver disease
NASH	Non-alcoholic steatohepatitis
NCBI	National Center for Biotechnology Information
NP1L1	Niemann Pick 1 like 1 receptor
NPR3	Natriuretic peptide receptor 3
NTCP	Sodium taurocholate Co-Transporting Polypeptide
O.C.T.	Optimum cutting temperature
OATP	Organic anion transport peptide
OCA	Obeticholic acid
OGTT	Oral glucose tolerance test
OST	Organic solute transporter
OTU	Operational Taxonomic Units
PBS	Phosphate buffered saline
PC	Phosphatidylcholine
PCA	Principle component analysis
PCR	Polymerase chain reaction
PE	Phosphatidylethanolamine
PE-P	Plasmalogen
PG	Phosphatidylgcerol
PGC1α	Peroxisome proliferator-activated receptor gamma coactivator 1-alpha
P-HFD	Palm oil based high-fat diet
P-HFD-BA	P-HFD plus 0.1 % cholic and chenodeoxycholic acid
PI	Phosphatidylinositol
PPAR	Peroxisome proliferator-activated receptor
PS	Phosphatidylserine
PUFA	Polyunsaturated fatty acid
PXR	Preganane X receptor
Q and H	Query and hit of blast analysis
qPCR	Quantitative polymerase chain reaction
RARα	Retinoic acid receptor
rRNA	Ribosomal ribonucleic acid
RT	Room temperature
RXR	Retinoid X receptor
SA	Saturated fatty acids
SCD1	Stearoyl-CoA desaturase 1
SCFA	Short chain fatty acids

SDS	Sodium Dodecyl Sulfate
sec	Seconds
SHP	Small heterodimer partner
SM	Sphingomyelin
sp.	Species
SPF	Specific pathogen free
SREBP1c	Sterol regulatory element binding protein 1c
T2D	Type 2 diabetes
TDCA	Tauro-conjugated deoxycholic acid
TGR5	G protein-coupled bile acid receptor
TLR	Toll-like receptor
TNF	Tumor necrosis factor
UPL	Universal Probe Library
V3/V4	Variable regions 3 and 4
VDR	Vitamin D receptor
VLDL	Very-low-density lipoprotein
WAT	White adipose tissue
WCA	Wilkins-Chalgren-Agar

References

1. Qin J, Li R, Raes J, Arumugam M, Burgdorf KS, Manichanh C, et al. A human gut microbial gene catalogue established by metagenomic sequencing. Nature. 2010;464:59–65. doi:10.1038/nature08821.

2. Sender R, Fuchs S, Milo R. Revised Estimates for the Number of Human and Bacteria Cells in the Body. PLoS Biol. 2016;14:e1002533. doi:10.1371/journal.pbio.1002533.

3. Xu J, Gordon JI. Honor thy symbionts. Proc Natl Acad Sci U S A. 2003;100:10452–9. doi:10.1073/pnas.1734063100.

4. Nicholson JK, Holmes E, Kinross J, Burcelin R, Gibson G, Jia W, Pettersson S. Host-gut microbiota metabolic interactions. Science. 2012;336:1262–7. doi:10.1126/science.1223813.

5. Vrieze A, Holleman F, Zoetendal EG, Vos WM de, Hoekstra JBL, Nieuwdorp M. The environment within: how gut microbiota may influence metabolism and body composition. Diabetologia. 2010;53:606–13. doi:10.1007/s00125-010-1662-7.

6. Ley RE, Peterson DA, Gordon JI. Ecological and evolutionary forces shaping microbial diversity in the human intestine. Cell. 2006;124:837–48. doi:10.1016/j.cell.2006.02.017.

7. Dore J, Simren M, Buttle L, Guarner F. Hot topics in gut microbiota. United European Gastroenterol J. 2013;1:311–8. doi:10.1177/2050640613502477.

8. Kamada N, Chen GY, Inohara N, Nunez G. Control of pathogens and pathobionts by the gut microbiota. Nat Immunol. 2013;14:685–90. doi:10.1038/ni.2608.

9. Goodrich JK, Waters JL, Poole AC, Sutter JL, Koren O, Blekhman R, et al. Human genetics shape the gut microbiome. Cell. 2014;159:789–99. doi:10.1016/j.cell.2014.09.053.

10. Faith JJ, Guruge JL, Charbonneau M, Subramanian S, Seedorf H, Goodman AL, et al. The long-term stability of the human gut microbiota. Science. 2013;341:1237439. doi:10.1126/science.1237439.

11. Kau AL, Ahern PP, Griffin NW, Goodman AL, Gordon JI. Human nutrition, the gut microbiome and the immune system. Nature. 2011;474:327–36. doi:10.1038/nature10213.

12. Round JL, Mazmanian SK. The gut microbiota shapes intestinal immune responses during health and disease. Nat Rev Immunol. 2009;9:313–23. doi:10.1038/nri2515.

13. Bäckhed F, Ding H, Wang T, Hooper LV, Koh GY, Nagy A, et al. The gut microbiota as an environmental factor that regulates fat storage. Proc Natl Acad Sci U S A. 2004;101:15718–23. doi:10.1073/pnas.0407076101.

14. Muccioli GG, Naslain D, Backhed F, Reigstad CS, Lambert DM, Delzenne NM, Cani PD. The endocannabinoid system links gut microbiota to adipogenesis. Mol Syst Biol. 2010;6:392. doi:10.1038/msb.2010.46.

15. Le Chatelier E, Nielsen T, Qin J, Prifti E, Hildebrand F, Falony G, et al. Richness of human gut microbiome correlates with metabolic markers. Nature. 2013;500:541–6. doi:10.1038/nature12506.

16. Turnbaugh PJ, Hamady M, Yatsunenko T, Cantarel BL, Duncan A, Ley RE, et al. A core gut microbiome in obese and lean twins. Nature. 2009;457:480–4. doi:10.1038/nature07540.

17. Cotillard A, Kennedy SP, Kong LC, Prifti E, Pons N, Le Chatelier E, et al. Dietary intervention impact on gut microbial gene richness. Nature. 2013;500:585–8. doi:10.1038/nature12480.

18. Brignardello J, Morales P, Diaz E, Romero J, Brunser O, Gotteland M. Pilot study: alterations of intestinal microbiota in obese humans are not associated with colonic inflammation or disturbances of barrier function. Aliment Pharmacol Ther. 2010;32:1307–14. doi:10.1111/j.1365-2036.2010.04475.x.

19. Karlsson CLJ, Onnerfalt J, Xu J, Molin G, Ahrne S, Thorngren-Jerneck K. The microbiota of the gut in preschool children with normal and excessive body weight. Obesity (Silver Spring). 2012;20:2257–61. doi:10.1038/oby.2012.110.

20. Turnbaugh PJ, Ley RE, Mahowald MA, Magrini V, Mardis ER, Gordon JI. An obesity-associated gut microbiome with increased capacity for energy harvest. Nature. 2006;444:1027–31. doi:10.1038/nature05414.

21. Ley RE, Turnbaugh PJ, Klein S, Gordon JI. Microbial ecology: human gut microbes associated with obesity. Nature. 2006;444:1022–3. doi:10.1038/4441022a.

22. Fleissner CK, Huebel N, Abd El-Bary MM, Loh G, Klaus S, Blaut M. Absence of intestinal microbiota does not protect mice from diet-induced obesity. Br J Nutr. 2010;104:919–29. doi:10.1017/S0007114510001303.

23. Armougom F, Henry M, Vialettes B, Raccah D, Raoult D. Monitoring bacterial community of human gut microbiota reveals an increase in Lactobacillus in obese patients and Methanogens in anorexic patients. PLoS ONE. 2009;4:e7125. doi:10.1371/journal.pone.0007125.

24. Duncan SH, Lobley GE, Holtrop G, Ince J, Johnstone AM, Louis P, Flint HJ. Human colonic microbiota associated with diet, obesity and weight loss. Int J Obes (Lond). 2008;32:1720–4. doi:10.1038/ijo.2008.155.

25. Schwiertz A, Taras D, Schafer K, Beijer S, Bos NA, Donus C, Hardt PD. Microbiota and SCFA in lean and overweight healthy subjects. Obesity (Silver Spring). 2010;18:190–5. doi:10.1038/oby.2009.167.

26. Zhang H, DiBaise JK, Zuccolo A, Kudrna D, Braidotti M, Yu Y, et al. Human gut microbiota in obesity and after gastric bypass. Proc Natl Acad Sci U S A. 2009;106:2365–70. doi:10.1073/pnas.0812600106.

27. Qin J, Li Y, Cai Z, Li S, Zhu J, Zhang F, et al. A metagenome-wide association study of gut microbiota in type 2 diabetes. Nature. 2012;490:55–60. doi:10.1038/nature11450.

28. Forslund K, Hildebrand F, Nielsen T, Falony G, Le Chatelier E, Sunagawa S, et al. Disentangling type 2 diabetes and metformin treatment signatures in the human gut microbiota. Nature. 2015;528:262–6. doi:10.1038/nature15766.

29. Larsen N, Vogensen FK, van den Berg FWJ, Nielsen DS, Andreasen AS, Pedersen BK, et al. Gut microbiota in human adults with type 2 diabetes differs from non-diabetic adults. PLoS ONE. 2010;5:e9085. doi:10.1371/journal.pone.0009085.

30. Wu X, Ma C, Han L, Nawaz M, Gao F, Zhang X, et al. Molecular characterisation of the faecal microbiota in patients with type II diabetes. Curr Microbiol. 2010;61:69–78. doi:10.1007/s00284-010-9582-9.

31. Zhang X, Shen D, Fang Z, Jie Z, Qiu X, Zhang C, et al. Human gut microbiota changes reveal the progression of glucose intolerance. PLoS ONE. 2013;8:e71108. doi:10.1371/journal.pone.0071108.

32. Karlsson FH, Tremaroli V, Nookaew I, Bergstrom G, Behre CJ, Fagerberg B, et al. Gut metagenome in European women with normal, impaired and diabetic glucose control. Nature. 2013;498:99–103. doi:10.1038/nature12198.

33. Clavel T, Lagkouvardos I, Hiergeist A. Microbiome sequencing: challenges and opportunities for molecular medicine. Expert Rev Mol Diagn. 2016;16:795–805. doi:10.1080/14737159.2016.1184574.

34. Falony G, Joossens M, Vieira-Silva S, Wang J, Darzi Y, Faust K, et al. Population-level analysis of gut microbiome variation. Science. 2016;352:560–4. doi:10.1126/science.aad3503.

35. Vrieze A, van Nood E, Holleman F, Salojarvi J, Kootte RS, Bartelsman JFWM, et al. Transfer of intestinal microbiota from lean donors increases insulin sensitivity in individuals with metabolic syndrome. Gastroenterology. 2012;143:913-6.e7. doi:10.1053/j.gastro.2012.06.031.

36. Mouzaki M, Comelli EM, Arendt BM, Bonengel J, Fung SK, Fischer SE, et al. Intestinal microbiota in patients with nonalcoholic fatty liver disease. Hepatology. 2013;58:120–7. doi:10.1002/hep.26319.

37. Le Roy T, Llopis M, Lepage P, Bruneau A, Rabot S, Bevilacqua C, et al. Intestinal microbiota determines development of non-alcoholic fatty liver disease in mice. Gut. 2013;62:1787–94. doi:10.1136/gutjnl-2012-303816.

38. Zhu L, Baker SS, Gill C, Liu W, Alkhouri R, Baker RD, Gill SR. Characterization of gut microbiomes in nonalcoholic steatohepatitis (NASH) patients: a connection between endogenous alcohol and NASH. Hepatology. 2013;57:601–9. doi:10.1002/hep.26093.

39. Wong VW-S, Tse C-H, Lam TT-Y, Wong GL-H, Chim AM-L, Chu WC-W, et al. Molecular characterization of the fecal microbiota in patients with nonalcoholic steatohepatitis--a longitudinal study. PLoS ONE. 2013;8:e62885. doi:10.1371/journal.pone.0062885.

40. Raman M, Ahmed I, Gillevet PM, Probert CS, Ratcliffe NM, Smith S, et al. Fecal microbiome and volatile organic compound metabolome in obese humans with nonalcoholic fatty liver disease. Clin Gastroenterol Hepatol. 2013;11:868-75.e1-3. doi:10.1016/j.cgh.2013.02.015.

41. Karlsson FH, Fak F, Nookaew I, Tremaroli V, Fagerberg B, Petranovic D, et al. Symptomatic atherosclerosis is associated with an altered gut metagenome. Nat Commun. 2012;3:1245. doi:10.1038/ncomms2266.

42. Serino M, Luche E, Gres S, Baylac A, Bergé M, Cenac C, et al. Metabolic adaptation to a high-fat diet is associated with a change in the gut microbiota. Gut. 2012;61:543–53. doi:10.1136/gutjnl-2011-301012.

43. de La Serre C, Ellis CL, Lee J, Hartman AL, Rutledge JC, Raybould HE. Propensity to high-fat diet-induced obesity in rats is associated with changes in the gut microbiota and gut inflammation. Am J Physiol Gastrointest Liver Physiol. 2010;299:8. doi:10.1152/ajpgi.00098.2010.

44. Parks BW, Nam E, Org E, Kostem E, Norheim F, Hui ST, et al. Genetic control of obesity and gut microbiota composition in response to high-fat, high-sucrose diet in mice. Cell Metab. 2013;17:141–52. doi:10.1016/j.cmet.2012.12.007.

45. Prpic V, Watson PM, Frampton IC, Sabol MA, Jezek GE, Gettys TW. Adaptive changes in adipocyte gene expression differ in AKR/J and SWR/J mice during diet-induced obesity. J Nutr. 2002;132:3325–32.

46. Vijay-Kumar M, Aitken JD, Carvalho FA, Cullender TC, Mwangi S, Srinivasan S, et al. Metabolic syndrome and altered gut microbiota in mice lacking Toll-like receptor 5. Science. 2010;328:228–31. doi:10.1126/science.1179721.

47. Spruss A, Kanuri G, Wagnerberger S, Haub S, Bischoff SC, Bergheim I. Toll-like receptor 4 is involved in the development of fructose-induced hepatic steatosis in mice. Hepatology. 2009;50:1094–104. doi:10.1002/hep.23122.

48. Cani PD, Amar J, Iglesias MA, Poggi M, Knauf C, Bastelica D, et al. Metabolic endotoxemia initiates obesity and insulin resistance. Diabetes. 2007;56:1761–72. doi:10.2337/db06-1491.

49. Lam YY, Ha CWY, Campbell CR, Mitchell AJ, Dinudom A, Oscarsson J, et al. Increased gut permeability and microbiota change associate with mesenteric fat inflammation and metabolic dysfunction in diet-induced obese mice. PLoS ONE. 2012;7:e34233. doi:10.1371/journal.pone.0034233.

50. Kless C, Müller VM, Schüppel VL, Lichtenegger M, Rychlik M, Daniel H, et al. Diet-induced obesity causes metabolic impairment independent of alterations in gut barrier integrity. Mol Nutr Food Res. 2015;59:968–78. doi:10.1002/mnfr.201400840.

51. Müller VM, Zietek T, Rohm F, Fiamoncini J, Lagkouvardos I, Haller D, et al. Gut barrier impairment by high-fat diet in mice depends on housing conditions. Mol Nutr Food Res. 2016;60:897–908. doi:10.1002/mnfr.201500775.

52. den Besten G, Bleeker A, Gerding A, van Eunen K, Havinga R, van Dijk TH, et al. Short-Chain Fatty Acids Protect Against High-Fat Diet-Induced Obesity via a PPARgamma-Dependent Switch From Lipogenesis to Fat Oxidation. Diabetes. 2015;64:2398–408. doi:10.2337/db14-1213.

53. Blaut M, Klaus S. Intestinal microbiota and obesity. Handb Exp Pharmacol. 2012:251–73. doi:10.1007/978-3-642-24716-3_11.

54. Bäckhed F, Manchester JK, Semenkovich CF, Gordon JI. Mechanisms underlying the resistance to diet-induced obesity in germ-free mice. Proc Natl Acad Sci U S A. 2007;104:979–84. doi:10.1073/pnas.0605374104.

55. Pedersen HK, Gudmundsdottir V, Nielsen HB, Hyotylainen T, Nielsen T, Jensen BAH, et al. Human gut microbes impact host serum metabolome and insulin sensitivity. Nature. 2016;535:376–81. doi:10.1038/nature18646.

56. Lips MA, van Klinken JB, van Harmelen V, Dharuri HK, Hoen PAC 't, Laros JFJ, et al. Roux-en-Y gastric bypass surgery, but not calorie restriction, reduces plasma branched-chain amino acids in obese women independent of weight loss or the presence of type 2 diabetes. Diabetes Care. 2014;37:3150–6. doi:10.2337/dc14-0195.

57. Shah SH, Crosslin DR, Haynes CS, Nelson S, Turer CB, Stevens RD, et al. Branched-chain amino acid levels are associated with improvement in insulin resistance with weight loss. Diabetologia. 2012;55:321–30. doi:10.1007/s00125-011-2356-5.

58. Dumas M-E, Barton RH, Toye A, Cloarec O, Blancher C, Rothwell A, et al. Metabolic profiling reveals a contribution of gut microbiota to fatty liver phenotype in insulin-resistant mice. Proc Natl Acad Sci U S A. 2006;103:12511–6. doi:10.1073/pnas.0601056103.

59. Buchman AL, Dubin MD, Moukarzel AA, Jenden DJ, Roch M, Rice KM, et al. Choline deficiency: A cause of hepatic steatosis during parenteral nutrition that can be reversed with intravenous choline supplementation. Hepatology. 1995;22:1399–403. doi:10.1002/hep.1840220510.

60. Tanaka N, Matsubara T, Krausz KW, Patterson AD, Gonzalez FJ. Disruption of phospholipid and bile acid homeostasis in mice with nonalcoholic steatohepatitis. Hepatology. 2012;56:118–29. doi:10.1002/hep.25630.

61. Cope K, Risby T, Diehl AM. Increased gastrointestinal ethanol production in obese mice: implications for fatty liver disease pathogenesis. Gastroenterology. 2000;119:1340–7.

62. Wewalka M, Patti M-E, Barbato C, Houten SM, Goldfine AB. Fasting serum taurine-conjugated bile acids are elevated in type 2 diabetes and do not change with intensification of insulin. J Clin Endocrinol Metab. 2014;99:1442–51. doi:10.1210/jc.2013-3367.

63. Cariou B, Chetiveaux M, Zair Y, Pouteau E, Disse E, Guyomarc'h-Delasalle B, et al. Fasting plasma chenodeoxycholic acid and cholic acid concentrations are inversely correlated with insulin sensitivity in adults. Nutr Metab (Lond). 2011;8:48. doi:10.1186/1743-7075-8-48.

64. Brufau G, Stellaard F, Prado K, Bloks VW, Jonkers E, Boverhof R, et al. Improved glycemic control with colesevelam treatment in patients with type 2 diabetes is not directly associated with changes in bile acid metabolism. Hepatology. 2010;52:1455–64. doi:10.1002/hep.23831.

65. Haeusler RA, Astiarraga B, Camastra S, Accili D, Ferrannini E. Human insulin resistance is associated with increased plasma levels of 12alpha-hydroxylated bile acids. Diabetes. 2013;62:4184–91. doi:10.2337/db13-0639.

66. Patti M-E, Houten SM, Bianco AC, Bernier R, Larsen PR, Holst JJ, et al. Serum bile acids are higher in humans with prior gastric bypass: potential contribution to improved glucose and lipid metabolism. Obesity (Silver Spring). 2009;17:1671–7. doi:10.1038/oby.2009.102.

67. Mouzaki M, Wang AY, Bandsma R, Comelli EM, Arendt BM, Zhang L, et al. Bile Acids and Dysbiosis in Non-Alcoholic Fatty Liver Disease. PLoS ONE. 2016;11:e0151829. doi:10.1371/journal.pone.0151829.

68. Ali AH, Carey EJ, Lindor KD. Recent advances in the development of farnesoid X receptor agonists. Ann Transl Med. 2015;3:5. doi:10.3978/j.issn.2305-5839.2014.12.06.

69. Porez G, Prawitt J, Gross B, Staels B. Bile acid receptors as targets for the treatment of dyslipidemia and cardiovascular disease. J Lipid Res. 2012;53:1723–37. doi:10.1194/jlr.R024794.

70. Cariou B, van Harmelen K, Duran-Sandoval D, van Dijk TH, Grefhorst A, Abdelkarim M, et al. The farnesoid X receptor modulates adiposity and peripheral insulin sensitivity in mice. J Biol Chem. 2006;281:11039–49. doi:10.1074/jbc.M510258200.

71. Zhang Y, Lee FY, Barrera G, Lee H, Vales C, Gonzalez FJ, et al. Activation of the nuclear receptor FXR improves hyperglycemia and hyperlipidemia in diabetic mice. Proc Natl Acad Sci U S A. 2006;103:1006–11. doi:10.1073/pnas.0506982103.

72. Evans MJ, Mahaney PE, Borges-Marcucci L, Lai K, Wang S, Krueger JA, et al. A synthetic farnesoid X receptor (FXR) agonist promotes cholesterol lowering in models of dyslipidemia. Am J Physiol Gastrointest Liver Physiol. 2009;296:G543-52. doi:10.1152/ajpgi.90585.2008.

73. Flatt B, Martin R, Wang T-L, Mahaney P, Murphy B, Gu X-H, et al. Discovery of XL335 (WAY-362450), a highly potent, selective, and orally active agonist of the farnesoid X receptor (FXR). J Med Chem. 2009;52:904–7. doi:10.1021/jm8014124.

74. Pellicciari R, Fiorucci S, Camaioni E, Clerici C, Costantino G, Maloney PR, et al. 6α-Ethyl-Chenodeoxycholic Acid (6-ECDCA), a Potent and Selective FXR Agonist Endowed with Anticholestatic Activity. J. Med. Chem. 2002;45:3569–72. doi:10.1021/jm025529g.

75. Li YTY, Swales KE, Thomas GJ, Warner TD, Bishop-Bailey D. Farnesoid x receptor ligands inhibit vascular smooth muscle cell inflammation and migration. Arteriosclerosis, Thrombosis, and Vascular Biology. 2007;27:2606–11. doi:10.1161/ATVBAHA.107.152694.

76. Wang XX, Jiang T, Shen Y, Caldas Y, Miyazaki-Anzai S, Santamaria H, et al. Diabetic nephropathy is accelerated by farnesoid X receptor deficiency and inhibited by farnesoid X receptor activation in a type 1 diabetes model. Diabetes. 2010;59:2916–27. doi:10.2337/db10-0019.

77. Adorini L, Pruzanski M, Shapiro D. Farnesoid X receptor targeting to treat nonalcoholic steatohepatitis. Drug Discov Today. 2012;17:988–97. doi:10.1016/j.drudis.2012.05.012.

78. Hirschfield GM, Mason A, Luketic V, Lindor K, Gordon SC, Mayo M, et al. Efficacy of obeticholic acid in patients with primary biliary cirrhosis and inadequate response to ursodeoxycholic acid. Gastroenterology. 2015;148:751-61.e8. doi:10.1053/j.gastro.2014.12.005.

79. Ubeda M, Lario M, Munoz L, Borrero M-J, Rodriguez-Serrano M, Sanchez-Diaz A-M, et al. Obeticholic acid reduces bacterial translocation and inhibits intestinal inflammation in cirrhotic rats. J Hepatol. 2016;64:1049–57. doi:10.1016/j.jhep.2015.12.010.

80. Mudaliar S, Henry RR, Sanyal AJ, Morrow L, Marschall H-U, Kipnes M, et al. Efficacy and safety of the farnesoid X receptor agonist obeticholic acid in patients with type 2 diabetes and nonalcoholic fatty liver disease. Gastroenterology. 2013;145:574-82.e1. doi:10.1053/j.gastro.2013.05.042.

81. Urizar NL, Liverman AB, Dodds DT, Silva FV, Ordentlich P, Yan Y, et al. A natural product that lowers cholesterol as an antagonist ligand for FXR. Science. 2002;296:1703–6. doi:10.1126/science.1072891.

82. Deng R. Therapeutic effects of guggul and its constituent guggulsterone: cardiovascular benefits. Cardiovasc Drug Rev. 2007;25:375–90. doi:10.1111/j.1527-3466.2007.00023.x.

83. Ulbricht C, Basch E, Szapary P, Hammerness P, Axentsev S, Boon H, et al. Guggul for hyperlipidemia: a review by the Natural Standard Research Collaboration. Complement Ther Med. 2005;13:279–90. doi:10.1016/j.ctim.2005.08.003.

84. Pellicciari R, Gioiello A, Macchiarulo A, Thomas C, Rosatelli E, Natalini B, et al. Discovery of 6alpha-ethyl-23(S)-methylcholic acid (S-EMCA, INT-777) as a potent and selective agonist for the TGR5 receptor, a novel target for diabesity. J Med Chem. 2009;52:7958–61. doi:10.1021/jm901390p.

85. Pols TWH, Nomura M, Harach T, Lo Sasso G, Oosterveer MH, Thomas C, et al. TGR5 activation inhibits atherosclerosis by reducing macrophage inflammation and lipid loading. Cell Metab. 2011;14:747–57. doi:10.1016/j.cmet.2011.11.006.

86. Thomas C, Pellicciari R, Pruzanski M, Auwerx J, Schoonjans K. Targeting bile-acid signalling for metabolic diseases. Nat Rev Drug Discov. 2008;7:678–93. doi:10.1038/nrd2619.

87. Woting A, Pfeiffer N, Loh G, Klaus S, Blaut M. Clostridium ramosum promotes high-fat diet-induced obesity in gnotobiotic mouse models. MBio. 2014;5:e01530-14. doi:10.1128/mBio.01530-14.

88. Everard A, Belzer C, Geurts L, Ouwerkerk JP, Druart C, Bindels LB, et al. Cross-talk between Akkermansia muciniphila and intestinal epithelium controls diet-induced obesity. Proc Natl Acad Sci U S A. 2013;110:9066–71. doi:10.1073/pnas.1219451110.

89. Dao MC, Everard A, Aron-Wisnewsky J, Sokolovska N, Prifti E, Verger EO, et al. Akkermansia muciniphila and improved metabolic health during a dietary intervention in obesity: relationship with gut microbiome richness and ecology. Gut. 2016;65:426–36. doi:10.1136/gutjnl-2014-308778.

90. Fei N, Zhao L. An opportunistic pathogen isolated from the gut of an obese human causes obesity in germfree mice. ISME J. 2013;7:880–4. doi:10.1038/ismej.2012.153.

91. Wade WG, Downes J, Dymock D, Hiom SJ, Weightman AJ, Dewhirst FE, et al. The family Coriobacteriaceae: reclassification of Eubacterium exiguum (Poco et al. 1996) and Peptostreptococcus heliotrinreducens (Lanigan 1976) as Slackia exigua gen. nov., comb. nov. and Slackia heliotrinireducens gen. nov., comb. nov., and Eubacterium lentum (Prevot 1938) as Eggerthella lenta gen. nov., comb. nov. Int J Syst Bacteriol. 1999;49 Pt 2:595–600. doi:10.1099/00207713-49-2-595.

92. Clavel T, Charrier C, Braune A, Wenning M, Blaut M, Haller D. Isolation of bacteria from the ileal mucosa of TNFdeltaARE mice and description of Enterorhabdus mucosicola gen. nov., sp. nov. International Journal of Systematic and Evolutionary Microbiology. 2009;59:1805–12. doi:10.1099/ijs.0.003087-0.

93. Clavel T, Duck W, Charrier C, Wenning M, Elson C, Haller D. Enterorhabdus caecimuris sp. nov., a member of the family Coriobacteriaceae isolated from a mouse model of spontaneous colitis, and emended description of the genus Enterorhabdus Clavel et al. 2009. International Journal of Systematic and Evolutionary Microbiology. 2010;60:1527–31. doi:10.1099/ijs.0.015016-0.

94. Anderson RC, Rasmussen MA, Jensen NS, Allison MJ. Denitrobacterium detoxificans gen. nov., sp. nov., a ruminal bacterium that respires on nitrocompounds. International Journal of

Systemiatic and Evolutionary Microbiology. 2000;50 Pt 2:633–8. doi:10.1099/00207713-50-2-633.

95. Dewhirst FE, Paster BJ, Tzellas N, Coleman B, Downes J, Spratt DA, Wade WG. Characterization of novel human oral isolates and cloned 16S rDNA sequences that fall in the family Coriobacteriaceae: description of olsenella gen. nov., reclassification of Lactobacillus uli as Olsenella uli comb. nov. and description of Olsenella profusa sp. nov. International Journal of Systemiatic and Evolutionary Microbiology. 2001;51:1797–804. doi:10.1099/00207713-51-5-1797.

96. Minamida K, Ota K, Nishimukai M, Tanaka M, Abe A, Sone T, et al. Asaccharobacter celatus gen. nov., sp. nov., isolated from rat caecum. International Journal of Systemiatic and Evolutionary Microbiology. 2008;58:1238–40. doi:10.1099/ijs.0.64894-0.

97. Copeland A, Sikorski J, Lapidus A, Nolan M, Del Rio TG, Lucas S, et al. Complete genome sequence of Atopobium parvulum type strain (IPP 1246T). Stand. Genomic Sci. 2009;1:166–73. doi:10.4056/sigs.29547.

98. Würdemann D, Tindall BJ, Pukall R, Lünsdorf H, Strömpl C, Namuth T, et al. Gordonibacter pamelaeae gen. nov., sp. nov., a new member of the Coriobacteriaceae isolated from a patient with Crohn's disease, and reclassification of Eggerthella hongkongensis Lau et al. 2006 as Paraeggerthella hongkongensis gen. nov., comb. nov. International Journal of Systemiatic and Evolutionary Microbiology. 2009;59:1405–15. doi:10.1099/ijs.0.005900-0.

99. Kageyama A, Benno Y, Nakase T. Phylogenetic evidence for the transfer of Eubacterium lentum to the genus Eggerthella as Eggerthella lenta gen. nov., comb. nov. Int J Syst Bacteriol. 1999;49 Pt 4:1725–32. doi:10.1099/00207713-49-4-1725.

100. Kageyama A, Benno Y, Nakase T. Phylogenetic and phenotypic evidence for the transfer of Eubacterium aerofaciens to the genus Collinsella as Collinsella aerofaciens gen. nov., comb. nov. Int J Syst Bacteriol. 1999;49 Pt 2:557–65. doi:10.1099/00207713-49-2-557.

101. Clavel T, Charrier C, Wenning M, Haller D. Parvibacter caecicola gen. nov., sp. nov., a bacterium of the family Coriobacteriaceae isolated from the caecum of a mouse. International Journal of Systemiatic and Evolutionary Microbiology. 2013;63:2642–8. doi:10.1099/ijs.0.045344-0.

102. Lagier J-C, Elkarkouri K, Rivet R, Couderc C, Raoult D, Fournier P-E. Non contiguous-finished genome sequence and description of Senegalemassilia anaerobia gen. nov., sp. nov. Stand Genomic Sci. 2013;7:343–56. doi:10.4056/sigs.3246665.

103. Maruo T, Sakamoto M, Ito C, Toda T, Benno Y. Adlercreutzia equolifaciens gen. nov., sp. nov., an equol-producing bacterium isolated from human faeces, and emended description of the genus Eggerthella. International Journal of Systemiatic and Evolutionary Microbiology. 2008;58:1221–7. doi:10.1099/ijs.0.65404-0.

104. Liu D. Molecular detection of human bacterial pathogens. Boca Raton, FL: Taylor & Francis/CRC Press; 2011.

105. Rodriguez Jovita M, Collins MD, Sjoden B, Falsen E. Characterization of a novel Atopobium isolate from the human vagina: description of Atopobium vaginae sp. nov. Int J Syst Bacteriol. 1999;49 Pt 4:1573–6. doi:10.1099/00207713-49-4-1573.

106. Eggerth AH. The Gram-positive Non-spore-bearing Anaerobic Bacilli of Human Feces. J Bacteriol. 1935;30:277–99.

107. Clavel T, Lepage P, Charrier C. The Family Coriobacteriaceae: The Prokaryotes. 2014:201–38. doi:10.1007/978-3-642-30138-4.

108. Munoz R, Yarza P, Ludwig W, Euzeby J, Amann R, Schleifer K-H, et al. Release LTPs104 of the All-Species Living Tree. Syst Appl Microbiol. 2011;34:169–70. doi:10.1016/j.syapm.2011.03.001.

109. Yarza P, Ludwig W, Euzeby J, Amann R, Schleifer K-H, Glockner FO, Rossello-Mora R. Update of the All-Species Living Tree Project based on 16S and 23S rRNA sequence analyses. Syst Appl Microbiol. 2010;33:291–9. doi:10.1016/j.syapm.2010.08.001.

110. Yarza P, Richter M, Peplies J, Euzeby J, Amann R, Schleifer K-H, et al. The All-Species Living Tree project: a 16S rRNA-based phylogenetic tree of all sequenced type strains. Syst Appl Microbiol. 2008;31:241–50. doi:10.1016/j.syapm.2008.07.001.

111. Kumar S, Stecher G, Tamura K. MEGA7: Molecular Evolutionary Genetics Analysis Version 7.0 for Bigger Datasets. Mol Biol Evol. 2016;33:1870–4. doi:10.1093/molbev/msw054.

112. Nei M, Kumar S. Molecular evolution and phylogenetics. Oxford, New York: Oxford University Press; 2000.

113. Felsenstein J. Confidence Limits on Phylogenies: An Approach Using the Bootstrap. Evolution. 1985;39:783. doi:10.2307/2408678.

114. Bokkenheuser VD, Winter J, Finegold SM, Sutter VL, Ritchie AE, Moore WE, Holdeman LV. New markers for Eubacterium lentum. Applied and Environmental Microbiology. 1979;37:1001–6.

115. Wegner K, Just S, Gau L, Mueller H, Gerard P, Lepage P, et al. Rapid analysis of bile acids in different biological matrices using LC-ESI-MS/MS for the investigation of bile acid transformation by mammalian gut bacteria. Anal Bioanal Chem. 2017;1231–45. doi:10.1007/s00216-016-0048-1.

116. Martínez I, Perdicaro DJ, Brown AW, Hammons S, Carden TJ, Carr TP, et al. Diet-induced alterations of host cholesterol metabolism are likely to affect the gut microbiota composition in hamsters. Applied and Environmental Microbiology. 2013;79:516–24. doi:10.1128/AEM.03046-12.

117. Claus SP, Ellero SL, Berger B, Krause L, Bruttin A, Molina J, et al. Colonization-induced host-gut microbial metabolic interaction. MBio. 2011;2:e00271-10. doi:10.1128/mBio.00271-10.

118. Martinez I, Wallace G, Zhang C, Legge R, Benson AK, Carr TP, et al. Diet-Induced Metabolic Improvements in a Hamster Model of Hypercholesterolemia Are Strongly Linked to Alterations of the Gut Microbiota. Applied and Environmental Microbiology. 2009;75:4175–84. doi:10.1128/AEM.00380-09.

119. Thorasin T, Hoyles L, McCartney AL. Dynamics and diversity of the 'Atopobium cluster' in the human faecal microbiota, and phenotypic characterization of 'Atopobium cluster' isolates. Microbiology (Reading, Engl). 2015;161:565–79. doi:10.1099/mic.0.000016.

120. Klappenbach JA, Saxman PR, Cole JR, Schmidt TM. rrndb: the Ribosomal RNA Operon Copy Number Database. Nucleic Acids Res. 2001;29:181–4.

121. Downes J, Munson MA, Spratt DA, Kononen E, Tarkka E, Jousimies-Somer H, Wade WG. Characterisation of Eubacterium-like strains isolated from oral infections. J Med Microbiol. 2001;50:947–51. doi:10.1099/0022-1317-50-11-947.

122. Kazor CE, Mitchell PM, Lee AM, Stokes LN, Loesche WJ, Dewhirst FE, Paster BJ. Diversity of Bacterial Populations on the Tongue Dorsa of Patients with Halitosis and Healthy Patients. Journal of Clinical Microbiology. 2003;41:558–63. doi:10.1128/JCM.41.2.558-563.2003.

123. Harmsen HJ, Wildeboer-Veloo AC, Grijpstra J, Knol J, Degener JE, Welling GW. Development of 16S rRNA-based probes for the Coriobacterium group and the Atopobium cluster and their application for enumeration of Coriobacteriaceae in human feces from volunteers of different age groups. Applied and Environmental Microbiology. 2000;66:4523–7.

124. Gullon B, Gullon P, Tavaria FK, Yanez R. Assessment of the prebiotic effect of quinoa and amaranth in the human intestinal ecosystem. Food Funct. 2016;7:3782–8. doi:10.1039/c6fo00924g.

125. Chen Y, Ji F, Guo J, Shi D, Fang D, Li L. Dysbiosis of small intestinal microbiota in liver cirrhosis and its association with etiology. Sci Rep. 2016;6:34055. doi:10.1038/srep34055.

126. Xie G, Wang X, Liu P, Wei R, Chen W, Rajani C, et al. Distinctly altered gut microbiota in the progression of liver disease. Oncotarget. 2016;7:19355–66. doi:10.18632/oncotarget.8466.

127. Geurts L, Lazarevic V, Derrien M, Everard A, van Roye M, Knauf C, et al. Altered Gut Microbiota and Endocannabinoid System Tone in Obese and Diabetic Leptin-Resistant Mice: Impact on Apelin Regulation in Adipose Tissue. Front. Microbio. 2011. doi:10.3389/fmicb.2011.00149.

128. Dray C, Debard C, Jager J, Disse E, Daviaud D, Martin P, et al. Apelin and APJ regulation in adipose tissue and skeletal muscle of type 2 diabetic mice and humans. Am J Physiol Endocrinol Metab. 2010;298:E1161-9. doi:10.1152/ajpendo.00598.2009.

129. Moore WE, Holdeman LV. Human fecal flora: the normal flora of 20 Japanese-Hawaiians. Appl Microbiol. 1974;27:961–79.

130. Kassinen A, Krogius-Kurikka L, Mäkivuokko H, Rinttilä T, Paulin L, Corander J, et al. The fecal microbiota of irritable bowel syndrome patients differs significantly from that of healthy subjects. Gastroenterology. 2007;133:24–33. doi:10.1053/j.gastro.2007.04.005.

131. Wang R-F, Beggs ML, Erickson BD, Cerniglia CE. DNA microarray analysis of predominant human intestinal bacteria in fecal samples. Mol Cell Probes. 2004;18:223–34. doi:10.1016/j.mcp.2004.03.002.

132. Tap J, Mondot S, Levenez F, Pelletier E, Caron C, Furet J-P, et al. Towards the human intestinal microbiota phylogenetic core. Environ Microbiol. 2009;11:2574–84. doi:10.1111/j.1462-2920.2009.01982.x.

133. Arumugam M, Raes J, Pelletier E, Le Paslier D, Yamada T, Mende DR, et al. Enterotypes of the human gut microbiome. Nature. 2011;473:174–80. doi:10.1038/nature09944.

134. Lahti L, Salonen A, Kekkonen RA, Salojärvi J, Jalanka-Tuovinen J, Palva A, et al. Associations between the human intestinal microbiota, Lactobacillus rhamnosus GG and serum lipids indicated by integrated analysis of high-throughput profiling data. PeerJ. 2013;1:e32. doi:10.7717/peerj.32.

135. Candela M, Biagi E, Soverini M, Consolandi C, Quercia S, Severgnini M, et al. Modulation of gut microbiota dysbioses in type 2 diabetic patients by macrobiotic Ma-Pi 2 diet. Br J Nutr. 2016;116:80–93. doi:10.1017/S0007114516001045.

136. Liu W, Zhang J, Wu C, Cai S, Huang W, Chen J, et al. Unique Features of Ethnic Mongolian Gut Microbiome revealed by metagenomic analysis. Sci Rep. 2016;6:34826. doi:10.1038/srep34826.

137. Saunders E, Pukall R, Abt B, Lapidus A, Glavina Del Rio T, Copeland A, et al. Complete genome sequence of Eggerthella lenta type strain (IPP VPI 0255). Stand Genomic Sci. 2009;1:174–82. doi:10.4056/sigs.33592.

138. Kutschera M, Engst W, Blaut M, Braune A. Isolation of catechin-converting human intestinal bacteria. J Appl Microbiol. 2011;111:165–75. doi:10.1111/j.1365-2672.2011.05025.x.

139. Takagaki A, Nanjo F. Bioconversion of (-)-epicatechin, (+)-epicatechin, (-)-catechin, and (+)-catechin by (-)-epigallocatechin-metabolizing bacteria. Biol Pharm Bull. 2015;38:789–94. doi:10.1248/bpb.b14-00813.

140. Clavel T, Henderson G, Alpert C-A, Philippe C, Rigottier-Gois L, Dore J, Blaut M. Intestinal bacterial communities that produce active estrogen-like compounds enterodiol and enterolactone in humans. Applied and Environmental Microbiology. 2005;71:6077–85. doi:10.1128/AEM.71.10.6077-6085.2005.

141. Lee M-R, Huang Y-T, Liao C-H, Chuang T-Y, Wang W-J, Lee S-W, et al. Clinical and microbiological characteristics of bacteremia caused by Eggerthella, Paraeggerthella, and Eubacterium species at

a university hospital in Taiwan from 2001 to 2010. Journal of Clinical Microbiology. 2012;50:2053–5. doi:10.1128/JCM.00548-12.

142. Gardiner BJ, Korman TM, Junckerstorff RK. Eggerthella lenta bacteremia complicated by spondylodiscitis, psoas abscess, and meningitis. Journal of Clinical Microbiology. 2014;52:1278–80. doi:10.1128/JCM.03158-13.

143. Venugopal AA, Szpunar S, Johnson LB. Risk and prognostic factors among patients with bacteremia due to Eggerthella lenta. Anaerobe. 2012;18:475–8. doi:10.1016/j.anaerobe.2012.05.005.

144. Matthies A, Clavel T, Gütschow M, Engst W, Haller D, Blaut M, Braune A. Conversion of daidzein and genistein by an anaerobic bacterium newly isolated from the mouse intestine. Applied and Environmental Microbiology. 2008;74:4847–52. doi:10.1128/AEM.00555-08.

145. Yang J, Summanen PH, Henning SM, Hsu M, Lam H, Huang J, et al. Xylooligosaccharide supplementation alters gut bacteria in both healthy and prediabetic adults: a pilot study. Front Physiol. 2015;6:216. doi:10.3389/fphys.2015.00216.

146. Vessey DA, Whitney J, Gollan JL. The role of conjugation reactions in enhancing biliary secretion of bile acids. Biochem J. 1983;214:923–7.

147. Stamp D, Jenkins G. An Overview of Bile-Acid Synthesis, Chemistry and Function. 2008.

148. Kosters A, Karpen SJ. Bile acid transporters in health and disease. Xenobiotica. 2008;38:1043–71. doi:10.1080/00498250802040584.

149. Löffler G, Heinrich PC, Petrides PE, editors. Biochemie und Pathobiochemie: Chapter 32.1.4 and 32.1.6. 8th ed. Berlin, Heidelberg: Springer Medizin Verlag Heidelberg; 2007.

150. Hofmann AF, Hagey LR. Bile acids: chemistry, pathochemistry, biology, pathobiology, and therapeutics. Cell Mol Life Sci. 2008;65:2461–83. doi:10.1007/s00018-008-7568-6.

151. Jenkins GJ, Hardie L. Bile Acids: An Overview of Bile-Acid Synthesis, Chemistry and Function: The Royal Society of Chemistry; 2008.

152. DANIELSSON H. Influence of bile acids on digestion and absorption of lipids. Am J Clin Nutr. 1963;12:214–9.

153. Chiang JYL. Bile acid metabolism and signaling. Compr Physiol. 2013;3:1191–212. doi:10.1002/cphy.c120023.

154. Hylemon PB, Harder J. Biotransformation of monoterpenes, bile acids, and other isoprenoids in anaerobic ecosystems. FEMS Microbiol Rev. 1998;22:475–88.

155. Hill MJ, Drasar BS. Degradation of bile salts by human intestinal bacteria. Gut. 1968;9:22–7.

156. Ridlon JM, Kang D-J, Hylemon PB. Bile salt biotransformations by human intestinal bacteria. J Lipid Res. 2006;47:241–59. doi:10.1194/jlr.R500013-JLR200.

157. Macdonald IA, Sutherland JD, Cohen BI, Mosbach EH. Effect of bile acid oxazoline derivatives on microorganisms participating in 7 alpha-hydroxyl epimerization of primary bile acids. J Lipid Res. 1983;24:1550–9.

158. Liu L, Aigner A, Schmid RD. Identification, cloning, heterologous expression, and characterization of a NADPH-dependent 7β-hydroxysteroid dehydrogenase from Collinsella aerofaciens. Appl Microbiol Biotechnol. 2011;90:127–35. doi:10.1007/s00253-010-3052-y.

159. Savino S, Ferrandi EE, Forneris F, Rovida S, Riva S, Monti D, Mattevi A. Structural and biochemical insights into 7beta-hydroxysteroid dehydrogenase stereoselectivity. Proteins. 2016;84:859–65. doi:10.1002/prot.25036.

160. Bokkenheuser VD, Winter J, Dehazya P, Kelly WG. Isolation and characterization of human fecal bacteria capable of 21-dehydroxylating corticoids. Applied and Environmental Microbiology. 1977;34:571–5.

161. Bokkenheuser VD, Winter J, O'Rourke S, Ritchie AE. Isolation and characterization of fecal bacteria capable of 16 alpha-dehydroxylating corticoids. Applied and Environmental Microbiology. 1980;40:803–8.

162. Eggert T, Bakonyi D, Hummel W. Enzymatic routes for the synthesis of ursodeoxycholic acid. J Biotechnol. 2014;191:11–21. doi:10.1016/j.jbiotec.2014.08.006.

163. Neimark E, Chen F, Li X, Shneider BL. Bile acid-induced negative feedback regulation of the human ileal bile acid transporter. Hepatology. 2004;40:149–56. doi:10.1002/hep.20295.

164. Raufman JP, Zimniak P, Bartoszko-Malik A. Lithocholyltaurine interacts with cholinergic receptors on dispersed chief cells from guinea pig stomach. Am J Physiol. 1998;274:1004.

165. Raufman JP, Chen Y, Cheng K, Compadre C, Compadre L, Zimniak P. Selective interaction of bile acids with muscarinic receptors: a case of molecular mimicry. Eur J Pharmacol. 2002;457:77–84.

166. Hylemon PB, Zhou H, Pandak WM, Ren S, Gil G, Dent P. Bile acids as regulatory molecules. J Lipid Res. 2009;50:1509–20. doi:10.1194/jlr.R900007-JLR200.

167. Le Y, Murphy PM, Wang JM. Formyl-peptide receptors revisited. Trends Immunol. 2002;23:541–8.

168. Seol W, Choi HS, Moore DD. Isolation of proteins that interact specifically with the retinoid X receptor: two novel orphan receptors. Mol Endocrinol. 1995;9:72–85. doi:10.1210/mend.9.1.7760852.

169. Forman BM, Goode E, Chen J, Oro AE, Bradley DJ, Perlmann T, et al. Identification of a nuclear receptor that is activated by farnesol metabolites. Cell. 1995;81:687–93.

170. Lefebvre P, Cariou B, Lien F, Kuipers F, Staels B. Role of bile acids and bile acid receptors in metabolic regulation. Physiol Rev. 2009;89:147–91. doi:10.1152/physrev.00010.2008.

171. Rizzo G, Disante M, Mencarelli A, Renga B, Gioiello A, Pellicciari R, Fiorucci S. The farnesoid X receptor promotes adipocyte differentiation and regulates adipose cell function in vivo. Molecular Pharmacology. 2006;70:1164–73. doi:10.1124/mol.106.023820.

172. Claudel T, Sturm E, Duez H, Torra IP, Sirvent A, Kosykh V, et al. Bile acid-activated nuclear receptor FXR suppresses apolipoprotein A-I transcription via a negative FXR response element. J. Clin. Invest. 2002;109:961–71. doi:10.1172/JCI200214505.

173. Hageman J, Herrema H, Groen AK, Kuipers F. A role of the bile salt receptor FXR in atherosclerosis. Arteriosclerosis, Thrombosis, and Vascular Biology. 2010;30:1519–28. doi:10.1161/ATVBAHA.109.197897.

174. Jung D, Elferink MGL, Stellaard F, Groothuis GMM. Analysis of bile acid-induced regulation of FXR target genes in human liver slices. Liver Int. 2007;27:137–44. doi:10.1111/j.1478-3231.2006.01393.x.

175. Caron S, Huaman Samanez C, Dehondt H, Ploton M, Briand O, Lien F, et al. Farnesoid X receptor inhibits the transcriptional activity of carbohydrate response element binding protein in human hepatocytes. Molecular and Cellular Biology. 2013;33:2202–11. doi:10.1128/MCB.01004-12.

176. Chiang JYL. Farnesoid X Receptor Responds to Bile Acids and Represses Cholesterol 7alpha -Hydroxylase Gene (CYP7A1) Transcription. Journal of Biological Chemistry. 2000;275:10918–24. doi:10.1074/jbc.275.15.10918.

177. Kliewer SA, Mangelsdorf DJ. Bile Acids as Hormones: The FXR-FGF15/19 Pathway. Dig Dis. 2015;33:327–31. doi:10.1159/000371670.

178. Swann JR, Want EJ, Geier FM, Spagou K, Wilson ID, Sidaway JE, et al. Systemic gut microbial modulation of bile acid metabolism in host tissue compartments. Proc Natl Acad Sci U S A. 2011;108 Suppl 1:4523–30. doi:10.1073/pnas.1006734107.

179. Lefebvre P, Chinetti G, Fruchart J-C, Staels B. Sorting out the roles of PPAR alpha in energy metabolism and vascular homeostasis. J Clin Invest. 2006;116:571–80. doi:10.1172/JCI27989.

180. Pineda Torra I, Claudel T, Duval C, Kosykh V, Fruchart J-C, Staels B. Bile acids induce the expression of the human peroxisome proliferator-activated receptor alpha gene via activation of the farnesoid X receptor. Mol Endocrinol. 2003;17:259–72. doi:10.1210/me.2002-0120.

181. Fiorucci S, Rizzo G, Antonelli E, Renga B, Mencarelli A, Riccardi L, et al. Cross-talk between farnesoid-X-receptor (FXR) and peroxisome proliferator-activated receptor gamma contributes to the antifibrotic activity of FXR ligands in rodent models of liver cirrhosis. J Pharmacol Exp Ther. 2005;315:58–68. doi:10.1124/jpet.105.085597.

182. Tyagi S, Gupta P, Saini AS, Kaushal C, Sharma S. The peroxisome proliferator-activated receptor: A family of nuclear receptors role in various diseases. J Adv Pharm Technol Res. 2011;2:236–40. doi:10.4103/2231-4040.90879.

183. Costa V, Gallo MA, Letizia F, Aprile M, Casamassimi A, Ciccodicola A. PPARG: Gene Expression Regulation and Next-Generation Sequencing for Unsolved Issues. PPAR Research 2010. doi:10.1155/2010/409168.

184. Abdelkarim M, Caron S, Duhem C, Prawitt J, Dumont J, Lucas A, et al. The farnesoid X receptor regulates adipocyte differentiation and function by promoting peroxisome proliferator-activated receptor-gamma and interfering with the Wnt/beta-catenin pathways. J Biol Chem. 2010;285:36759–67. doi:10.1074/jbc.M110.166231.

185. Nakahara M, Furuya N, Takagaki K, Sugaya T, Hirota K, Fukamizu A, et al. Ileal bile acid-binding protein, functionally associated with the farnesoid X receptor or the ileal bile acid transporter, regulates bile acid activity in the small intestine. J Biol Chem. 2005;280:42283–9. doi:10.1074/jbc.M507454200.

186. Wang H, Chen J, Hollister K, Sowers LC, Forman BM. Endogenous Bile Acids Are Ligands for the Nuclear Receptor FXR/BAR. Molecular Cell. 1999;3:543–53. doi:10.1016/S1097-2765(00)80348-2.

187. Calkin AC, Tontonoz P. Transcriptional integration of metabolism by the nuclear sterol-activated receptors LXR and FXR. Nat Rev Mol Cell Biol. 2012;13:213–24. doi:10.1038/nrm3312.

188. Schmitt J, Kong B, Stieger B, Tschopp O, Schultze SM, Rau M, et al. Protective effects of farnesoid X receptor (FXR) on hepatic lipid accumulation are mediated by hepatic FXR and independent of intestinal FGF15 signal. Liver Int. 2015;35:1133–44. doi:10.1111/liv.12456.

189. Thomas AM, Hart SN, Kong B, Fang J, Zhong X-B, Guo GL. Genome-wide tissue-specific farnesoid X receptor binding in mouse liver and intestine. Hepatology. 2010;51:1410–9. doi:10.1002/hep.23450.

190. Watanabe M, Houten SM, Wang L, Moschetta A, Mangelsdorf DJ, Heyman RA, et al. Bile acids lower triglyceride levels via a pathway involving FXR, SHP, and SREBP-1c. J. Clin. Invest. 2004;113:1408–18. doi:10.1172/JCI200421025.

191. Kawamata Y. A G Protein-coupled Receptor Responsive to Bile Acids. Journal of Biological Chemistry. 2003;278:9435–40. doi:10.1074/jbc.M209706200.

192. Keitel V, Reinehr R, Gatsios P, Rupprecht C, Görg B, Selbach O, et al. The G-protein coupled bile salt receptor TGR5 is expressed in liver sinusoidal endothelial cells. Hepatology. 2007;45:695–704. doi:10.1002/hep.21458.

193. Keitel V, Cupisti K, Ullmer C, Knoefel WT, Kubitz R, Häussinger D. The membrane-bound bile acid receptor TGR5 is localized in the epithelium of human gallbladders. Hepatology. 2009;50:861–70. doi:10.1002/hep.23032.

194. Watanabe M, Houten SM, Mataki C, Christoffolete MA, Kim BW, Sato H, et al. Bile acids induce energy expenditure by promoting intracellular thyroid hormone activation. Nature. 2006;439:484–9. doi:10.1038/nature04330.

195. Thomas C, Gioiello A, Noriega L, Strehle A, Oury J, Rizzo G, et al. TGR5-mediated bile acid sensing controls glucose homeostasis. Cell Metab. 2009;10:167–77. doi:10.1016/j.cmet.2009.08.001.

196. Chen X, Lou G, Meng Z, Huang W. TGR5: a novel target for weight maintenance and glucose metabolism. Exp Diabetes Res. 2011;2011:853501. doi:10.1155/2011/853501.

197. Pols TWH, Noriega LG, Nomura M, Auwerx J, Schoonjans K. The bile acid membrane receptor TGR5: a valuable metabolic target. Dig Dis. 2011;29:37–44. doi:10.1159/000324126.

198. Charlton M. Obesity, hyperlipidemia, and metabolic syndrome. Liver Transpl. 2009;15 Suppl 2:S83-9. doi:10.1002/lt.21914.

199. Shi Y, Burn P. Lipid metabolic enzymes: emerging drug targets for the treatment of obesity. Nat Rev Drug Discov. 2004;3:695–710. doi:10.1038/nrd1469.

200. Wang TY, Liu M, Portincasa P, Wang DQ-H. New insights into the molecular mechanism of intestinal fatty acid absorption. Eur J Clin Invest. 2013;43:1203–23. doi:10.1111/eci.12161.

201. Cao J, Hawkins E, Brozinick J, Liu X, Zhang H, Burn P, Shi Y. A predominant role of acyl-CoA:monoacylglycerol acyltransferase-2 in dietary fat absorption implicated by tissue distribution, subcellular localization, and up-regulation by high fat diet. J Biol Chem. 2004;279:18878–86. doi:10.1074/jbc.M313272200.

202. Mostafa N, Bhat BG, Coleman RA. Increased hepatic monoacylglycerol acyltransferase activity in streptozotocin-induced diabetes: characterization and comparison with activities from adult and neonatal rat liver. Biochim Biophys Acta. 1993;1169:189–95.

203. Luan Y, Hirashima T, Man Z-W, Wang M-W, Kawano K, Sumida T. Pathogenesis of obesity by food restriction in OLETF rats-increased intestinal monoacylglycerol acyltransferase activities may be a crucial factor. Diabetes Res Clin Pract. 2002;57:75–82.

204. Klop B, Elte JWF, Cabezas MC. Dyslipidemia in obesity: mechanisms and potential targets. Nutrients. 2013;5:1218–40. doi:10.3390/nu5041218.

205. Trauner M, Claudel T, Fickert P, Moustafa T, Wagner M. Bile acids as regulators of hepatic lipid and glucose metabolism. Dig Dis. 2010;28:220–4. doi:10.1159/000282091.

206. Horton JD, Goldstein JL, Brown MS. SREBPs: Activators of the complete program of cholesterol and fatty acid synthesis in the liver. J. Clin. Invest. 2002;109:1125–31. doi:10.1172/JCI200215593.

207. Shimomura I, Bashmakov Y, Horton JD. Increased Levels of Nuclear SREBP-1c Associated with Fatty Livers in Two Mouse Models of Diabetes Mellitus. Journal of Biological Chemistry. 1999;274:30028–32. doi:10.1074/jbc.274.42.30028.

208. Steffensen KR, Gustafsson J-A. Putative Metabolic Effects of the Liver X Receptor (LXR). Diabetes. 2004;53:S36-S42. doi:10.2337/diabetes.53.2007.S36.

209. Joseph SB, McKilligin E, Pei L, Watson MA, Collins AR, Laffitte BA, et al. Synthetic LXR ligand inhibits the development of atherosclerosis in mice. Proc Natl Acad Sci U S A. 2002;99:7604–9. doi:10.1073/pnas.112059299.

210. Hodson L, Fielding BA. Stearoyl-CoA desaturase: rogue or innocent bystander? Prog Lipid Res. 2013;52:15–42. doi:10.1016/j.plipres.2012.08.002.

211. Peter A, Cegan A, Wagner S, Lehmann R, Stefan N, Konigsrainer A, et al. Hepatic lipid composition and stearoyl-coenzyme A desaturase 1 mRNA expression can be estimated from plasma VLDL fatty acid ratios. Clin Chem. 2009;55:2113–20. doi:10.1373/clinchem.2009.127274.

212. Miyazaki M, Ntambi JM. Role of stearoyl-coenzyme A desaturase in lipid metabolism. Prostaglandins, Leukotrienes and Essential Fatty Acids. 2003;68:113–21. doi:10.1016/S0952-3278(02)00261-2.

213. Enser M. Desaturation of stearic acid by liver and adipose tissue from obese-hyperglycaemic mice (ob/ob). Biochem J. 1975;148:551–5.

214. Enser M. The role of insulin in the regulation of stearic acid desaturase activity in liver and adipose tissue from obese--hyperglycaemic (ob/ob) and lean mice. Biochem J. 1979;180:551–8.

215. Smith SB, Mersmann HJ, Smith EO, Britain KG. Stearoyl-coenzyme A desaturase gene expression during growth in adipose tissue from obese and crossbred pigs. J Anim Sci. 1999;77:1710. doi:10.2527/1999.7771710x.

216. Waters KM, Ntambi JM. Polyunsaturated fatty acids inhibit hepatic stearoyl-CoA desaturase-1 gene in diabetic mice. Lipids. 1996;31:S33-S36. doi:10.1007/BF02637047.

217. Li J, Jia H, Cai X, Zhong H, Feng Q, Sunagawa S, et al. An integrated catalog of reference genes in the human gut microbiome. Nat Biotechnol. 2014;32:834–41. doi:10.1038/nbt.2942.

218. Altschul SF, Gish W, Miller W, Myers EW, Lipman DJ. Basic local alignment search tool. J Mol Biol. 1990;215:403–10. doi:10.1016/S0022-2836(05)80360-2.

219. Dashkevicz MP, Feighner SD. Development of a Differential Medium for Bile Salt Hydrolase-Active Lactobacillus spp. Applied and Environmental Microbiology. 1989:11–6.

220. Begley M, Hill C, Gahan CGM. Bile salt hydrolase activity in probiotics. Applied and Environmental Microbiology. 2006;72:1729–38. doi:10.1128/AEM.72.3.1729-1738.2006.

221. Kouker G, Jaeger KE. Specific and sensitive plate assay for bacterial lipases. Applied and Environmental Microbiology. 1987;53:211–3.

222. Haarman M, Knol J. Quantitative real-time PCR analysis of fecal Lactobacillus species in infants receiving a prebiotic infant formula. Applied and Environmental Microbiology. 2006;72:2359–65. doi:10.1128/AEM.72.4.2359-2365.2006.

223. Kläring K, Hanske L, Bui N, Charrier C, Blaut M, Haller D, et al. Intestinimonas butyriciproducens gen. nov., sp. nov., a butyrate-producing bacterium from the mouse intestine. International Journal of Systemiatic and Evolutionary Microbiology. 2013;63:4606–12. doi:10.1099/ijs.0.051441-0.

224. Godon JJ, Zumstein E, Dabert P, Habouzit F, Moletta R. Molecular microbial diversity of an anaerobic digestor as determined by small-subunit rDNA sequence analysis. Applied and Environmental Microbiology. 1997;63:2802–13.

225. Klindworth A, Pruesse E, Schweer T, Peplies J, Quast C, Horn M, Glöckner FO. Evaluation of general 16S ribosomal RNA gene PCR primers for classical and next-generation sequencing-based diversity studies. Nucleic Acids Res. 2013;41:e1. doi:10.1093/nar/gks808.

226. Berry D, Ben Mahfoudh K, Wagner M, Loy A. Barcoded primers used in multiplex amplicon pyrosequencing bias amplification. Applied and Environmental Microbiology. 2011;77:7846–9. doi:10.1128/AEM.05220-11.

227. Lagkouvardos I, Kläring K, Heinzmann SS, Platz S, Scholz B, Engel K, et al. Gut metabolites and bacterial community networks during a pilot intervention study with flaxseeds in healthy adult men. Mol Nutr Food Res 2015. doi:10.1002/mnfr.201500125.

228. Lagkouvardos I, Joseph D, Kapfhammer M, Giritli S, Horn M, Haller D, Clavel T. IMNGS: A comprehensive open resource of processed 16S rRNA microbial profiles for ecology and diversity studies. Sci Rep. 2016;6:33721. doi:10.1038/srep33721.

229. Edgar RC. UPARSE: highly accurate OTU sequences from microbial amplicon reads. Nat Methods. 2013;10:996–8. doi:10.1038/nmeth.2604.

230. Quast C, Pruesse E, Yilmaz P, Gerken J, Schweer T, Yarza P, et al. The SILVA ribosomal RNA gene database project: improved data processing and web-based tools. Nucleic Acids Res. 2013;41:6. doi:10.1093/nar/gks1219.

231. Wang Q, Garrity GM, Tiedje JM, Cole JR. Naive Bayesian classifier for rapid assignment of rRNA sequences into the new bacterial taxonomy. Applied and Environmental Microbiology. 2007;73:5261–7. doi:10.1128/AEM.00062-07.

232. Lagkouvardos I, Fischer S, Kumar N, Clavel T. Rhea: A transparent and modular R pipeline for microbial profiling based on 16S rRNA gene amplicons. PeerJ. 2017;5:e2836. doi:10.7717/peerj.2836.

233. Chun J, Lee J-H, Jung Y, Kim M, Kim S, Kim BK, Lim Y-W. EzTaxon: a web-based tool for the identification of prokaryotes based on 16S ribosomal RNA gene sequences. International Journal of Systematic and Evolutionary Microbiology. 2007;57:2259–61. doi:10.1099/ijs.0.64915-0.

234. Ecker J, Scherer M, Schmitz G, Liebisch G. A rapid GC-MS method for quantification of positional and geometric isomers of fatty acid methyl esters. J Chromatogr B Analyt Technol Biomed Life Sci. 2012;897:98–104. doi:10.1016/j.jchromb.2012.04.015.

235. Sjogren P, Sierra-Johnson J, Gertow K, Rosell M, Vessby B, Faire U de, et al. Fatty acid desaturases in human adipose tissue: relationships between gene expression, desaturation indexes and insulin resistance. Diabetologia. 2008;51:328–35. doi:10.1007/s00125-007-0876-9.

236. Ecker J, Liebisch G, Scherer M, Schmitz G. Differential effects of conjugated linoleic acid isomers on macrophage glycerophospholipid metabolism. J Lipid Res. 2010;51:2686–94. doi:10.1194/jlr.M007906.

237. Bligh EG, Dyer WJ. A rapid method of total lipid extraction and purification. Can J Biochem Physiol. 1959;37:911–7. doi:10.1139/o59-099.

238. Amann RI, Binder BJ, Olson RJ, Chisholm SW, Devereux R, Stahl DA. Combination of 16S rRNA-targeted oligonucleotide probes with flow cytometry for analyzing mixed microbial populations. Applied and Environmental Microbiology. 1990;56:1919–25.

239. Cox J, Mann M. MaxQuant enables high peptide identification rates, individualized p.p.b.-range mass accuracies and proteome-wide protein quantification. Nat Biotechnol. 2008;26:1367–72. doi:10.1038/nbt.1511.

240. Cox J, Neuhauser N, Michalski A, Scheltema RA, Olsen JV, Mann M. Andromeda: a peptide search engine integrated into the MaxQuant environment. J Proteome Res. 2011;10:1794–805. doi:10.1021/pr101065j.

241. Cox J, Hein MY, Luber CA, Paron I, Nagaraj N, Mann M. Accurate proteome-wide label-free quantification by delayed normalization and maximal peptide ratio extraction, termed MaxLFQ. Mol Cell Proteomics. 2014;13:2513–26. doi:10.1074/mcp.M113.031591.

242. Wisniewski JR, Hein MY, Cox J, Mann M. A "proteomic ruler" for protein copy number and concentration estimation without spike-in standards. Mol Cell Proteomics. 2014;13:3497–506. doi:10.1074/mcp.M113.037309.

243. Livak KJ, Schmittgen TD. Analysis of relative gene expression data using real-time quantitative PCR and the 2(-Delta Delta C(T)) Method. Methods. 2001;25:402–8. doi:10.1006/meth.2001.1262.

244. Jo J, Gavrilova O, Pack S, Jou W, Mullen S, Sumner AE, et al. Hypertrophy and/or Hyperplasia: Dynamics of Adipose Tissue Growth. PLoS Comput Biol. 2009;5:e1000324. doi:10.1371/journal.pcbi.1000324.

245. Wolf MJ, Adili A, Piotrowitz K, Abdullah Z, Boege Y, Stemmer K, et al. Metabolic activation of intrahepatic CD8+ T cells and NKT cells causes nonalcoholic steatohepatitis and liver cancer via cross-talk with hepatocytes. Cancer Cell. 2014;26:549–64. doi:10.1016/j.ccell.2014.09.003.

246. Silva J, Dasgupta S, Wang G, Krishnamurthy K, Ritter E, Bieberich E. Lipids isolated from bone induce the migration of human breast cancer cells. J Lipid Res. 2006;47:724–33. doi:10.1194/jlr.M500473-JLR200.

247. Berger E, Heraud S, Mojallal A, Lequeux C, Weiss-Gayet M, Damour O, Geloen A. Pathways commonly dysregulated in mouse and human obese adipose tissue: FAT/CD36 modulates differentiation and lipogenesis. Adipocyte. 2015;4:161–80. doi:10.4161/21623945.2014.987578.

248. Ecker J, Liebisch G. Application of stable isotopes to investigate the metabolism of fatty acids, glycerophospholipid and sphingolipid species. Prog Lipid Res. 2014;54:14–31. doi:10.1016/j.plipres.2014.01.002.

249. Million M, Lagier J-C, Yahav D, Paul M. Gut bacterial microbiota and obesity. Clin Microbiol Infect. 2013;19:305–13. doi:10.1111/1469-0691.12172.

250. Walker AW, Ince J, Duncan SH, Webster LM, Holtrop G, Ze X, et al. Dominant and diet-responsive groups of bacteria within the human colonic microbiota. ISME J. 2011;5:220–30. doi:10.1038/ismej.2010.118.

251. Angelakis E, Bastelica D, Ben Amara A, El Filali A, Dutour A, Mege J-L, et al. An evaluation of the effects of Lactobacillus ingluviei on body weight, the intestinal microbiome and metabolism in mice. Microb Pathog. 2012;52:61–8. doi:10.1016/j.micpath.2011.10.004.

252. Newgard CB, An J, Bain JR, Muehlbauer MJ, Stevens RD, Lien LF, et al. A branched-chain amino acid-related metabolic signature that differentiates obese and lean humans and contributes to insulin resistance. Cell Metab. 2009;9:311–26. doi:10.1016/j.cmet.2009.02.002.

253. Wang TJ, Larson MG, Vasan RS, Cheng S, Rhee EP, McCabe E, et al. Metabolite profiles and the risk of developing diabetes. Nat Med. 2011;17:448–53. doi:10.1038/nm.2307.

254. Schneeberger M, Everard A, Gomez-Valades AG, Matamoros S, Ramirez S, Delzenne NM, et al. Akkermansia muciniphila inversely correlates with the onset of inflammation, altered adipose tissue metabolism and metabolic disorders during obesity in mice. Sci Rep. 2015;5:16643. doi:10.1038/srep16643.

255. Gauffin Cano P, Santacruz A, Moya A, Sanz Y. Bacteroides uniformis CECT 7771 ameliorates metabolic and immunological dysfunction in mice with high-fat-diet induced obesity. PLoS ONE. 2012;7:e41079. doi:10.1371/journal.pone.0041079.

256. Yin Y-N, Yu Q-F, Fu N, Liu X-W, Lu F-G. Effects of four Bifidobacteria on obesity in high-fat diet induced rats. World J Gastroenterol. 2010;16:3394–401.

257. An HM, Park SY, Lee DK, Kim JR, Cha MK, Lee SW, et al. Antiobesity and lipid-lowering effects of Bifidobacterium spp. in high fat diet-induced obese rats. Lipids Health Dis. 2011;10:116. doi:10.1186/1476-511X-10-116.

258. Fak F, Backhed F. Lactobacillus reuteri prevents diet-induced obesity, but not atherosclerosis, in a strain dependent fashion in Apoe-/- mice. PLoS ONE. 2012;7:e46837. doi:10.1371/journal.pone.0046837.

259. Wang J, Tang H, Zhang C, Zhao Y, Derrien M, Rocher E, et al. Modulation of gut microbiota during probiotic-mediated attenuation of metabolic syndrome in high fat diet-fed mice. ISME J. 2015;9:1–15. doi:10.1038/ismej.2014.99.

260. Li F, Jiang C, Krausz KW, Li Y, Albert I, Hao H, et al. Microbiome remodelling leads to inhibition of intestinal farnesoid X receptor signalling and decreased obesity. Nat Commun. 2013;4:2384. doi:10.1038/ncomms3384.

261. Koza RA, Nikonova L, Hogan J, Rim J-S, Mendoza T, Faulk C, et al. Changes in gene expression foreshadow diet-induced obesity in genetically identical mice. PLoS Genet. 2006;2:e81. doi:10.1371/journal.pgen.0020081.

262. Kovacova Z, Tharp WG, Liu D, Wei W, Xie H, Collins S, Pratley RE. Adipose tissue natriuretic peptide receptor expression is related to insulin sensitivity in obesity and diabetes. Obesity (Silver Spring). 2016;24:820–8. doi:10.1002/oby.21418.

263. Morton NM, Nelson YB, Michailidou Z, Di Rollo EM, Ramage L, Hadoke PWF, et al. A stratified transcriptomics analysis of polygenic fat and lean mouse adipose tissues identifies novel candidate obesity genes. PLoS ONE. 2011;6:e23944. doi:10.1371/journal.pone.0023944.

264. Sengenes C, Zakaroff-Girard A, Moulin A, Berlan M, Bouloumie A, Lafontan M, Galitzky J. Natriuretic peptide-dependent lipolysis in fat cells is a primate specificity. Am J Physiol Regul Integr Comp Physiol. 2002;283:R257-65. doi:10.1152/ajpregu.00453.2001.

265. Birkenfeld AL, Boschmann M, Moro C, Adams F, Heusser K, Franke G, et al. Lipid mobilization with physiological atrial natriuretic peptide concentrations in humans. J Clin Endocrinol Metab. 2005;90:3622–8. doi:10.1210/jc.2004-1953.

266. Galitzky J, Sengenes C, Thalamas C, Marques MA, Senard JM, Lafontan M, Berlan M. The lipid-mobilizing effect of atrial natriuretic peptide is unrelated to sympathetic nervous system activation or obesity in young men. J Lipid Res. 2001;42:536–44.

267. Morigny P, Houssier M, Mouisel E, Langin D. Adipocyte lipolysis and insulin resistance. Biochimie. 2016;125:259–66. doi:10.1016/j.biochi.2015.10.024.

268. de Wit N, Derrien M, Bosch-Vermeulen H, Oosterink E, Keshtkar S, Duval C, et al. Saturated fat stimulates obesity and hepatic steatosis and affects gut microbiota composition by an enhanced overflow of dietary fat to the distal intestine. Am J Physiol Gastrointest Liver Physiol. 2012;303:G589-99. doi:10.1152/ajpgi.00488.2011.

269. Lovejoy JC. The influence of dietary fat on insulin resistance. Curr Diab Rep. 2002;2:435–40.

270. Lovejoy JC, Smith SR, Champagne CM, Most MM, Lefevre M, DeLany JP, et al. Effects of diets enriched in saturated (palmitic), monounsaturated (oleic), or trans (elaidic) fatty acids on insulin sensitivity and substrate oxidation in healthy adults. Diabetes Care. 2002;25:1283–8.

271. Montgomery MK, Hallahan NL, Brown SH, Liu M, Mitchell TW, Cooney GJ, Turner N. Mouse strain-dependent variation in obesity and glucose homeostasis in response to high-fat feeding. Diabetologia. 2013;56:1129–39. doi:10.1007/s00125-013-2846-8.

272. Cani PD, Bibiloni R, Knauf C, Waget A, Neyrinck AM, Delzenne NM, Burcelin R. Changes in gut microbiota control metabolic endotoxemia-induced inflammation in high-fat diet-induced obesity and diabetes in mice. Diabetes. 2008;57:1470–81. doi:10.2337/db07-1403.

273. Zardooz H, Rostamkhani F, Zaringhalam J, Faraji Shahrivar F. Plasma corticosterone, insulin and glucose changes induced by brief exposure to isoflurane, diethyl ether and CO2 in male rats. Physiol Res. 2010;59:973–8.

274. He M, Pei Z, Mohsen A-W, Watkins P, Murdoch G, van Veldhoven PP, et al. Identification and characterization of new long chain acyl-CoA dehydrogenases. Mol Genet Metab. 2011;102:418–29. doi:10.1016/j.ymgme.2010.12.005.

275. Polz E, Kostner GM. The binding of beta 2-glycoprotein-I to human serum lipoproteins: distribution among density fractions. FEBS Letters. 1979;102:183–6.

276. Polz E, Kostner GM, HOLASEK A. Studies on the Protein Composition of Human Serum Very Low Density Lipoproteins: Demonstration of the β2 -Glycoprotein-I. Hoppe-Seyler´s Zeitschrift für physiologische Chemie. 1979;360:1061–8. doi:10.1515/bchm2.1979.360.2.1061.

277. Nakaya Y, Schaefer EJ, Brewer H. Activation of human post heparin lipoprotein lipase by apolipoprotein H (β2-glycoprotein I). Biochem Biophys Res Commun. 1980;95:1168–72. doi:10.1016/0006-291X(80)91595-8.

278. Crook M, Chng SI, Lumb P, Reid F. Serum apolipoprotein H and its relationship to blood pressure, serum lipids, fasting plasma glucose and insulin in normal individuals. Ann Clin Biochem. 2001;38:494–8.

279. Graham TE, Yang Q, Bluher M, Hammarstedt A, Ciaraldi TP, Henry RR, et al. Retinol-binding protein 4 and insulin resistance in lean, obese, and diabetic subjects. N Engl J Med. 2006;354:2552–63. doi:10.1056/NEJMoa054862.

280. Castro A, Lazaro I, Selva DM, Cespedes E, Girona J, NuriaPlana, et al. APOH is increased in the plasma and liver of type 2 diabetic patients with metabolic syndrome. Atherosclerosis. 2010;209:201–5. doi:10.1016/j.atherosclerosis.2009.09.072.

281. Morak M, Schmidinger H, Riesenhuber G, Rechberger GN, Kollroser M, Haemmerle G, et al. Adipose triglyceride lipase (ATGL) and hormone-sensitive lipase (HSL) deficiencies affect expression of lipolytic activities in mouse adipose tissues. Mol Cell Proteomics. 2012;11:1777–89. doi:10.1074/mcp.M111.015743.

282. Singh M, Kaur R, Lee M-J, Pickering RT, Sharma VM, Puri V, Kandror KV. Fat-specific protein 27 inhibits lipolysis by facilitating the inhibitory effect of transcription factor Egr1 on transcription of adipose triglyceride lipase. J Biol Chem. 2014;289:14481–7. doi:10.1074/jbc.C114.563080.

283. Ito M, Nagasawa M, Hara T, Ide T, Murakami K. Differential roles of CIDEA and CIDEC in insulin-induced anti-apoptosis and lipid droplet formation in human adipocytes. J Lipid Res. 2010;51:1676–84. doi:10.1194/jlr.M002147.

284. Matsusue K, Kusakabe T, Noguchi T, Takiguchi S, Suzuki T, Yamano S, Gonzalez FJ. Hepatic steatosis in leptin-deficient mice is promoted by the PPARgamma target gene Fsp27. Cell Metab. 2008;7:302–11. doi:10.1016/j.cmet.2008.03.003.

285. Langhi C, Baldan A. CIDEC/FSP27 is regulated by peroxisome proliferator-activated receptor alpha and plays a critical role in fasting- and diet-induced hepatosteatosis. Hepatology. 2015;61:1227–38. doi:10.1002/hep.27607.

286. Nishino N, Tamori Y, Tateya S, Kawaguchi T, Shibakusa T, Mizunoya W, et al. FSP27 contributes to efficient energy storage in murine white adipocytes by promoting the formation of unilocular lipid droplets. J Clin Invest. 2008;118:2808–21. doi:10.1172/JCI34090.

287. Langhi C, Arias N, Rajamoorthi A, Basta J, Lee RG, Baldan A. Therapeutic silencing of Fat Specific Protein 27 improves glycemic control in mouse models of obesity and insulin resistance. J Lipid Res 2016. doi:10.1194/jlr.M069799.

288. Moreno-Navarrete JM, Ortega F, Serrano M, Rodriguez-Hermosa JI, Ricart W, Mingrone G, Fernandez-Real JM. CIDEC/FSP27 and PLIN1 gene expression run in parallel to mitochondrial genes in human adipose tissue, both increasing after weight loss. Int J Obes (Lond). 2014;38:865–72. doi:10.1038/ijo.2013.171.

289. Guilherme A, Virbasius JV, Puri V, Czech MP. Adipocyte dysfunctions linking obesity to insulin resistance and type 2 diabetes. Nat Rev Mol Cell Biol. 2008;9:367–77. doi:10.1038/nrm2391.

290. Bjursell M, Wedin M, Admyre T, Hermansson M, Bottcher G, Goransson M, et al. Ageing Fxr deficient mice develop increased energy expenditure, improved glucose control and liver damage resembling NASH. PLoS ONE. 2013;8:e64721. doi:10.1371/journal.pone.0064721.

291. Jiang C, Xie C, Lv Y, Li J, Krausz KW, Shi J, et al. Intestine-selective farnesoid X receptor inhibition improves obesity-related metabolic dysfunction. Nat Commun. 2015;6:10166. doi:10.1038/ncomms10166.

292. Zhang Y, Ge X, Heemstra LA, Chen W-D, Xu J, Smith JL, et al. Loss of FXR protects against diet-induced obesity and accelerates liver carcinogenesis in ob/ob mice. Mol Endocrinol. 2012;26:272–80. doi:10.1210/me.2011-1157.

293. Parseus A, Sommer N, Sommer F, Caesar R, Molinaro A, Stahlman M, et al. Microbiota-induced obesity requires farnesoid X receptor. Gut 2016. doi:10.1136/gutjnl-2015-310283.

294. Prawitt J, Abdelkarim M, Stroeve JHM, Popescu I, Duez H, Velagapudi VR, et al. Farnesoid X receptor deficiency improves glucose homeostasis in mouse models of obesity. Diabetes. 2011;60:1861–71. doi:10.2337/db11-0030.

295. Watanabe M, Horai Y, Houten SM, Morimoto K, Sugizaki T, Arita E, et al. Lowering bile acid pool size with a synthetic farnesoid X receptor (FXR) agonist induces obesity and diabetes through reduced energy expenditure. J Biol Chem. 2011;286:26913–20. doi:10.1074/jbc.M111.248203.

296. Fang S, Suh JM, Reilly SM, Yu E, Osborn O, Lackey D, et al. Intestinal FXR agonism promotes adipose tissue browning and reduces obesity and insulin resistance. Nat Med. 2015;21:159–65. doi:10.1038/nm.3760.

297. Vidal-Puig A, Jimenez-Linan M, Lowell BB, Hamann A, Hu E, Spiegelman B, et al. Regulation of PPAR gamma gene expression by nutrition and obesity in rodents. J Clin Invest. 1996;97:2553–61. doi:10.1172/JCI118703.

298. Memon RA, Tecott LH, Nonogaki K, Beigneux A, Moser AH, Grunfeld C, Feingold KR. Up-regulation of peroxisome proliferator-activated receptors (PPAR-alpha) and PPAR-gamma messenger ribonucleic acid expression in the liver in murine obesity: troglitazone induces expression of PPAR-gamma-responsive adipose tissue-specific genes in the liver of obese diabetic mice. Endocrinology. 2000;141:4021–31. doi:10.1210/endo.141.11.7771.

299. Bedoucha M, Atzpodien E, Boelsterli UA. Diabetic KKAy mice exhibit increased hepatic PPARgamma1 gene expression and develop hepatic steatosis upon chronic treatment with antidiabetic thiazolidinediones. J Hepatol. 2001;35:17–23.

300. Matsusue K, Haluzik M, Lambert G, Yim S-H, Gavrilova O, Ward JM, et al. Liver-specific disruption of PPARgamma in leptin-deficient mice improves fatty liver but aggravates diabetic phenotypes. J Clin Invest. 2003;111:737–47. doi:10.1172/JCI17223.

301. Chawla A, Boisvert WA, Lee CH, Laffitte BA, Barak Y, Joseph SB, et al. A PPAR gamma-LXR-ABCA1 pathway in macrophages is involved in cholesterol efflux and atherogenesis. Molecular Cell. 2001;7:161–71.

302. Caron-Jobin M, Mauvoisin D, Michaud A, Veilleux A, Noel S, Fortier MP, et al. Stearic acid content of abdominal adipose tissues in obese women. Nutr Diabetes. 2012;2:e23. doi:10.1038/nutd.2011.19.

303. Kunesova M, Hlavaty P, Tvrzicka E, Stankova B, Kalouskova P, Viguerie N, et al. Fatty acid composition of adipose tissue triglycerides after weight loss and weight maintenance: the DIOGENES study. Physiol Res. 2012;61:597–607.

304. Miyata M, Matsuda Y, Tsuchiya H, Kitada H, Akase T, Shimada M, et al. Chenodeoxycholic acid-mediated activation of the farnesoid X receptor negatively regulates hydroxysteroid sulfotransferase. Drug Metab Pharmacokinet. 2006;21:315–23.

305. Werner A, Kuipers F, Verkade HJ. Fat Absorption and Lipid Metabolism in Cholestasis. In: Trauner M, Jansen PLM, editors. Molecular Pathogenesis of Cholestasis. Boston, MA: Springer Verlag; 2013. p. 314–328. doi:10.1007/978-1-4419-9034-1_23.

306. Iqbal J, Hussain MM. Intestinal lipid absorption. Am J Physiol Endocrinol Metab. 2009;296:94. doi:10.1152/ajpendo.90899.2008.

307. Gomez MX, Polin D. Influence of cholic acid on the utilization of fats in the growing chicken. Poult Sci. 1974;53:773–81.

308. Coburn CT, Hajri T, Ibrahimi A, Abumrad NA. Role of CD36 in membrane transport and utilization of long-chain fatty acids by different tissues. J Mol Neurosci. 2001;16:117-21; discussion 151-7. doi:10.1385/JMN:16:2-3:117.

309. Henkin AH, Cohen AS, Dubikovskaya EA, Park HM, Nikitin GF, Auzias MG, et al. Real-time noninvasive imaging of fatty acid uptake in vivo. ACS Chem Biol. 2012;7:1884–91. doi:10.1021/cb300194b.

310. Utsunomiya H, Yamamoto Y, Takeshita E, Tokumoto Y, Tada F, Miyake T, et al. Upregulated absorption of dietary palmitic acids with changes in intestinal transporters in non-alcoholic steatohepatitis (NASH). J Gastroenterol 2017. doi:10.1007/s00535-016-1298-6.

311. Koutsari C, Ali AH, Mundi MS, Jensen MD. Storage of circulating free fatty acid in adipose tissue of postabsorptive humans: quantitative measures and implications for body fat distribution. Diabetes. 2011;60:2032–40. doi:10.2337/db11-0154.

312. Rey FE, Gonzalez MD, Cheng J, Wu M, Ahern PP, Gordon JI. Metabolic niche of a prominent sulfate-reducing human gut bacterium. Proc Natl Acad Sci U S A. 2013;110:13582–7. doi:10.1073/pnas.1312524110.

313. Kübeck R, Bonet-Ripoll C, Hoffmann C, Walker A, Muller VM, Schuppel VL, et al. Dietary fat and gut microbiota interactions determine diet-induced obesity in mice. Mol Metab. 2016;5:1162–74. doi:10.1016/j.molmet.2016.10.001.

314. Wainfan E, Henkin G, Rittenberg SC, Marx W. Metabolism of cholesterol by intestinal bacteria in vitro. J Biol Chem. 1954;207:843–9.

315. Yan L, Combs GF, JR, DeMars LC, Johnson LK. Effects of the physical form of the diet on food intake, growth, and body composition changes in mice. J Am Assoc Lab Anim Sci. 2011;50:488–94.

316. Desmarchelier C, Ludwig T, Scheundel R, Rink N, Bader BL, Klingenspor M, Daniel H. Diet-induced obesity in ad libitum-fed mice: food texture overrides the effect of macronutrient composition. Br J Nutr. 2013;109:1518–27. doi:10.1017/S0007114512003340.

317. Anegawa E, Kotorii N, Ishimaru Y, Okuro M, Sakai N, Nishino S. Chronic Powder Diet After Weaning Induces Sleep, Behavioral, Neuroanatomical, and Neurophysiological Changes in Mice. PLoS ONE. 2015;10:e0143909. doi:10.1371/journal.pone.0143909.

318. Clavel T, Desmarchelier C, Haller D, Gérard P, Rohn S, Lepage P, Daniel H. Intestinal microbiota in metabolic diseases: from bacterial community structure and functions to species of pathophysiological relevance. Gut Microbes. 2014;5:544–51. doi:10.4161/gmic.29331.

319. Sayin SI, Wahlström A, Felin J, Jäntti S, Marschall H-U, Bamberg K, et al. Gut microbiota regulates bile acid metabolism by reducing the levels of tauro-beta-muricholic acid, a naturally occurring FXR antagonist. Cell Metab. 2013;17:225–35. doi:10.1016/j.cmet.2013.01.003.

320. Zietak M, Kovatcheva-Datchary P, Markiewicz LH, Stahlman M, Kozak LP, Backhed F. Altered Microbiota Contributes to Reduced Diet-Induced Obesity upon Cold Exposure. Cell Metab. 2016;23:1216–23. doi:10.1016/j.cmet.2016.05.001.

321. Islam S, Fukiya S, Hagio M, Fujii N, Ishizuka S, Ooka T, et al. Bile acid is a host factor that regulates the composition of the cecal microbiota in rats. Gastroenterology. 2011;141:1773–81. doi:10.1053/j.gastro.2011.07.046.

322. Ridlon JM, Alves JM, Hylemon PB, Bajaj JS. Cirrhosis, bile acids and gut microbiota: unraveling a complex relationship. Gut Microbes. 2013;4:382–7. doi:10.4161/gmic.25723.

323. Pfeiffer N, Desmarchelier C, Blaut M, Daniel H, Haller D, Clavel T. Acetatifactor muris gen. nov., sp. nov., a novel bacterium isolated from the intestine of an obese mouse. Arch Microbiol. 2012;194:901–7. doi:10.1007/s00203-012-0822-1.

324. Hildebrandt MA, Hoffmann C, Sherrill-Mix SA, Keilbaugh SA, Hamady M, Chen Y-Y, et al. High-fat diet determines the composition of the murine gut microbiome independently of obesity. Gastroenterology. 2009;137:1716-24.e1-2. doi:10.1053/j.gastro.2009.08.042.

325. Zhang C, Zhang M, Pang X, Zhao Y, Wang L, Zhao L. Structural resilience of the gut microbiota in adult mice under high-fat dietary perturbations. ISME J. 2012;6:1848–57. doi:10.1038/ismej.2012.27.

326. Zhang C, Zhang M, Wang S, Han R, Cao Y, Hua W, et al. Interactions between gut microbiota, host genetics and diet relevant to development of metabolic syndromes in mice. ISME J. 2010;4:232–41. doi:10.1038/ismej.2009.112.

327. Andoh A, Nishida A, Takahashi K, Inatomi O, Imaeda H, Bamba S, et al. Comparison of the gut microbial community between obese and lean peoples using 16S gene sequencing in a Japanese population. J Clin Biochem Nutr. 2016;59:65–70. doi:10.3164/jcbn.15-152.

328. van der Wielen P, Rovers G, Scheepens J, Biesterveld S. Clostridium lactatifermen tans sp. nov., a lactate-fermenting anaerobe isolated from the caeca of a chicken. International Journal of Systemiatic and Evolutionary Microbiology. 2002;52:921–5. doi:10.1099/00207713-52-3-921.

329. Brugiroux S, Beutler M, Pfann C, Garzetti D, Ruscheweyh H-J, Ring D, et al. Genome-guided design of a defined mouse microbiota that confers colonization resistance against Salmonella enterica serovar Typhimurium. Nat Microbiol. 2016;2:16215. doi:10.1038/nmicrobiol.2016.215.

Publications and Presentations

Publications

- Wegner, Just, Gau, Mueller, Gerard, Lepage, Clavel, and Rohn (2017). **Rapid analysis of bile acids in different biological matrices using LC-ESI-MS/MS for the investigation of bile acid transformation by mammalian gut bacteria**. Analytical and bioanalytical chemistry; 409; 1231-1245.
- Lagkouvardos, Pukall, Abt, Foesel, Meier-Kolthoff, Kumar, Bresciani, Martínez, Just, Ziegler, Brugiroux, Garzetti, Wenning, Bui, Wang, Hugenholtz, Plugge, Peterson, Hornef, Baines, Smidt, Walter, Kristiansen, Nielsen, Haller, Overmann, Stecher, Clavel. (2016) **The Mouse Intestinal Bacterial Collection (miBC) provides host-specific insight into cultured diversity and functional potential of the gut microbiota**. Nature Microbiology; 1(10):16131.
- Zantow, Just, Lagkouvardos, Kisling, Dübel, Lepage, Clavel, and Hust (2016) **Mining gut microbiome oligopeptides by functional metaproteome display**. Scientific Reports; 6:34337.

Manuscripts in preparation:

- Just, Streidl, Ecker, Wegner, Gau, Haller, Gerard, Rohn, Lepage, and Clavel. Intestinal *Coriobacteriaceae* **influence lipid metabolism in mice**.
- Just, Mondot, Wegner, Gau, Ecker, Dunkel, Haller, Gerard, Rohn, Lepage, and Clavel. **Gut microbiota-dependent impact of dietary fat type on diet-induced obesity**.

Oral presentations

- *CorioFunc* **consortium meetings**: Hamburg (01.10.2014), Paris (18.06.2015; 15.10.2016), Freising (10.01.2014; 08.11.2016)
- **24. – 26.6.2016**: 9th Seeon Conference, Microbiota, Probiota and Host; "Gut-derived *Coriobacteriaceae* increase white adipose tissue deposition in mice".
- **05. – 08.03.2017**: 5th Joint Conference of the DGHM & VAAM, Würzburg; "Gut-derived *Coriobacteriaceae* increase white adipose tissue deposition in mice".